공학박사학위논문

Study of Producing α-Si_3N_4 Powder by Low-temperature Vapor-phase Reaction Method

저온기상합성법에 의한 알파상 질화규소 분말 제조 연구

2016 년 8 월

서울대학교 대학원

재료공학부

정용권

Study of Producing α-Si_3N_4 Powder by Low-temperature Vapor-phase Reaction method

지도교수 박 찬

이 논문을 공학박사학위 논문으로 제출함

2016 년 8 월

서울대학교 대학원

재료공학부

정용권

정용권의 박사학위논문을 인준함

2016 년 8 월

위 원 장 유 상 임 (인)

부위원장 박 찬 (인)

위 원 장 호 원 (인)

위 원 한 지 현 (인)

위 원 김 진 상 (인)

Abstract

Study of Producing α-Si_3N_4 Powder by Low-temperature Vapor-phase Reaction Method

Yong-Kwon Chung
Department of Materials Science and Engineering
The Graduate School
Seoul National University

Most silicon nitride powders, industrially used in various applications under extreme conditions, are produced by the diimide process. The synthesis of diimide is carried out in the range −50–0 °C using liquid-phase reactants with organic solvent. This process, however, consumes a considerable amount of energy. One promising method for the synthesis of silicon nitride powder is the vapor-phase reaction of $SiCl_4$ with NH_3, and this synthetic process is also energy efficient. In this study, the processing parameters of the vapor-phase reaction for the synthesis of silicon nitride were investigated for producing diimide. The vapor-phase reaction completed at room temperature with a down-top flow, and solid products were obtained at the bottom of the reactor. $Si(NH)_2$ decomposed at temperatures >150 °C according to the result of the thermogravimetric analysis,

limiting the reaction temperature. The reaction temperature increased with increasing flow rates of the reactants and decreased with increasing flow rate of the carrier gas. The reaction yield decreased with increasing flow rate of the carrier gas. Under the optimized reaction conditions, 87% yield was obtained. Amorphous silicon nitride powder prepared by low-temperature vapor-phase reaction was heated at various temperatures for different periods of time to examine the crystallization behavior. The effects of the heat-treatment temperature and duration on the degree of crystallization were investigated along with the effect of the heat-up rate on the particle size, and the distribution of the crystallized α-phase silicon nitride powder. A phase transition from amorphous to α-phase occurred at temperatures >1,400 °C. The crystallization process was completed after heating at 1,500 °C for 3 h or 1,550 °C for 1 h. The crystallization process starts at the surface of the amorphous particle, whereas the outer regions of the particle become crystalline and the inner part remains amorphous. The re-arrangement of the Si and N atoms on the surface of the amorphous particle leads to the formation of hexagonal crystals that are separated from the host amorphous particle. The particle size and size distribution were controlled by varying the heat-treatment profile (namely, the heat-treatment temperature, heating rate, and heating duration at the specified temperature) and can be used to control the relative extent of the nucleation and growth. The completion of most of the nucleation process by lowering the heat-up rate was used to achieve a singlet particle size distribution. A bimodal particle size distribution was achieved by fast heating during the crystallization process.

In this study, we developed a novel synthesis method for the preparation of Si_3N_4 nanowires from the amorphous silicon nitride (a-Si_3N_4) powder synthesized by low-temperature vapor-phase reaction method. Highly crystallized α-Si_3N_4 nanowires were synthesized by heating Si_3N_4 powder under ammonia atmosphere. The surface of the nanowires was smooth and clean without any attached particles. The thickness of the nanowires was in the range 200–300 nm with lengths of tens of micrometers. The nucleation of nanowires from the reaction between SiO and N_2 occurs on the surface of a-Si_3N_4 powder, covered by a thin layer of SiO_2, and the nanowires grow from the re-arrangement of Si and N atoms of the a-Si_3N_4 powder. The reduction of SiO_2 to SiO by ammonia was promoted by the presence of Ni catalyst, and thus the growth was observed at lower temperature when Ni was added to the a-Si_3N_4 powder. The growth of α-Si_3N_4 nanowires occurs along the [100] and [101] directions and follows Vapor–Solid–Solid mechanism. Silicon nitride is an alternative material widely used for silica crucibles for directional solidification of multi-Si ingots, and its main advantages is the reusability in successive castings and elimination for a source for oxygen contamination of the ingot. In this study, multi-Si ingot was cast in the synthesized Si_3N_4 coated-crucibles and compared to the reference ingots cast in commercial crucibles. The quality assessment of the coating layer was investigated. The thickness of the coating layer was 257 μm with a uniformity of 27.15%. The inside crack and inclusion were not observed in the 25 bricks. The average MCLT and resistivity of the slugs were 3.9 μs and 4.4 Ω·s, respectively. The contents of O, C, and metal impurities were 4.4, 1.1, and 7.3 ppm, respectively. These results indicate that the performance of the synthesized Si_3N_4 coated-crucible was almost similar to the

commercial one. For application in the structural ceramics, pressureless sintering of the synthesized powder was carried out. Density and microstructure of the sintered body were measured, and the results were compared to the sintered body from Ube E10 powder. The pressureless sintering of the synthesized powder showed 99% sintering density at 1,650 °C, whereas Ube E10 powder showed 96% sintering density. The density of the synthesized powder was higher than that of Ube E10 powder. The Si_3N_4 powder synthesized by low-temperature vapor-phase reaction would be a good candidate for coating and the structural ceramic materials.

Keywords: silicon diimide, $Si(NH)_2$, silicon nitride, Si_3N_4, vapor-phase reaction, imide decomposition, crystallization, nanowire, Si_3N_4 powder coating

Student Number: 2013-30187

Contents

List of Figures

List of Tables

Chapter 1. General Introduction

1.1 Introduction

Silicon nitride has attracted significant attention for the first time as a possible raw material for the technical synthesis of ammonia. A series of patents published in the period 1909–1918 have described the synthesis of ammonia by heating Si_3N_4 with solutions or dispersions of basic oxides, hydroxides, or salts, by the treatment with hot water vapor, or by heating in the presence of hydrogen. Because of the concurrent development of the Haber–Bosch process, these methods never gained any importance. It is not surprising, therefore, that this early interest in silicon nitride soon declined. However, silicon nitride saw a remarkable renaissance after the discovery, as it can be converted into a ceramic material. Silicon nitride ceramics significantly extend the limits of metallic materials under combined thermal and mechanical stress in corrosive environments.

1.2 Silicon Nitride as Ceramic Material

Silicon nitride is of great interest as a heavy-duty material for applications in chemical engineering, wear technology, metal networking, energy technology, and especially in engine and turbine construction.[12–24] This broad interest arises from a favorable combination of great hardness, wear resistance, chemical stability, low density, and high mechanical strength at temperatures up to 1300 °C. The

application of Si_3N_4 ceramic parts in combustion engines and gas turbines promises significant advantages such as higher efficiency and better fuel use because of higher combustion temperatures, faster response of oscillating or rotating engine components (valves, pistons, turbocharger, and turbine rotors) due to low density, and longer service intervals due to a generally improved wear behavior. Silicon nitride ceramics are produced either by nitriding silicon powder compacts or by sintering Si_3N_4 powder compacts [25,26]. The first method produces a porous, reaction bonded silicon nitride (RBSN) material, reaction-bonded with almost negligible shrinkage; this material is used either directly or may be densified by a following sintering step, and the resulting material is named as sintered RBSN (SRBSN).[25–30] The second method, which is covered comprehensively in this article, leads to Si_3N_4 ceramics of superior quality. These are of special interest to advanced engine construction and advanced mechanical engineering. To demonstrate their technological benefits reliably, Si_3N_4 components require a perfect and economical control of the entire manufacturing process from the synthesis of the Si_3N_4 powder, processing, forming, and sintering to the precise finishing of the structural component. Non-uniformity of the starting powder, for example, even just a few extraneous particles, ill-defined particle clusters, or particle morphologies such as a mass of disordered, more or less agglomerated lumps, fibers, or nanowires, as well as extraneous particles or impurities dragged in through powder processing induce fracture-causing structural defects, which cannot be remediated in the following manufacturing steps, resulting in products of inferior quality and reliability. Because powder-inherent sources of defects can hardly be eliminated by subsequent ceramic processing, the powder producer has a

special responsibility to supply extremely well-defined and high-quality powders. To avoid environmental contamination such as dust particles, the transfer of powder processing, shaping, and sintering into clean rooms has been discussed.[31,32] Repeatedly, this measure has been described to improve the fracture strength and reliability.[33,34] Furthermore, defects also arise during shaping, sintering, and finishing. These nowise trivial problems have to be solved convincingly to allow an economical and large-scale production of silicon nitride components. Here, chemistry plays an important role, because powder synthesis and component manufacturing touch many problems of fundamental solid-state chemistry, surface chemistry, tribochemistry, and chemical engineering.

1.3 The Structure of Silicon Nitride-origin of Hardness, Durability, and Strength.

Crystalline silicon nitride exists in two hexagonal modifications, alpha and beta, which are built up from a three-dimensional network of Si_3N_4 tetrahedrons.[36,37] Rigid structure and strong covalent bonds provide extraordinary hardness, durability, and mechanical strength to this material. Fig. 2 shows the crystal structure of Si_3N_4, built from Si_6N_8 units along the crystallographic c-axis, and channels with a diameter of ~0.15 nm play a certain role in the diffusion of atoms, even large ones. α-Si_3N_4 is built from a $Si1_2N_{16}$ unit cell, [24] and because of the absence of channels this structure, diffusion is much more difficult than that in β-Si_3N_4. Early work on the conditions leading to formation of either the α or β phase indicated that the α phase, assumed to be an oxygen-stabilized low-temperature

modification with a narrow range of existence, has the empirical formula $Si_{11.4–11.5}N_{15}O_{0.3}$ (actually no oxinitride phase).[36,40–42] However, the formation of the α phase required significantly less oxygen than presumed.[43] By chemical vapor deposition it was possible to produce α-Si_3N_4 single crystals extremely low in oxygen [39,44–47] Nowadays, α- and β-Si_3N_4 are regarded as polymorphic modifications; α-Si_3N_4 is the stable low-temperature modification, as the α-Si_3N_4 content of a powder increases with decreasing synthesis temperature and α to β transformation occurs only at temperatures exceeding 1650 °C. Probably for kinetic reasons, α to β transformation has not yet been observed. The α/β ratio of commercially available powders is usually determined not only by X-ray [48, 49], but also IR [50–52] and ^{29}Si MAS NMR spectroscopy.[53–55] ^{29}Si MAS NMR spectroscopy is particularly useful as it can be used to distinguish and quantify not only the crystalline phases but also amorphous Si_3N_4. [54] This method is also suitable for the study of sintering phenomenon.[56,57]

1.4 The Synthesis of Si_3N_4 Powders

For the technical synthesis of high-quality Si_3N_4 powders, three following methods are important: nitridation of silicon powder [Eq. (a)], [58–61] carbothermal reduction of SiO_2 in the presence of nitrogen [Eq. (b)] or ammonia,[62–66] and ammonolysis of reactive silicon compounds [Eqs. (c) and (d)]. [67–71]

$$3Si + 2N_2 \rightarrow Si_3N_4 \text{ at } 1100–1400\ °C \quad (a)$$

$$3SiO_2 + 2N_2 + 6C \rightarrow Si_3N_4 + 6CO \text{ at } 1450–1600\ °C \quad (b)$$

$$3SiCl_4 + 4NH_3 \rightarrow Si_3N_4 + 12HCl \text{ at } 25–1400\ °C \quad (c)$$

$3SiH_4 + 4NH_3 \rightarrow Si_3N_4 + 12H_2$ at 600–1400 °C (d)

In contrast to direct nitridation or carbothermal reduction, ammonolysis does not yield crystalline Si_3N_4 directly. The reaction initially leads to extremely moisture-sensitive silicon diimide [Eq. (e)], which is then transformed to α-Si_3N_4 by pyrolysis via amorphous Si_3N_4 [Eqs. (f) and (g)] [67–69,72].

$SiCl_4 + 6NH_3 \rightarrow Si(NH)_2 + 4NH_4Cl$ at 25 °C (e)

$3Si(NH)_2 \rightarrow a\text{-}Si_3N_4 + 2NH_3$ at 900–1200 °C (f)

$a\text{-}Si_3N_4 \rightarrow c\text{-}Si_3N_4$ at 1300–1600°C (g)

Several other reactions [Eq. (h), [73–75] (i), [76] (j) [77,78]] have not gained importance for technological or economic reasons such as cost effectiveness, slow reaction kinetics, or the development of undesirable particle morphologies.

$3SiS_2 + 4NH_3 \rightarrow Si_3N_4 + 6H_2S$ (h)

$3SiC + 4NH_3 \rightarrow Si_3N_4 + 3CH_4$ (i)

$3SiO_2 + 4NH_3 \rightarrow Si_3N_4 + 6H_2O$ (j)

Furthermore, there have been numerous attempts to synthesize Si_3N_4 by pyrolysis or carbothermical reduction from silazanes or siloxanes.[79] Because of the comparatively complicated and costly production and handling of silazanes, this method is less interesting for powder synthesis than for the manufacturing of Si_3N_4 fibers or coatings. Polymeric silazanes of suitable structure may be processed by spinning to produce fibers or by melt or solution coating; subsequent pyrolysis

usually provides 60–80% ceramic yield. There is also some fundamental interest in the use of silazanes as binders or plasticizers for silicon nitride powder molding by dry pressing or injection molding, because pyrolysis leaves nothing but Si_3N_4.

1.4.1 Required Powder Properties

Si_3N_4 powder qualified for applications in advanced ceramics has to meet numerous demands regarding chemical and physical properties. Important criteria for powder quality include purity, crystallinity, particle shape, particle size distribution, degree of particle agglomeration, and α/β ratio, as well as technological properties such as good processing behavior in different powder shaping techniques and good sintering activity. To minimize shrinkage and avoid the development of density gradients during sintering, powder shaping has to aim at particle packing densities as high and as homogeneous as possible. This has been achieved by defined particle size distributions, spherical particle shapes, mean particle sizes <1 pm, and exclusion of coarse or hard agglomerated particles. These factors, together with defined C and O contents, exclusion of extraneous particles, and a high α/β ratio, are important characteristics of powders with good sintering behavior and favor the development of a homogeneous grain structure during sintering. The spectrum of all these properties affects the general sintering activity of a powder. Roughly, sintering activity increases with decreasing particle size. However, powder processing becomes increasingly difficult (dust generation, bad densification behavior in dry pressing, and high sintering shrinkage) as particle sizes decrease. Therefore, the search for universally applicable powders often requires a compromise between opposing demands. These circumstances, in turn,

offer possibilities for special "powder designs", that is, tailor-made powders with special advantages in certain manufacturing processes. A free-flowing granulated Si_3N_4 powder, which will not crumble into dust particles but is easy to densify, is favorable for charging automated dry presses and may illustrate this point. Some powder properties such as the α/β ratio have to be adjusted during the Si_3N_4 synthesis; others properties including particle size, particle size distribution, or C and O content, may be affected subsequently by suitable powder processing (e. g., milling, screening, or annealing). In order to minimize the efforts on powder processing, it is advantageous to adjust as many of the required properties as possible during the synthesis. The extent of the technological feasibility and economic of the approach depends on the synthetic method chosen.

1.4.2 Si_3N_4 Synthesis by Direct Nitridation of Elemental Silicon

Direct nitridation of elemental silicon, the process used more than 80 years ago to show the correct stoichiometry of silicon nitride to be Si_3N_4 [80], is still the dominant procedure for the industrial synthesis of silicon nitride powder. [45,46] The main processing steps are nitridation of silicon powder, milling, and finally purification of the crude product (Fig. 4). The selection of silicon powders of different purities strongly affects the impurity level of Si_3N_4. Besides commercially available, low-cost, metallurgical-grade silicon of different levels of purity, it is possible to use semiconductor grade silicon of extremely high purity as the starting material.[81] For the actual synthesis, piles of silicon powder are allowed to react with nitrogen either discontinuously in chamber furnaces or continuously in conveyor-type pusher furnaces according to Equation (a) ($\Delta H = -750$ kJ mol^{-1}).

The reaction proceeds at a reasonable rate only at –1100 °C. Reaction rates strongly depend on the particle size and chemical purity of the silicon powder.[66,61,82,83] Especially traces of Fe catalyze the nitridation.[82,84] Owing to its strong exothermal characteristic, the reaction has to be controlled carefully. In general, low temperatures and the presence of hydrogen in the nitriding gas favor the formation of α-phase material.[60,61,85] Too high temperatures cause not only the formation of undesired β-Si_3N_4 but also strongly sintered agglomerates of Si_3N_4 primary particles, which finally require a more intensive milling process. Careful control of the exothermic reaction is also necessary to avoid an uncontrolled temperature rise exceeding the melting point of silicon in the powder bed.[60,61,85] The evolution of heat can be reduced by lowering the concentration of nitrogen in the nitriding atmosphere after the onset of the reaction ("exothermal control"[86]). It may also be limited by a suitable, often empirically determined temperature control depending on nitridation kinetics, powder packing density, depth of powder bed, charge size, and type of furnace.[60,61,82] After synthesis, the sintered product is crushed and finally milled to the desired particle size. Depending on the powder processing, possible metallic impurities because of the milling wear are removed by subsequent acid leaching. A variation in the direct nitridation described here as self-propagating high-temperature (SHS) synthesis.[87–90] Here the reaction proceeds very fast ("thermite-like") after local ignition under increased N_2 pressure.[91–95] Under these conditions, the reaction zone moves with a speed of up to 0.1 m s^{-1} through the powder bed with temperatures often exceeding 1700 °C. The product is a high β-phase material (β >95%), requiring the usual processing by milling and acid leaching.[95] So far the question whether high β-phase Si_3N_4

powder is suitable for manufacturing advanced silicon nitride ceramics has been answered positively only sporadically;[96,97] further investigation is required.[95] Other open questions in the further development of SHS synthesis, which may also be used for the production of other refractory compound, [87–90,94] concern the control of the α/β ratio and the development of cost efficient, large-scale production. Whether SHS synthesis will allow direct manufacturing of high-quality sintered components is another interesting issue.

1.4.3 Si_3N_4 Synthesis by Carbothermal Reduction

This method uses the reaction of SiO_2 powder with carbon at temperatures of 1500 °C in a N_2 atmosphere, producing Si_3N_4 via a series of reactions [e.g., Eqs. (a), (I), and (m)]. The overall reaction is given by Eq. (b).

$$SiO_2 + C \rightarrow SiO + CO \quad (l)$$

$$SiO + C \rightarrow Si + CO \quad (m)$$

$$3Si + 2N_2 \rightarrow Si_3N_4 \quad (n)$$

Because inexpensive and readily available silicate raw materials may be used, carbothermal reduction attracted early interest during the first attempts to synthesize Si_3N_4 as the starting material for industrial-scale ammonia synthesis.[5–11,98] There was no concern about the chemical purity or particle morphology; reaction mixtures of quartz sand, silicates, carbon, and coke were even compounded with metal oxides to decrease the reaction temperature. Purification of the product from metallic impurities and nonreacted carbon was first achieved

by acid leaching and oxidative treatment.[11] Modern procedures ensure chemical purity by careful control of the purity levels of the starting materials. Besides high-purity, synthetic materials from pyrolysis [62] or sol–gel reactions,[63, 99, 100] natural products such as quartz sand [98] and clay [101] may also be used, although at the expense of purity. Though stoichiometry requires a SiO_2/C ratio by weight of just 1:0.4 for a complete reaction, a considerable excess of carbon is required in practice. Usually, the SiO_2/C ratios of 1:2 to 1:10 have been employed.[62–66,102,103] Very good results yield extremely fine SiO_2 and C powders from, for example, gas-phase pyrolysis.[62,103,104] An intensive homogenization of the powders is necessary to ensure that the reaction is homogeneous and proceeds to completion. A very good alternative is provided by the sol–gel type methods, in which the polycondensation of silicon halides with alcohols is prone to polymerization (e. g., furfural) yield easy-to-handle polymeric granules containing Si, O, and C in ultradisperse distribution. Thermal cracking yields an extremely homogeneous SiO_2/C mixture, which undergoes ready carbothermal reduction.[105] Because carbothermal reduction may also proceed reversibly, CO formed in the course of the reaction has to be removed. In practice, the reaction is carried out either continuously in conveyor-type pusher furnaces or in chamber kilns, where the CO partial pressure is kept low by flowing N_2. Though Si_3N_4 formation generally increases with increasing temperature, increasing amounts of SiC, depending on CO partial pressure, are formed at temperatures exceeding 1450 °C; the SiC is practically inseparable from the Si_3N_4 [65,99–106] (Fig. 5). Particle size and particle morphology may be controlled by adding either crystalline spheroidal Si_3N_4 particles or Si_3N_4 nanowires as nuclei to the reaction.

Since carbon acts also as a nucleation center for the Si_3N_4 formation, its particle size also affects Si_3N_4 powder characteristics. Very fine, high-surface carbon powders favor the formation of spheroidal Si_3N_4 particles; coarse, low-surface powders favor nanowire formation.[99,1021 After synthesis the reaction product is milled to adjust the desired particle size and the particle size distribution (Fig. 6). By tempering in the air, [66] NH_3 or chlorine-containing atmospheres [107,108] in temperatures range 600–800 °C, excess carbon is removed. If required, incompletely reacted SiO_2 may be removed by HF leaching.

1.4.4 Ammonolysis of Reactive Silicon Compounds

1.4.4.1 Si_3N_4 Synthesis by Liquid-Phase Reaction of $SiCl_4$ and NH_3

The study on the liquid-phase reaction of $SiCl_4$ and NH_3 dates back to 1830, when Persoz [109] isolated a white precipitate, which he considered to be silicon tetraamide, $Si(NH_2)_4$. Subsequently, however, this precipitate was identified as silicon diimide, $Si(NH)_2$. Though this reaction may be described in its most simple form by Eq. (e), further investigation showed a very complex process, leading to differently polymerized, extremely moisture-sensitive $[Si(NH)_2]x$. [112] Subsequent high-temperature pyrolysis leads to stable, processable α-Si_3N_4 via several intermediates and amorphous Si_3N_4 accompanied by NH_3 or N_2/H_2 liberation.[67–69,112–117] The transformation of amorphous silicon nitride to crystalline α-Si_3N_4 proceeds at >1200 °C in a diffusion-controlled manner with an activation energy of 306 kJ mol^{-1}.[118]

It is remarkable that NH_4Cl still present from the $SiCl_4/NH_3$ reaction [Eq. (e)] affects the $Si(NH)_2$ pyrolysis.[115] In the absence of NH_4CI, $Si(NH)_2$ is stable up

to 200 °C; it gradually loses NH_3 with increasing temperature, until finally amorphous Si_3N_4 is formed. However, thermal decomposition in the reaction of $Si(NH)_2$ and HCl in the presence of NH_4CI provides a compound of the composition $Si_2N_3H_2CI$, which decomposes to amorphous silicon nitride at >800 °C. The pyrolysis of $Si(NH)_2$ at temperatures <1200 K leads to the formation of an extremely fine, moisture-sensitive, amorphous Si_3N_4 powder showing primary particle sizes of ~10–30 nm and BET surfaces greater than 100 m^2 per g. Prolonged heating in the temperature range 1200–1400 °C induces crystallization of α-Si_3N_4 accompanied by particle coarsening. At temperatures >1500 °C, mainly β-Si_3N_4 is formed. [69] Particle morphology, particle size, and α/β ratio are affected by temperature, retention time, and impurities.[119,120] Since $SiCI_4/NH_3$ liquid-phase reaction allows the synthesis of a very pure and fine Si_3N_4 powder from easily purified and readily available starting materials, this method (often referred as the diimide process) has been developed on a pilot scale (Fig. 7). The $SiCI_4/NH_3$ reaction is carried out in a two-phase system consisting of an organic solvent and liquid NH_3 [72,116–117,121] or by reacting $SiCl_4$ vapor with excess liquid NH_3 [122] thus dissolving the by-product NH_4CI. The $Si(NH)_2$ precipitate is filtered and washed with liquid ammonia to remove residual NH_4Cl and finally calcined and crystallized to afford α-Si_3N_4. In contrast to thermal NH_4Cl separation by sublimation, in this procedure no corrosive NH_3/HCl vapors are generated, thus offering a technological advantage. However, upscaling has to take into consideration the large amount of NH_4Cl by-product, generated according to Eq. (o). An economically favorable and ecologically safe application or disposal has yet to be found for NH_4Cl by-product.

$$3SiCl_4 + 16NH_3 \rightarrow SI_3N_4 + 12NH_4Cl \quad (o)$$

1.4.4.2 Si_3N_4 Synthesis by Gas-Phase Reactions of $SiCl_4$ or SiH_4 with NH_3

Owing mainly to homogeneous nuclei formation, gas-phase reactions have a great potential for the production of extremely tine powders.[123] After the formation and growth of nuclei in the reaction zone, particles cluster to aggregates and agglomerates, which may be separated as fine dust (Fig. 8). For economical and technical reasons gas-phase reactions of $SiCl_4$ or SiH_4 with NH_3 are of special interest. From a technological point of view, the use of inexpensive $SiCl_4$ requires the separation of the corrosive NH_4Cl by-product through either hot gas filtration, extraction, or sublimation. Because of spontaneous ignition of SiH_4 in contact with air, however, the use of expensive SiH_4 requires extensive safety precautions. A technological advantage is the formation of hydrogen as gaseous by-product, which is easily separated. If $SiCl_4$ is used, reaction parameters may be adjusted to approach the stoichiometry of the reaction [Eq. (p)], thus keeping the amount of solid NH_4Cl by-product low compared to the corresponding liquid-phase reaction.

$$SiCl_4 + 2NH_3 \rightarrow Si(NH)_2 + 4HCl \quad (p)$$

Instead of using expensive pressure vessels, gas-phase reactions are run at atmospheric pressure in heated tube reactors (Fig. 9). Similar to industrial-scale synthesis of SiO_2 and TiO_2 powders, these reactions represent a good technological basis for a continuous and large-scale production of fine powders. As liquid-phase

reactions, $SiH_4/SiCl_4$-NH_3 gas-phase reactions also yield amorphous Si_3N_4 precursors, because of the short retention times of gas and particle streams in the hot reaction zone. These amorphous precursors have to be crystallized separately in a subsequent step. The reaction of SiH_4 and NH_3 in the temperature range 500–900 °C yielded amorphous powders with particle sizes in the range 30–200 nm and BET surfaces up to 26 m^2 g^{-1}. [70,71] Our investigations on $SiCl_4/NH_3$ gas-phase reactions in the temperature range 300–1700 °C showed the formation of extremely fine, spheroidal, and amorphous particles with BET surfaces up to 300 m^2g^{-1}.[124,125] Crystallization of these precursors induces particle coarsening, thus the BET surface may be adjusted in the range 2–20 m^2g^{-1}.[70,125] Strict control of impurities, temperature, and retention time is important for the generation of very fine, uniform, and high α-phase Si_3N_4 particles by the crystallization of amorphous Si_3N_4 (Fig. 10). The powders from $SiCl_4/NH_3$ gas-phase reactions require significantly less processing (Fig. 11) than the products from direct nitridation or carbothermal reduction, because of their inherent fine particle size and weak agglomeration. They are characterized by high chemical purity, good manufacturing properties, and high sintering activity.

1.4.5 Si_3N_4 Synthesis by Laser-Induced and Plasma chemical Reactions

The study on laser-induced [126–129] and plasma chemical reactions [130–134] as alternatives to "usual" thermal gas-phase reactions tries to avoid any heterogeneous nuclei formation, because of the contact of the reacting gases with hot reactor walls, guarantying an extremely high degree of particle fineness and uniformity. Characteristic properties of both the processes, which are based on chemical

reactions already described above, are extremely fast heating and cooling rates of 105 to 106 K s^{-1} and fast reaction rates of an order of 10^{-3} s. Figs. 12 and 13 show the experimental setups for laser-induced and plasma chemical Si_3N_4 synthesis from the reactions of SiH_4 or $SiCl_4$ with NH_3. Particle size, crystallinity, α/β ratio, and stoichiometric composition of the reaction product are affected by mass flow, pressure, stoichiometric ratio of reactants, and laser or plasma generator power output. A major problem of laser-induced synthesis is the small reaction diameter of the laser beam, allowing only product formation rates of the order of just a few grams per hour. Because of the extreme temperatures of several thousand K in plasma chemical reactions, the reactants are broken apart to different radicals, which may recombine in various ways in the temperature gradients of the reaction zone. Since fluid dynamics is also very important, precisely controlling the reaction is very difficult. Both laser-induced and plasma chemical synthesis allow the generation of extremely fine powders with particle sizes in the range 10–30 nm and BET surfaces >100 m^2 g^{-1}. However, the products often showing incorrect stoichiometric composition are amorphous or possess changing, not exactly reproducible α/β ratios. Furthermore, they may contain free silicon as an undesired by-product from the decomposition reactions. Because of these difficulties, laser-induced and plasma chemical reactions are not yet of importance to large-scale synthesis of Si_3N_4 powders, despite intense research.

1.5 Silicon Nitride Nanowires

After the discovery of crystal nanowires with unusual mechanical strength, [135] interest in the properties, production, and applications of ceramic nanowires have grown.[136,137] The use of nanowires to reinforce metallic or ceramic materials aims at improving fracture toughness or, more generally, mechanical properties of the matrix material. In spite of the strong general interest in ceramic nanowires, there are still problems in producing pure and uniform nanowires on a large scale in an economical way. The development of nanowire production and processing methods especially has to take into account health precautions to exclude a potential hazard arising from asbestos fibers.[138,139] Chemically, the same methods as in the synthesis of spheroidal Si_3N_4 powder particles are used for the production of Si_3N_4 nanowires. However, additional measures are required to apply general techniques such as vapor-phase transport or crystallization by vapor–liquid–solid (VLS) mechanisms to favor nanowire formation.

1.5.1 Nanowires from the Reaction of Si and N_2

In direct nitridation of elemental silicon, Si_3N_4 nanowires are formed by the reaction of silicon vapor and N_2. Fig. 14 shows a simple experimental setup for this production method. Silicon is evaporated from a crucible at the bottom; a stream of inert carrier gas is used to guide the Si vapor into a reaction zone in the upper part of the apparatus, where it reacts with N_2 or NH_3. The Si_3N_4 nanowires precipitate onto graphite baffles from where they may be collected.

1.5.2 Nanowires from Carbothermal Reduction of SiO_2

This process, which may be run continuously in conveyor-type pusher furnaces, yields nanowires from the gas-phase reaction of SiO and N_2 or NH_3 in CO-containing atmosphere.[141–143] By adjusting the stoichiometry, the particle size, homogeneity, and packing density of the reaction mixture of silica and carbon raw materials, addition of silicon or metal oxides, and control of the reaction temperature, the amount of SiO generation, and consequently Si_3N_4 nanowire formation is optimized. Nanowire formation is also favored if Si_3N_4 nanowires are added to the reaction mixture as the growth nuclei.[143]

1.5.3 Nanowires from the Reaction of $SiCl_4$ with NH_3

As described above, the reaction of $SiCl_4$ with NH_3 leads to $Si(NH)_2$, which further yields amorphous Si_3N_4 on calcination. If small amounts of Fe or SiO_2 are added to this material and the resulting mixture is heated to 1200–1500 °C in the absence of oxygen, Si_3N_4 nanowires are formed by the VLS mechanism from Fe- or silicate-containing eutectic melt droplets [72,143] (Fig. 15).

1.5.4 Nanowires from the Reaction of SiS_2 with NH_3

Originally intended to produce high-purity Si_3N_4 powder, the reaction of SiS_2 with NH_2 offers a good way to produce the reaction of Si powder with H_2S at high temperature [Eq. (q)].

$$Si + 2H_2S \rightarrow SiS_2 + 2H_2 \text{ at } 900\ ^\circ C \qquad (q)$$

The high vapor pressure of SiS_2, which forms because of the dissociation of SiS_2, leads to SiS_2 nanowire growth by the VLS mechanism from the eutectic droplets of SiS and sulfur vapor. The reaction of SiS_2 with NH_3 affords a (Si–S–N–H)x polymer, which thermally decomposes under NH_3 to yield amorphous silicon nitride. The amorphous silicon nitride is obtained in "spaghetti-like" morphology (Fig. 16) and may be crystallized to α-Si_3N_4 with the retention of morphology.

1.5.5 Nanowires from the Reaction of SiC and NH_3

The reaction of SiC with NH_3 is remarkable, as it leads to Si_3N_4 particles of unusual morphology. By heating a mixture of SiC and Fe powder in NH_3 to 1440 °C followed by a short-term temperature rise to 1480 °C, Glemser and Horn [176] obtained spiral-shaped α-Si_3N_4 nanowires (Fig. 17, left). Some of these spirals could be observed with the naked eye. Recently, similar observations have been made in the investigation of vapor-phase deposition of Si_3N_4 from Si_2CI_6, NH_3, and H_2 at 1200 °C onto a graphite substrate coated with Fe-containing compounds.[144,145] The spiral-shaped nanowires (Fig. 17, right) are ~0.5–1.0 pm thick and consist of α-phase Si_3N_4 slightly contaminated by carbon and oxygen. They show a quite uniform morphology with a regular pitch, spiral diameter, and length in the range 3–5 pm, 5–10 pm, and of 50–100 μm, respectively. Obviously, spirals are formed only in a narrow fiber-diameter range of ~0.1–5 μm.

1.5.6 Properties of Si_3N_4 Nanowires

The principal problems in nanowire production are the requirements of high chemical purity and uniform nanowire morphology. Because of technological

difficulties in producing a homogeneous distribution of Si_3N_4 nanowires in a matrix material, fracture-causing structural defects are often induced during material processing; in these cases, the originally intended toughening of the matrix actually turns out week.[146,147] Fundamental problems in nanowire processing are often connected with shaping and sintering, because the heaps of needle like particles are much more difficult to compact by dry pressing than the heaps of spheroidal particles.

1.6 Remarks on the Procedures for Synthesis of Si_3N_4 Powders

A comparison of chemical and physical characteristics of powders from commercially used synthetic methods shows that direct nitridation, carbothermal reduction, and ammonolysis of reactive silicon compounds are principally able to furnish very fine, high-purity Si_3N_4 powders for advanced applications. Often variations in the particle sizes, particle size distribution, and particle surface properties, which are important to ceramic processing, may be carried out after Si_3N_4 synthesis by suitable powder processing. Direct nitridation and carbothermal reduction use inexpensive raw materials and directly yield crystalline Si_3N_4. However, the reaction products require extensive subsequent processing. In contrast, ammonolysis of reactive silicon compounds yields moisture-sensitive products, which require further thermal treatment for crystallization to yield α-Si_3N_4. Because of their inherent fine particle size and only weak particle agglomeration, the extent of subsequent powder processing is considerably reduced

compared to direct nitridation and carbothermal reduction. Direct nitridation and $SiCl_4/NH_3$ gas-phase reactions seem to offer the best chances to furnish economically high-quality powders for the manufacturing of broadly applicable silicon nitride ceramics. The production of Si_3N_4 nanowires is not yet commercially important, as Si_3N_4 nanowire-reinforced materials have not found broad applications because of high costs and a lack of large-scale production methods for reliable components. For technological and economic reasons, especially carbothermal reduction and nanowire growth from amorphous $S_{i3}N_4$ should be suited best to meet an eventually increasing demand.

1.7 The Manufacture of Sintered Si_3N_4 Ceramics

1.7.1 Fundamentals of Sintering and Structural Development

1.7.1.1 Physical and Chemical Aspects of Si_3N_4 Sintering

"Dry" sintering techniques used in the densification of oxide ceramics cannot be applied to the sintering of Si_3N_4 powder compacts. Strong covalent Si–N bonds hinder useful mass transport through grain-boundary or lattice diffusion. The activation of diffusion by simply raising the sintering temperature is limited by ever-increasing thermal decomposition. Since a N_2 partial pressure of 1 bar is reached at ~1900 °C, several precautions have to be taken to prevent excessive decomposition during the sintering of Si_3N_4 at high temperatures. Most important is the addition of compounds that form molten silicate phases and allow densification by liquid-phase sintering mechanisms. Well-suited additives include alkaline-earth oxides and rare-earth oxides either alone or in combination with

Al_2O_3 or AlN.[148–152] Above 1300 °C sintering additives react with SiO_2 or Si_2N_2O always present in Si_3N_4 powders to yield molten silicate phases. In the case of sufficient wetting and solubility of Si_3N_4, these silicate melts allow densification by capillary-force-induced particle rearrangements and dissolution/reprecipitation processes. The efficiency of these mechanisms is illustrated by a model experiment using a pre-synthesized, nitrogen-saturated Mg-Al silicate glass as the sintering additive. At 1300 °C, the dilatometric monitoring of the process showed densification by capillary-force-induced particle rearrangement, because nitrogen saturation of the silicate glass does not allow further dissolution of N_2 or Si_3N_4. With increasing temperature, Si_3N_4 solubility increases and densification via dissolution/reprecipitation is observed. A Si_3N_4 sample without sintering additives shows a completely unsatisfactory densification. Another important precaution is sintering under high N_2 pressure to suppress decomposition.

1.7.1.2 Structural Development

After particle rearrangement at low temperatures, which increases the packing density almost without affecting the particle shape and particle size distribution, true sintering by dissolution/reprecipitation occurs at higher temperatures. At present, structural development is thought to depend on the type of Si_3N_4 starting powder. Starting from α-Si_3N_4, reprecipitation of dissolved α-Si_3N_4 from almost saturated or slightly oversaturated solutions leads to crystallization of needle or rod like β-Si_3N_4 grains far from the energetic minimum.[154] Because a fine-grained, needle like structure has a positive effect on the fracture-mechanical properties for numerous applications, this grain morphology is desired.[155,156] If β-Si_3N_4

powder is used, dissolution/reprecipitation occurs almost in equilibrium. The surface energy difference between small and large particles causes a continuous dissolution of small particles and their reprecipitation on large grains. This process allows grain growth with the minimization of boundary surface energy leading to the development of approximately globular particles. Prolonged thermal treatment, far beyond the moment when densification is complete, favors the grain growth by minimization of boundary energy ("Ostwald ripening") also in needle-grained structures and leads to grain coarsening with growth of spheroidal grains. In this case, structural development leads to the formation of globular grains, no matter whether α- or β-Si_3N_4 is used as the starting material. A study on the structural development on prolonged heat treatment of α-phase Si_3N_4 is shown in Fig. 18. After sintering, all these materials contain an amorphous or semicrystalline secondary phase in between the grain boundaries or in grain triple points. Because material properties at high temperatures are significantly affected by the secondary phase, the reduction, modification, or complete elimination of this phenomenon is of major importance for the optimization of Si_3N_4 ceramic properties.

1.7.1.3 Influence of Sintering Additives

The amount and chemistry of the molten silicate phase, which is formed by sintering additives, are of importance to the course of sintering, as they determine sintering kinetics. For example, the kinetics of MgO-doped systems is governed by dissolution, whereas the rate of diffusion is crucial in Y_2O_3-doped Si_3N_4. The effect of typical additives on the sintering behavior is shown in Fig. 19. For instance, the densification of Y_2O_3-doped Si_3N_4, which sinters at relatively high temperatures,

may proceed at a low temperature level of ($MgO + Al_2O_3$)-doped materials if Al_2O_3 is added. Different additive systems may form compounds of the type α'-Me(Si,Al)3(N,O)4 or β'-Si6-xAlxO_xN_{8-x}, with newly precipitated Si_3N_4 grains.[162,163] The expectation that Si_3N_4 ceramics free of secondary grain-boundary phases can be produced by using this principle has only been fulfilled for Be-doped Si_3N_4.[149,160] The amount and type of additives also affect the structural development and thus material properties. Fine-grained Si_3N_4 structures are favored in the systems where the molten silicate phase shows a relatively high viscosity at sintering temperatures (e. g., systems doped with rare-earth oxides). The effect of additives is especially clear in the structural development of β-SiAlON materials, where globular grains are favored.

1.7.1.4 Influence of Powder Characteristics

Besides the type and amount of additives, the sintering behavior, structural development, and finally the material properties strongly depend on the powder characteristics of the starting Si_3N_4 powder. Of further importance are the powder properties resulting from processing prior to shaping and sintering; in particular, breaking up particle agglomerates is necessary to produce a homogeneous distribution of sintering additives. Relevant powder properties can be divided based on physical, chemical, and technical characteristics, which together determine the processing behavior and sintering activity in a complex way. The effect of α/β-Si_3N_4 ratio has already been mentioned and is still a subject of intensive discussion.[54,124,155,164,165] A high α-phase content enhances the sintering activity and favors the development of rod like β-Si_3N_4 grains. With respect to

sintering activity, amorphous Si_3N_4 would be of even greater advantage. However, its large-scale use is complicated owing to its sensitivity towards hydrolysis and its low powder-packing density, resulting in enormous shrinkage during sintering. Among chemical powder characteristics, the oxygen content is of special importance, as it affects the softening behavior and the amount and viscosity of the silicate phase formed in the reaction with sintering additives. Although a great amount of low-viscosity silicate melt phase enhances sintering, it has a negative effect on the high-temperature properties of the material if the silicate phase remains as an amorphous, glassy grain-boundary phase. Thus, the oxygen content has to be adjusted based on the amount of sintering additives required (or vice versa); it is a compromise between the beneficial effects on the sintering behavior and detrimental effects on high-temperature material properties. Usually, commercially available powders possess an oxygen content in the range of 1–2%. Moreover, the distribution of oxygen in the particle itself is of importance. If oxygen is concentrated on the particle surfaces, it is directly available for silicate phase formation by reaction with sintering additives. In this way, surface oxygen considerably improves sintering activity.[166,167] Therefore, high-quality Si_3N_4 powders usually possess oxygen-enriched particle surfaces, thus allowing fine-tuning of the amount of sintering additives required for complete densification and thereby improve the material properties. Free carbon has a negative effect on the sintering behavior, because it reduces the oxygen content of the powder with the formation of volatile SiO and CO. The resulting ill-defined variations in the silicate phase chemistry may cause incomplete sintering and undesired structural development, leading to poor material properties.[153,169] Chemically bonded

carbon in the form of SiC is much less critical. Because of its inherent stability, this material may be considered as an inert filler.[108,147] The effects of other impurities have to be judged by their behavior in sintering; they may dissolve in the liquid phase with incorporation in the silicate structure, or they may remain as particle inclusions with or without the reaction with the Si_3N_4 matrix. Metal oxides and metal halides either evaporate during sintering or dissolve in the liquid phase, lowering its viscosity with the already discussed effects on the sintering behavior, structural development, and material properties. Metal particles such as Fe, Mn, and Ti react with the Si_3N_4 matrix to form silicides or nitrides.[170] Compared to the original particle sizes, inhomogeneities because of chemical reactions are larger [170] and thus generally detrimental to the mechanical properties such as fracture strength (Fig. 20). Granulometric powder properties, which involve particle size distribution, particle morphology, and particle agglomeration, affect the processing behavior and the extent of powder processing required to produce an admixture of high sintering activity. Since sintering activity increases with increasing surface energy, "sub-µm" powders with a high content of particles <1 µm are advantageous. The amount of "coarse grains" attracts special attention, because these particles will dissolve comparatively slowly in the silicate phase. Therefore, sintering slows down, and some particles may survive more or less unchanged to form structural inhomogeneities. Nanowire- or fiber like Si_3N_4 particles cause similar effects, making powder shaping more difficult. "Coarse grains" >1 µm, as well as deviant particle morphologies, usually are not destroyed during powder processing to generate the sintering admixture. Powder processing has to guarantee that agglomerates of primary crystallites, which are principally present, are broken

apart, because their size and the lack of sintering additives in their cores would induce very large defects and thus limit the strength and reliability of the sintered component. Furthermore, the size and hardness of these agglomerates determine the dispersibility and homogeneity of the sintering admixture; these properties are very important quality criteria. A qualitative and quantitative description of agglomeration mechanisms and agglomerate properties is steadily gaining importance as a goal of research.[172] The shape-sharp-edged to spheroidal/globular-and the size distribution of primary crystallites also determine the limits of densification and the extent of sintering shrinkage. Green densities (i. e., the densities of the powder-shaped bodies prior to sintering) must be as high as possible to reduce the danger of critical tensions due to high shrinkage; these tensions would otherwise form cracks and fissures during the temperature treatment. Physical, chemical, and technological powder properties have a complex effect on the sintering behavior, structural development, and final material properties. The relative effect of a single powder property may be estimated by the means of statistical calculations.[167,171]

1.7.2 Powder shaping

Axial or isostatic dry pressing, extrusion, slip casting, or injection molding are used for powder shaping (Fig. 21). These procedures are well known in the ceramic industry. Selection criteria depend on the component complexity, economics, and, feasibility of large-scale production. Dry pressing is used mainly for the production of components with simple geometry such as plates, tubes, or cylinders. Slip casting and injection molding are favored to produce net-shape components of

complex geometry on a large scale. All shaping techniques require certain, usually organic, processing additives. Binders ensure the stability of powder compacts in dry pressing, and dispersion agents produce highly particle-loaded, stable slips for slip casting, and plasticizers allowing injection molding. Because especially injection molding promises an economical, large-scale production of complex components, its development has attracted worldwide attention.[176–178] All organic additives have to be burned out quickly and quantitatively prior to sintering without inducing defects such as pores, cracks, or fissures. Because of high amount of plasticizers, usually ~10–25 wt%, this step is especially critical in injection molding. Although shaping is finished in a few seconds, plasticizer burnout requires several hours to several days depending on the component thickness and type of plasticizer. To improve this situation, the development of new organic plasticizer systems, which may be decomposed either chemically or thermally after powder shaping, is of fundamental importance.

1.7.3 Sintering

The sintering techniques used for the manufacturing of Si_3N_4 ceramics are compiled in Fig. 22 together with the process characteristics. Axial hot pressing in graphite matrices is used almost only for the components of relatively simple geometry such as rods, plates, or cylinders. Hot isostatic pressing (HIP), however, allows sintering of complex component.[179] Powder compacts are sealed gas-tight in metals or glasses of high melting point; plastic deformation of the softening material of the capsule results in uniform application of the external gas pressure on the powder compact. Densification occurs with very precise retention of shape.

After complete sintering, the capsule is removed mechanically (sandblasting) or chemically (etching). Thus, this so called capsule-hipping is an expensive and slow procedure not suited for low-cost mass production of ceramic components. Usually, it is applied for the production of components, which are used under extreme conditions and would otherwise require an even greater effort for production.[180] However, "hipping" allows the manufacturing of Si_3N_4 sintered materials with very good high-temperature properties owing to only very small amount-or even absence-of an amorphous grain-boundary phase.[181,182] These developments, to date on laboratory scale, may gain importance for the manufacturing of Si_3N_4 components, showing long-term mechanical strength at high temperatures. Cost-efficient mass production of near-finished Si_3N_4 components is possible by N_2 gas-pressure sintering, which was developed during the seventies and is meanwhile industrially employed.[149] In this process, a powder compact is heated to sintering temperature in a powder bed consisting of Si_3N_4 and BN. The course of temperature and pressure has to be adjusted based on the furnace geometry, sintering additives, and powder compact geometry. Sintering under normal pressure limits the maximum temperature to ~1820 °C owing to the decomposition of $S_{i3}N_4$. However, sintering at increased N_2 pressure allows a further temperature increase and results in a pressure-assisted densification, which is effective only if the stage of closed porosity, >93% of theoretical density, was reached by normal pressure sintering. This method shortens the overall time required for complete densification and has a limited ability to increase the strength and reliability of Si_3N_4-sintered components because of some defect healing.

1.8 Physical and Chemical Properties

1.8.1 Physical Properties

The scattering range of the data is mainly due to structural differences, which are affected by starting powder characteristics, amount and type of sintering additives, powder shaping, and sintering techniques as well as temperature, pressure, and soaking time during sintering. Fracture strength is surely the characteristic property determined most often; usually it is considered as a key criterion of quality. Some years ago, a significant dependence of material properties on the method of producing the starting powder was observed.[187] However, these differences almost vanished as a result of constant efforts to improve Si_3N_4 powder quality and production methods. The effect of sintering techniques on the material properties is reflected in the so-called Weibull modulus (a statistical parameter to characterize the property distribution over a manifold of samples) used to characterize the scattering of fracture strength and thus the reliability of the material. The (limited) ability of a particular sintering process to anneal defects such as pores, bubbles, internal cracks, and fissures is thereby quantified to a certain extent. The following values are typical for the Weibull modull of commercial materials: pressureless sintered Si_3N_4 > 10; gas-pressure-sintered Si_3N_4 (GP-SSN) > 15; isostatically hot-pressed Si_3N_4 (HIP-SSN), > 20. A general comparison of the fracture strength is difficult, because materials for specialized applications have been developed. Here, the main criteria of quality not only include the fracture strength, but also the strength level at temperatures >1000 °C, fracture toughness, and hardness or wear resistance. Today, the state of the art is a strength level in the range 800–1000 MPa at room temperature; however, materials with the fracture strengths exceeding 1000

MPa have been developed. By controlled structural development (*in situ* nanowire reinforcement), it is possible to increase the fracture toughness of Si_3N_4 materials from a level of ~7 MPa $m^{1/2}$ to almost 10 MPa $m^{1/2}$.[190] A conventional material is compared to an "*in situ* nanowire reinforced" material. The toughness level attained here could formerly be achieved only by reinforcement with extraneous particles (such as nanowires or platelets).[192,193] At temperatures exceeding 1000 °C, a decrease in the strength of many materials is caused by slowly softening amorphous grain-boundary glass phases. The amount and type of these phases determine creep and long-time fracture strength. All the modifications of materials or technological processes to inscribe prove the dependence of the fracture strength on temperature and to improve the strength level at high temperatures aiming at reducing the amounts of amorphous grain-boundary glass phases or at generating higher refractory, crystallized grain boundary phases together with the optimization of structure. Recently, a successful realization of these concepts has been reported.[189] An evaluation of a commercially available MgO-doped material is given in Fig. 23.[194] Here, the failure probability resulting from the Weibull analysis is in the range of linear elastic stress up to 900 °C, and probable reasons for positive or negative deviations caused by defect annealing or defect induction is shown. Fig. 23 also shows the life expectancy of the material below short-time fracture load. To avoid premature failure at a given temperature, the material should bear only considerably lower mechanical stresses than short time fracture strengths would indicate.

1.8.2 Chemical Properties

Owing to the broad possible applications of sintered Si_3N_4, its chemical properties have been investigated with special regard to corrosive behavior.[195–198] Silicon nitride is inert to numerous molten metals (e. g., Al, Zn, Sn, Pb, Cu, Ag, and Cd); however, in contact with molten transition metals such as Fe, Co, Ni, V, and Cr, it reacts readily to form metal silicides and N_2. In contract with molten salts, oxidic slags, and glasses, only slow corrosion occurs. With the exception of hydrofluoric acid, Si_3N_4 ceramics are resistant to mineral acids. Mainly porous Si_3N_4 materials are attacked by hot strong caustic solutions or melts with the formation of NH_3. For the applications in engine components made of Si_3N_4 (e. g., valves, turbocharger, gas turbines), the oxidation behavior of sintered Si_3N_4 is especially important. Because Si_3N_4 is coated with a thin protective layer of SiO_2 on heating in air, a good oxidation resistance is shown up to 1400 °C. In high-temperature oxidation, two fundamentally different mechanisms of damage were observed.[196] The first mechanism is based on the diffusion of sintering additives and impurities along the grain boundaries owing to the higher oxygen potential at the surface of the material. Reaction with SiO_2 at the surface forms oxidic glass phases of low viscosity, which induce enhanced corrosion accompanied by N_2 formation. N_2 pores and modification change the grain-boundary phases leading to different thermal expansion coefficients between glass phase and matrix material induce defects, which lower the fracture strength of the material. A second mechanism will lead to complete destruction, if crystalline phase is formed during sintering depending on sintering additives and are readily oxidized with concomitant volume expansion. Internal stress may build up so strongly that the sintered component is completely destroyed in a short time. This phenomenon has been observed primarily in some

ternary Y–Si–O–N and Ce–Si–O–N phases.[199] A suitable selection of sintering additives, the use of high-purity starting powders, and a reduction in the additive and oxygen content are important for the development of high-temperature oxidation-resistant sintered Si_3N_4 materials.

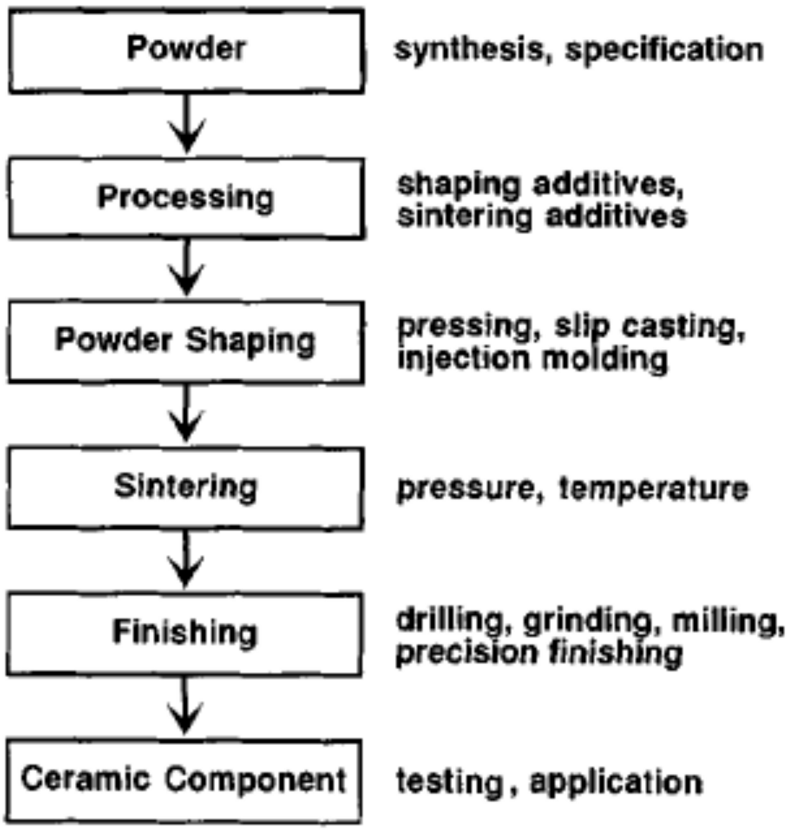

Fig. 1-1. Manufacturing process

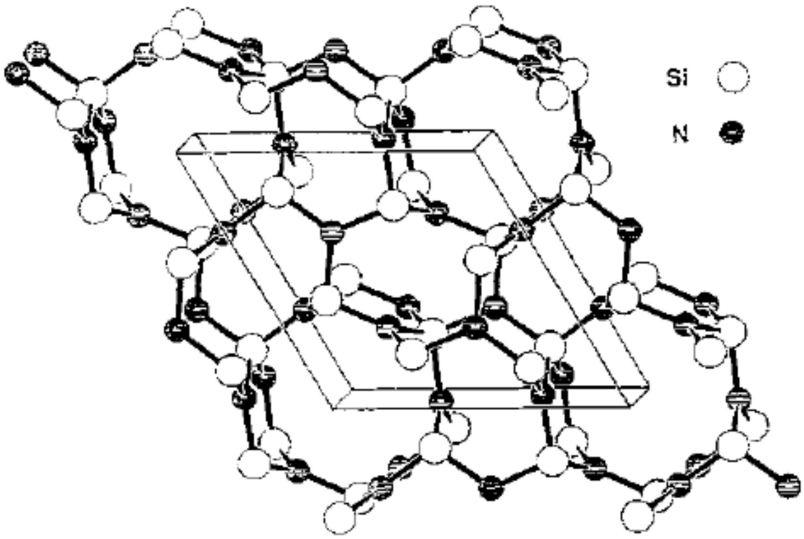

Fig. 1-2. Crystal structure of β-Si3N4

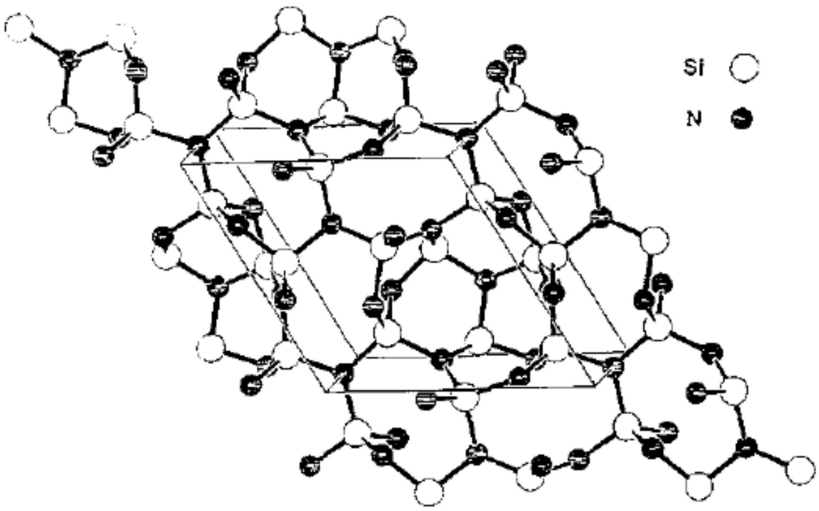

Fig. 1-3. Crystal structure of α-Si3N4

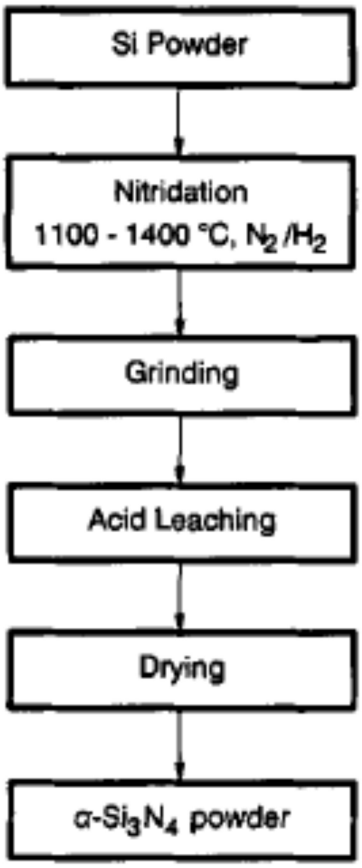

Fig. 1-4. Process for Si3N4 synthesis by direct nitridation

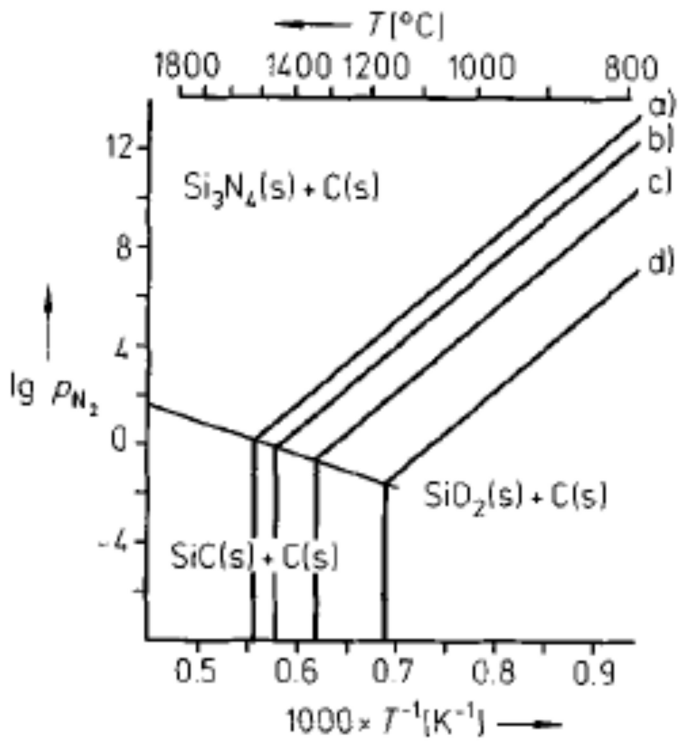

Fig. 1-5. Stability diagram for the system SiC/Si3M4/SiO2/C under varying CO partial pressures [106].

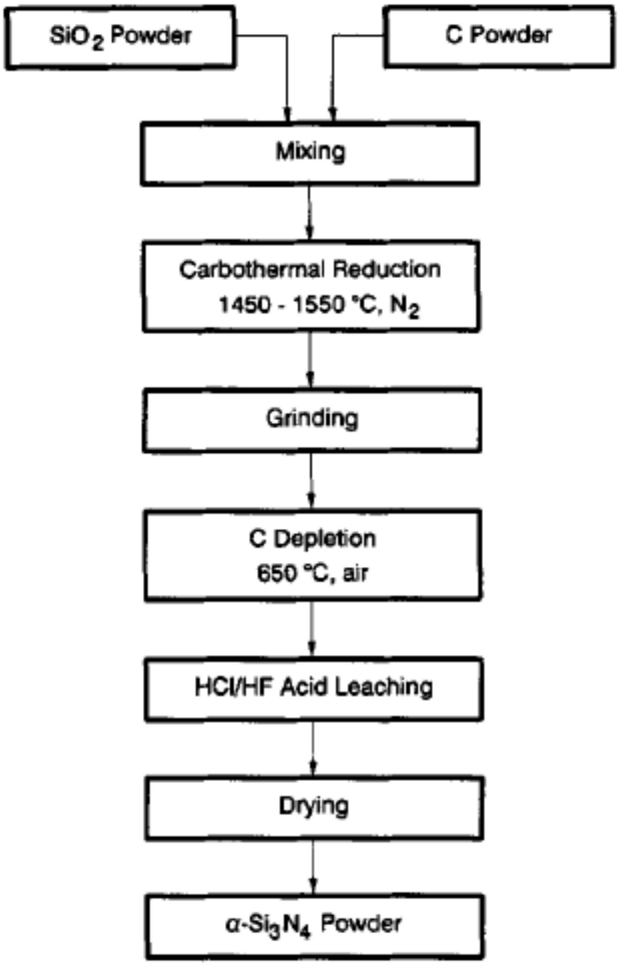

Fig. 1-6. Process for Si3N4 synthesis by carbothermal reduction

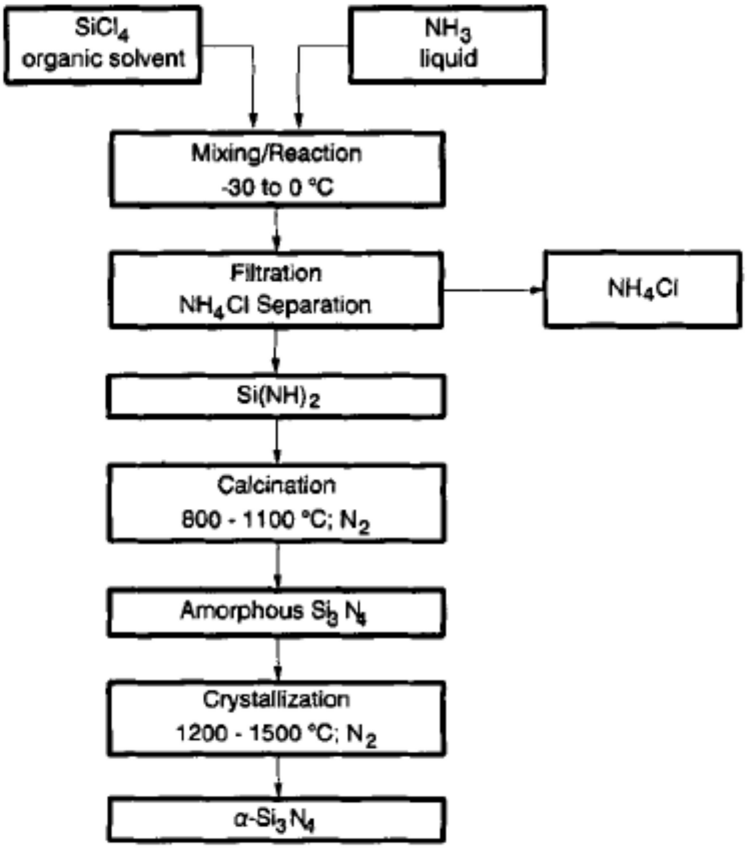

Fig. 1-7. Process for Si3N4 synthesis by SiCl4/NH3 liquid-phase reaction

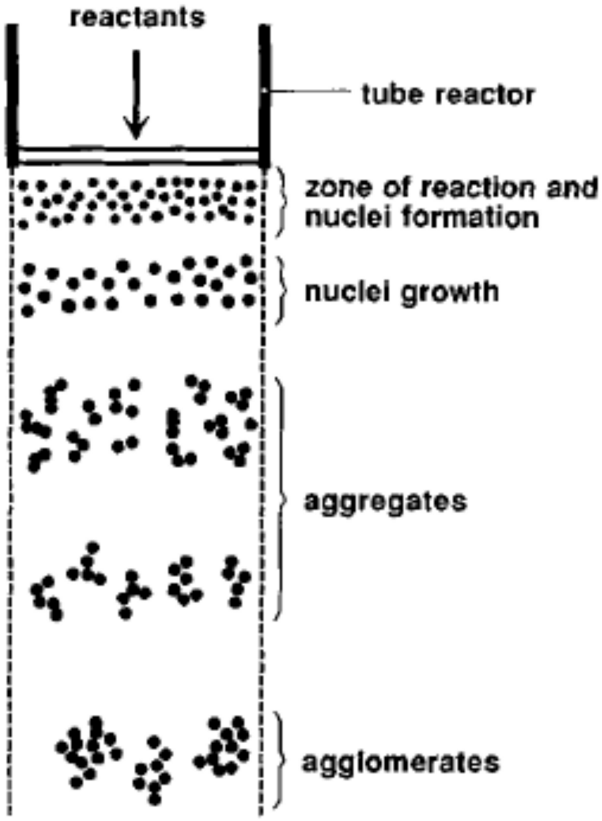

Fig. 1-8. Particle formation in gas-phase reaction [123]

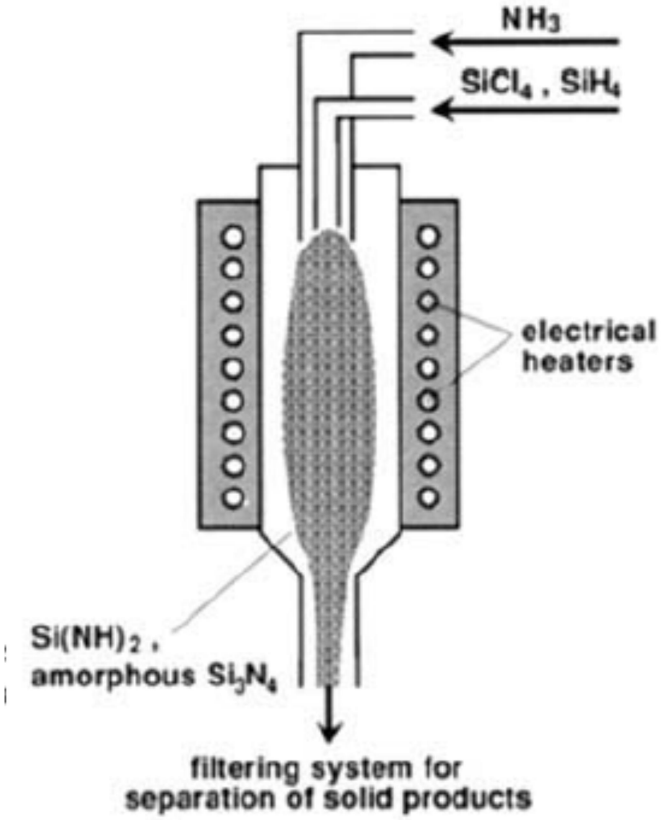

Fig. 1-9. Set-up of a gas-phase reactor for the synthesis of Si3N4 from SiCl4 and NH3

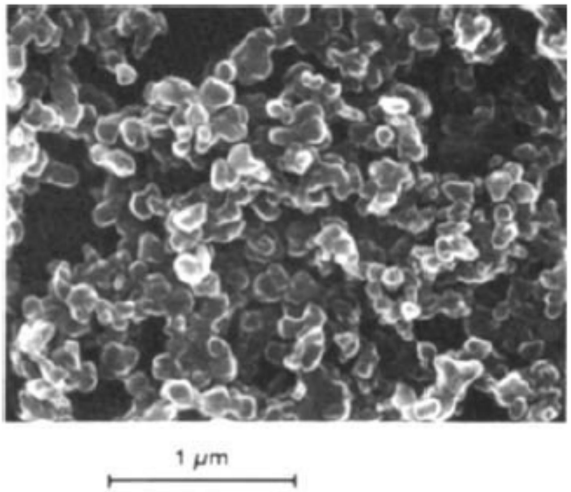

Fig. 1-10. α-Si3N4 powder by crystallization of amorphous Si3N4 from SiCl4/NH3 gas-phase reaction

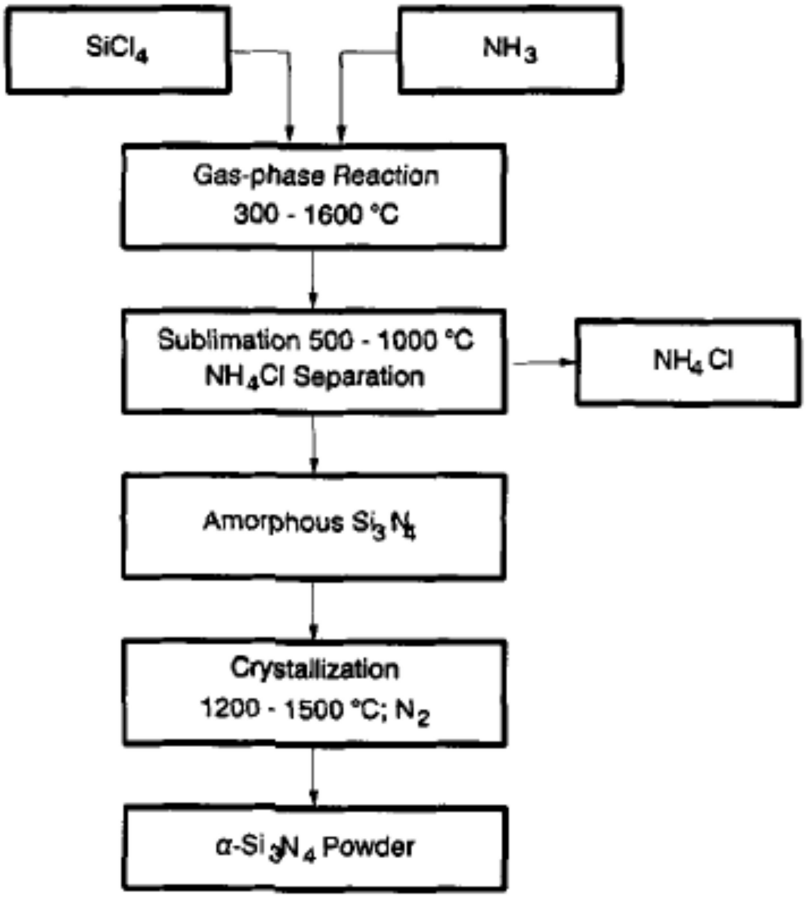

Fig. 1-11. Process for Si3N4 synthesis by SiCl4/NH3 gas-phase reaction

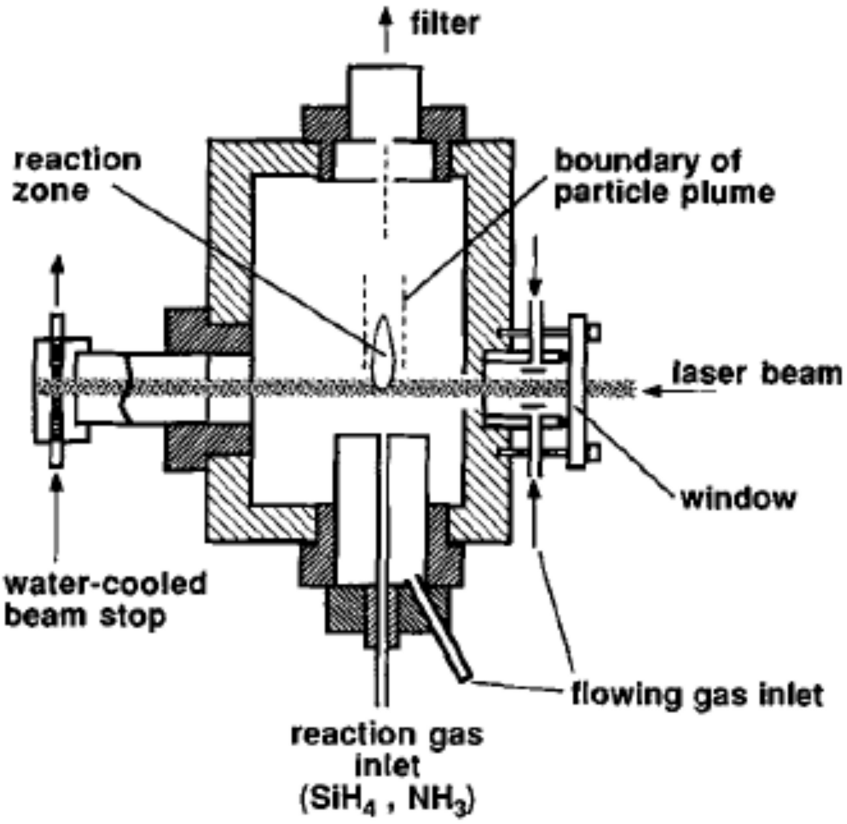

Fig. 1-12. Reactor for laser-induced Si3N4 synthesis from SiH4 and NH3 [126]

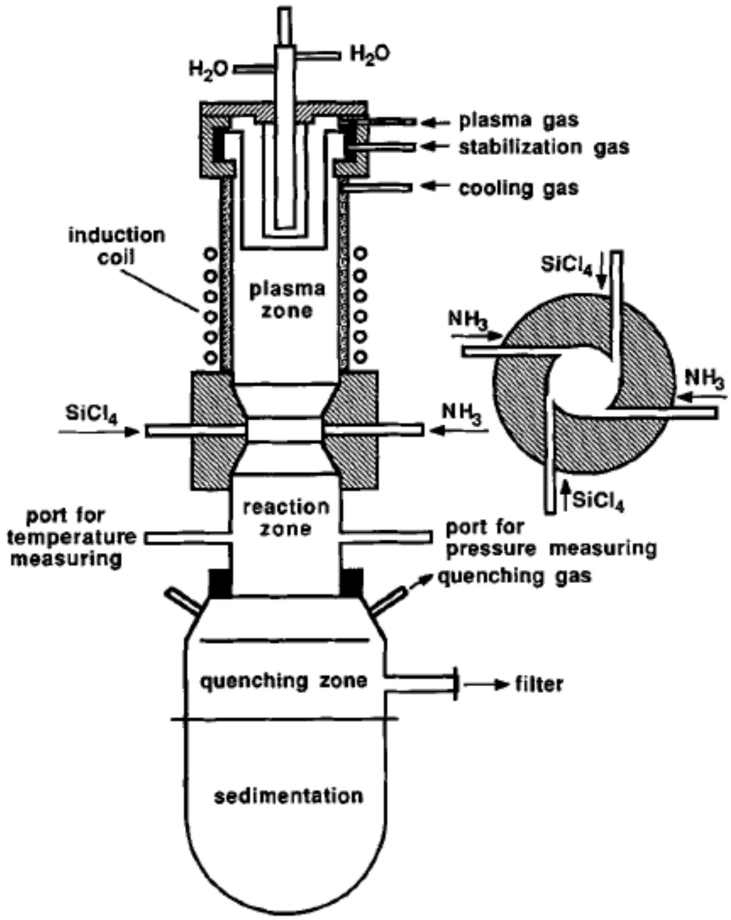

Fig. 1-13. Reactor for plasma chemical synthesis of Si3N4 from SiCl4 and NH3

[133]

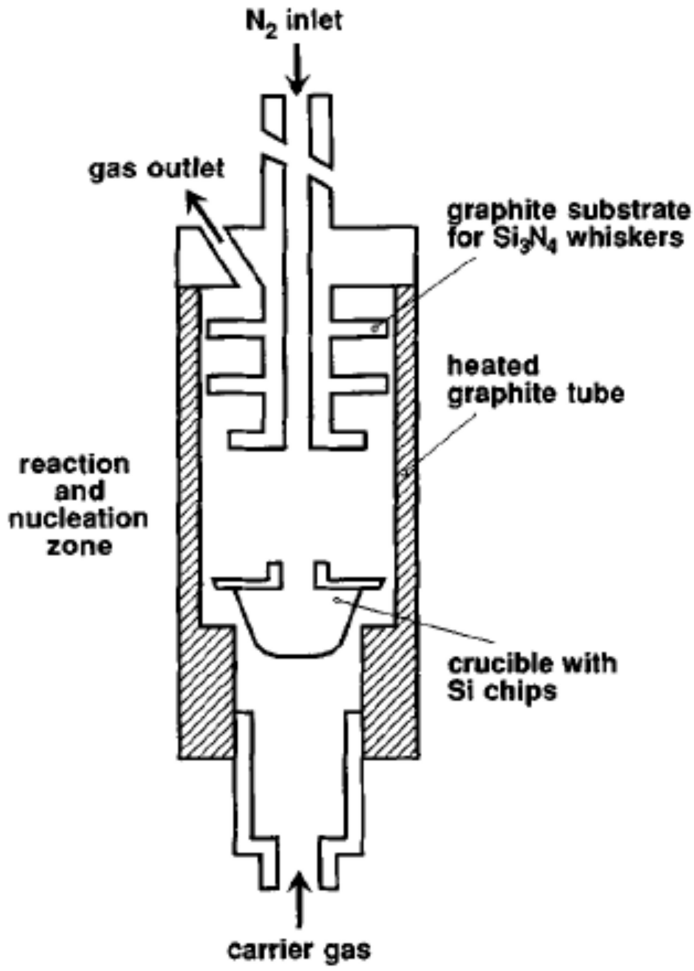

Fig. 1-14. Reactor for Si3N4 whisker synthesis from a Si/N2 gas-phase reactor

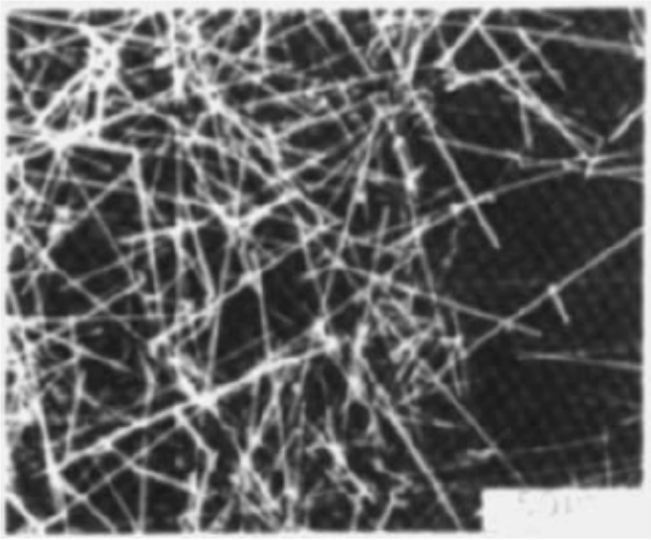

Fig. 1-15. α-Si3N4 whisker by crystallization of amorphous Si3N4 [72]

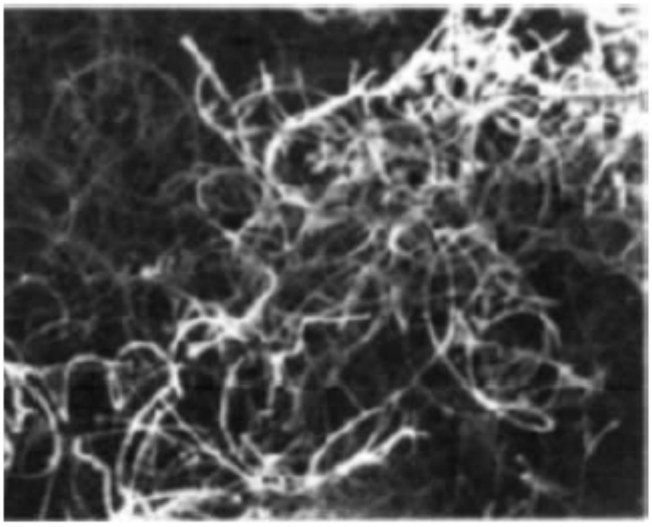

Fig. 1-16. Amorphous Si3N4 “spaghetti” from thermal decomposition of (Si-S-N-H)x polymers [74]

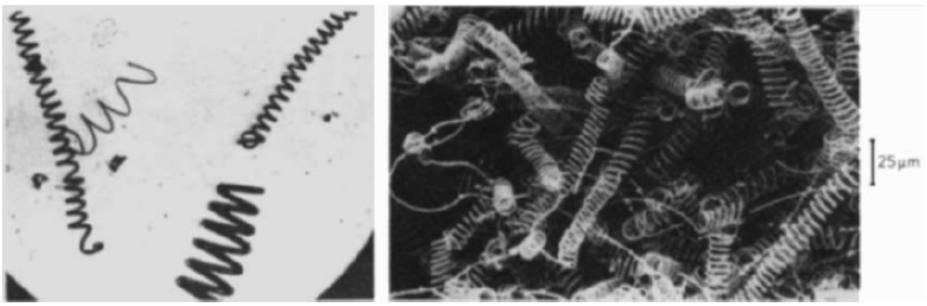

Fig. 1-17. Left: α-Si3N4 spirals from the reaction of SiC and NH3 in presense of Fe [76]. Right: α-Si3N4 spirals by vapor-phase deposition from a mixture of Si2Cl6, NH3, and H2 onto a Fe-coated graphite substrate [144]

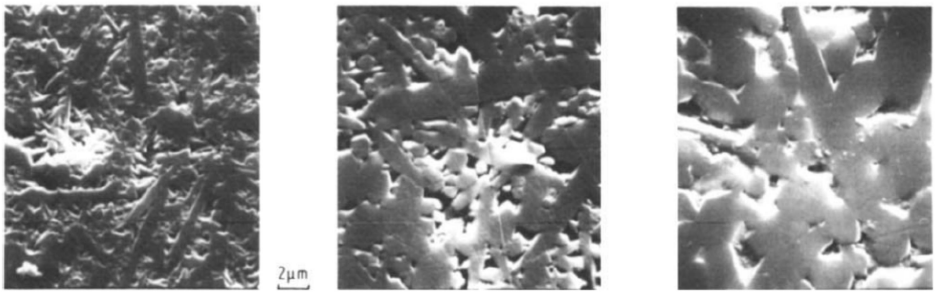

Fig. 1-18. Structure development in sintering of a Y2O3/Al2O3-doped Si3N4 powder [158]. Left: 1800°C (10min), Middle: 1800°C (2h), then 1820°C (2h), Right: 50 sintering cycles (see middle for conditions). Additives: 15wt% Y2O3+3.4wt% Al2O3

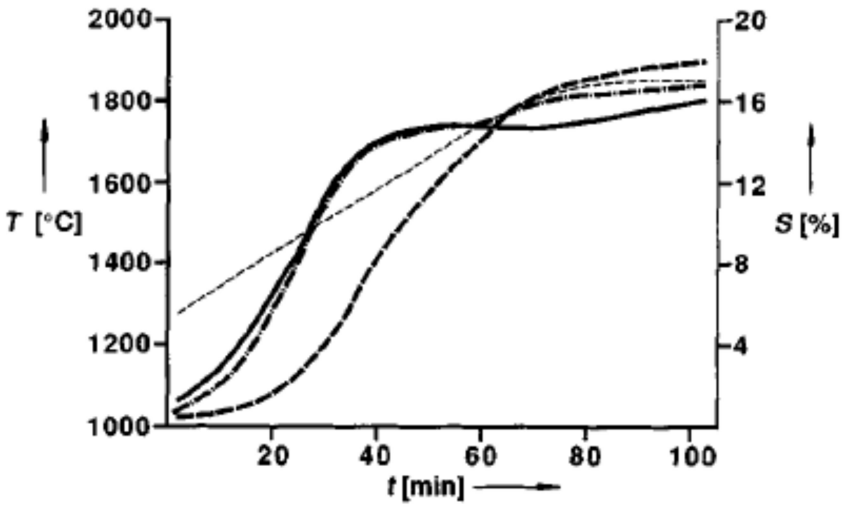

Fig. 1-19. Influence of type of additives on sintering behavior

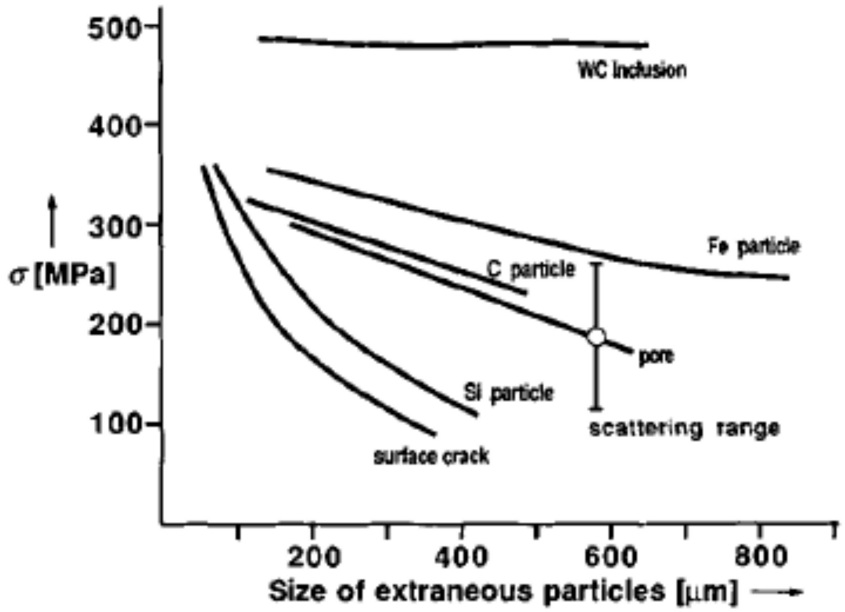

Fig. 1-20. Dependence of fracture stress σ on size of extraneous particle in Si3N4 sintered ceramics [171]

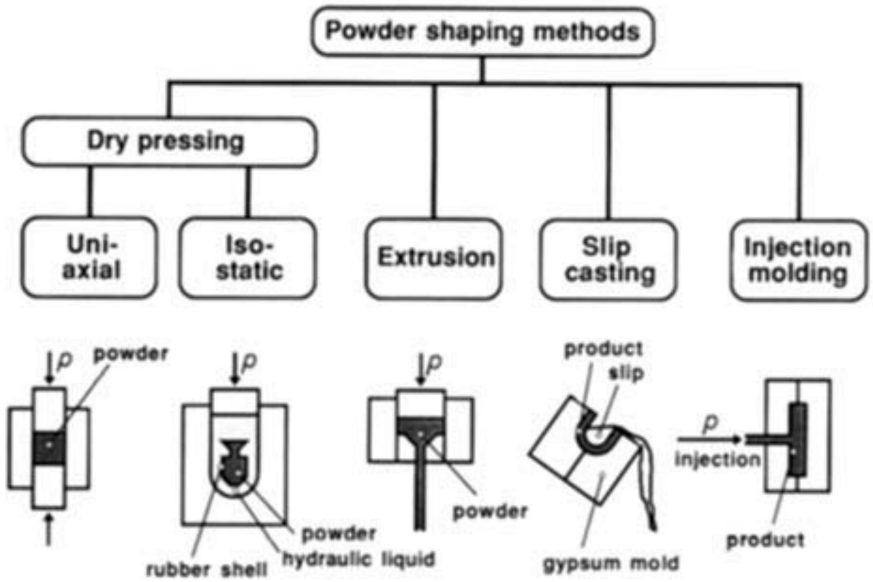

Fig. 1-21. Ceramic powder shaping methods

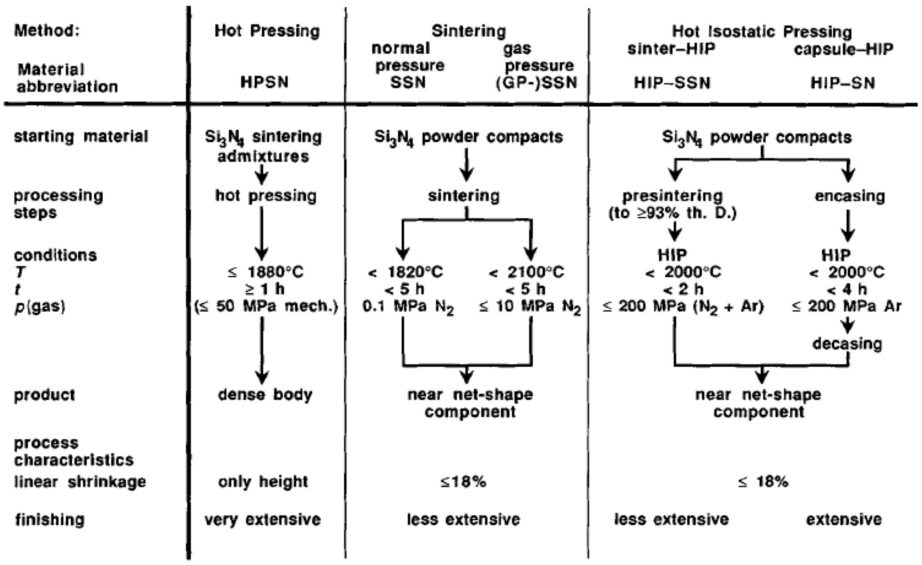

Fig. 1-22. Sintering process for the manufacturing of dense Si3N4 components

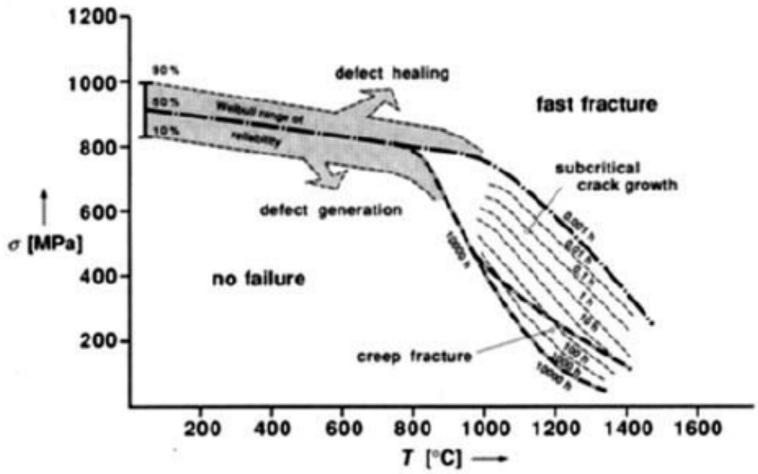

Fig. 1-23. Fracture strength of hot-pressed. MgO-doped Si3N4 as a function of temperature and time [164]

Reference

[1] H. Sainte-Claire Deville, F. Wohler, Ann. Chem. Pharm. 34 (1859) 248.

[2] DRP 236342 (1909); Zus.-Pat. 236892 (1909); 2us.-Pat. 241 510 (1909), BASF

[3] G. L. Williams, H. W. Campbell, US 1379668 (1918).

[4] H. Mehner, DRP 88999 (1899).

[5] A. S . Larsen, 0. J. Storm, DRP 229638 (1909).

[6] BE 13 091 (1913), Societe Generale des Nitrures.

[7] A. R. Lindblad, US 1311 568 (1918).

[8] A. S . Larsen, 0. J. Storm, DRP 231 090 (1910).

[9] DRP 234129 (1909), BASE

[10] F. von Bichowsky, US 1415280 (1921).

[11] DRP 237436 (1909), BASF.

[12] E. M. Leqoe, R. N. Katz, J. J. Burke: Ceramics /or High Performance App1icatio.t~II I, Plenum, New York 1979.

[13] F. L. Riley, Sprechsaal 118 (1985) 225.

[14] W. Bunk, M. BBhmer, H. KiDler : Keramische Komponentenfur Fahrzeug-gusturbinen 11, Springer, Berlin 1984.

[15] P. Walzer, M. Langer, Motortech. 2. 44 (1983) 1.

[16] M. Taguchi, Adv. Ceram. Marer. 2 (1987) 754.

[17] E. Gugel, Keram. Z. 39 (1987) 698.

[18] K. H. Jack, Endeavour 11 (1987) 80.

[19] F. Thummler, G. Grathwohl, Keram. Z. 40 (1988) 157.

[20] D. Fingerle, M. Fripan, U. Dworak, ZWFZ. wirtsch. Fertigung82(1987)392.

[21] J. Heinrich, J. Huber, P. Stingl, ZWFZ. wirtsch. Fertigung 82 (1987) 487.

[22] H. Knoch, K. Hunold, Tech. Mitt. 80 (1987) 31.

[23] D. Steinmann, Chem. Anlagen + Verjahren, 1988, 11.

[24] K. Uppenbrock, Sprechsaall21(1988) 135; ibid. 121 (1988)494; ibid. 122

[25] G. Ziegler, J. Heinrich, G. Wotting, J. Muter. Sci. 22 (1987) 3041.

[26] C. Boberski, R. Hamminger, M. Peuckert, F. Aldinger, R. Dillinger, J Heinrich, J. Huber, Angew. Chem. Adv. Muter. 10f (1989) 1592; Aagew. Chem. Int. Ed. Engl. 28 (1989) 1560; Adv. Muter. 1989, 378. BASE App1icatio.t~II I, Plenum, New York 1979. gusturbinen 11, Springer, Berlin 1984. 392. (1989) 232.

[27] A. J. Moulson, J. Mater. Sci. 14 (1979) 1017.

[28] L. Michalowsky, A. Rendtel, Silikattechnik 38 (1987) 78.

[29] M. E. Washburn, W S. Coblenz, Am. Cerum. SOC. Bull. 67 (1988) 356.

[30] H.-J. Kleebe, Dissertation, Universitat Koln (1988).

[31] H. Schubert, Fortschrittsber. der Dtsch. Kerum. Ges. 5 (1990) 29.

[32] J. R. Alcock, F. L. Riley, J. Eur. Ceram. SOC. 6 (1990) 339.

[33] G. Bandyopadhyay, F. M. Mahoney, D. L. Sordelet, K. French in V. J. Tennery (Ed.): Ceramic Materials and Components /or Engines, Am. Ceram. SOC. (1989), p. 1397.

[34] J. T. Neil, A. E. Pasto, L. J. Bowen, Adv. Cerum. Muter. 3 (1988) 225.

[35] F. Aldinger, H.-J. Kaltz. Angew. Chem. 99 (1987) 381; Angew. Chem. Int. Ed. Engl. 26 (1987) 371.

[36] S. N. Ruddlesden, P. Popper, Acta Crystallogr. 11 (1958) 465.

[37] S. Wild, P. Grieveson, K. H. Jack, Spec. Cerum. 5 (1972) 385.

[38] R. Grun, Acta Crystallogr. Sect. B35 (1979) 800.

[39] K. Kato, Z. Inoue, K. Kijima, I. Kawada, H. Tanaka, T. Yamane, J. Am. Ceram. Soc. 58 (1975) 90.

[40] D. H. Hardie, K. H. Jack, Nature 180 (1957) 323.

[41] K. Blegen, Spec. Ceram. 6 (1975) 223.

[42] K. H. Jack in F. L. Riley (Ed.): Progress in Nitrogen Ceramics, Nijhoff, Leyden 1977, p. 45.

[43] US 1937792 (1976), Lucas Jnd. Ltd.

[44] H. Haag, W. D. Glaser, B. Krismer in F, L. Riley (Ed.): Progress in Nitrogen Ceramics, Nijhoff, Leyden 1977, p. 315ff.

[45] I. Kohatsu, J. W. McCauley, Mater. Res. Bull. 9 (1974) 917.

[46] K. Kijima, N. Setaka, H. Tanaka, J. Cryst. Growth 24/25 (1974) 183.

[47] H. F. Priest, F. C. Burns, G. L. Priest, E. C. Skaar, J. Am. Ceram. SOC. 56 (1973) 395.

[48] C. P. Gazzara, D. R. Messier, Am. Ceram. SOC. Bull. 56 (1977) 777.

[49] K. Suzuki, Y Kano, Yogyo Kyokaishi 92 (1984) 101.

[50] J. P. Luongo, J. Electrochem. Soc. 130 (1983) 1560.

[51] R. A. Andrievskii, M. A. Leontev, Inorg. Muter. 20 (1984) 1786.

[52] T. K. Trout, J. M. Bellama, F. E. Brinckman, R. A. Faltynek, J. Mater. Res. 4 (1989) 399.

[53] G. R. Hatfield, K. R. Carduner, J. Mater. Sci. 24 (1989) 4209.

[54] K. R. Carduner, R. 0. Carter, M. E. Milberg, G. M. Crosbie, Anal. Chem. 59 (1987) 2794.

[55] K. R. Carduner, C. S. Blackwell, W. B. Hammond, F. Reidinger, G. R. Ed. Engl. 26 (1987) 371. Ceram. Soc. 58 (1975) 90. Leyden 1977, p. 45. Nitrogen

Ceramics, Nijhoff, Leyden 1977, p. 315ff. (1973) 395. Res. 4 (1989) 399. Chem. 59 (1987) 2794. Hatfield, J. Am. Chem. SOC.1 12 (1990) 4676.

[56] R. Dupree, M. H. Lewis, G. Leng-Ward, D. S. Williams, J. Muter. Sci. Lett. 4 (1985) 393.

[57] K. R. Carduner, R. 0. Carter, M. J. Kokosz, C. Peters, G. Crosbie, E. D. Stiles, Chem. Mater. i(1989) 302.

[58] G. Schwier, G. Nietfeld, Werksto/fe and Konsrruktion 2 (1988) 149.

[59] G. Schwier, G. Nietfeld, Sprechsaal 121 (1988) 174.

[60] G. Boden, S. Klemm, K. Quaritsch, Silikatrechiiik 38 (1987) 161.

[61] G. Boden, R. Irmisch, G. Himpel, T. Reetz, Sprechsaal 122 (1989) 224.

[62] Y Tuohino, R. Laitinen, K. Torkell in G. L. Messing, S. Hirano, H. Hausner (Ed.): Proc. 3rd Int. Con/. Powder Processing Sci., Am. Ceram. SOC. 1990, p. 337. Lett. 4 (1985) 393. Stiles, Chem. Mater. (1989) 302.

[63] K. Komeya, H. Inoue, J. Muter. Sci. 10 (1975) 1243.

[64] H. Jnoue, K. Komeya, A. Tsuge, J. Am. Cerum. SQC. 65 (1982) 205.

[65] M. Mori, H. Jnoue, T. Chirai in F. L. Riley (Ed.): Progress in Nirrogen Ceramics, Nijhoff, Den Haag 1983, p. 149ff.

[66] T. Ishii, A. Sano, 1. Imai in S. Somiya, A. Mitomo, M. Yoshimura (Ed.): Silicon Nitride - f, Elsevier Appl. Sci., London 1990, p. 59 ff.

[67] M. Blix, W. Wirbelauer, Ber. Dtsch. Chem. Ges. 36 (1903) 4220.

[68] 0. Glemser, P. Naumann, 2. Anorg. AlIg. Chem. 298 (1959) 134.

[69] K. S. Mazdiyasni, C. M. Cooke, J. Am. Ceram. SOC. 56 (1973) 628.

[70] S. Prochazka. C. Greskovich, Am. Ceram. Soc. BUN. 57 (1978) 579.

[71] W. M. Shen, EP 365295 (1989), Union Carbide Corp.

[72] Y Kohtoku in S. Somiya, M. Nitomo, M. Yoshimura (Eds.): Silicon Nitride - 1, Elsevier Appl. Sci., London 1989, p. 71 ff.

[73] P. E. D. Morgan, US. Dept. o/Energy, DOE-Report 83-004283 (1983).

[74] P. E. D. Morgan, E. A. Pugar, J. Am. Ceram. Soc. 68 (1985) 699.

[75] P. E. D. Morgan, US 4552740 (1985).

[76] 0. Glemser, H.G. Horn, Naturwissenschaften 49 (1962) 538.

[77] M. Hoch, K. Nair, Bull Am. Cerum. SOC. 58 (1979) 187.

[78] K. Komeya, H. Inoue, J. Maw. Sci. 10 (1975) 1243.

[79] M. Peockert, T. Vaahs, M. Bruck, Adv. Muter. 2 (1990) 398.

[80] L. Weiss, T. Engelhardt, 2. Anorg. Chem. 65 (1910) 38.

[81] A. Atkinson, A. J. Moulson, E. W. Roberts, J. Am. Ceram. SOC5.9 (1976)

[82] H. M. Jennings, J. Muter. Sci. 18 (1983) 951.

[83] R. Pompe, L. Hermansson, T. Johansson, E. Djurle, D. E. Hatcher, Mater. Sci. Eng. 71 (1985), 355.

[84] M. Mitomo, J. Marer. Sci. 12 (1977) 273.

[85] H. M. Jennings, B. J. Dalgleish, P. L. Pratt, J. Marer. Sci. 23 (1988) 2573.

[86] J. A. Mangels, Am. Ceram. SOC. Bull. 60 (1981) 613.

[87] A. G. Merzhanov. P. Borovinskaja, Dokl. Akad. Nauk SSSR 204 (1972)

[88] V. Hlavacek, Am. Ceram. SOC. Bull. 70 (1991) 240.

[89] Z. A. Munir, J. B. Holt, J. Mater. Sci. 22 (1987) 710.

[90] A. G. Merzhanov, Adv. Muter. 2 (1990) 570.

[91] K. Hirao, Y Miyamoto, M. Koizumi, J. Am. Ceram. SOC6. 9 (1986) C60.

[92] A. S. Muskasyan, V. M. Martynenko, A. G. Merzhanov, I. P. Borovin- skaya, M. Yu. Blinov, Fiz. Goreniya Vzryva 22 (1986) 43.

[93] K. Hirao, Y Miyamoto, M. Koizumi, Adv. Ceram. Mater. 2 (1987) 780.

[94] S. Kumar, J. A. Puszinski, V. Hlavacek in Z. A. Munir, J. B. Holt (Ed.):Combustion and Plasma Synthesis of High Temperature Materials, VCH Publishers, New York 1990.

[95] J. Lis, S. Majovrowski, J. A. Puszynski, V. Hlavacek, Am. Ceram. SOC. Bull. 70 (1991) 244.

[96] M. Shimada, T. Okamoto, M. Koizumi, Mem. Inst. Sci. Ind. Res., Osaka Univ. 41 (1984) 1.

[97] T. Nishioka, M. Myake, H. Matsumoto, M. Higuchi, JP 6389459 (1988).

[98] E. Friedrich, L. Sittig, Z. Anorg. A&. Chem. 143 (1925) 293.

[99] A. Szweda, A. Henry, K. H. Jack, Proc. Br. Ceram. SOC. 31 (1981) 107.

[100] M. Mitomo, Y Yoshioka, Adv. Ceram. Mater. 2 (1987) 253.

[101] Y Sugahara, J. Miyamoto, K. Kuoda, C. Kato, Appl. Clay Sci. 4 (1989) 11.

[102] S. J. P. Durham, K. Shanker, R. L. Drew in H. Hausner, G. L. Messing, S . Hirano (Ed.): Proc. 2nd Int. Powder Process. Sci. Conf, Deutsche Keramische Gesellschaft, Cologne 1988, p. 31 3ff. Ceramics, Nijhoff, Den Haag 1983, p. 149. Silicon Nitride -1, Elsevier, London 1990, p. 59-285.

[103] A. Hendry, K. H. Jack, Spec. Ceram. 6 (1975) 199.

[104] K. Shanker, S. Grenier, R. A. L. Drew in G. L. Messing, S . Hirano, H. Hausner (Ed.): Proc. 3rd Int. Powder Process. Sci. Conf. Am. Ceram. SOC. 1990, p. 329.

[105] W Krumbe, B. Laubach, G. Franz, EP 362605 (1989), Bayer AG.

[106] A. Yamaguchi, Refractories 38 (1986) 2. Engl. Transl., Tokyo 1986.

[107] W Krumbe, B. Laubach, G. Franz, EP 237680 (1990), Bayer AG.

[108] L. Schonfelder, G. Franz, U. Wickel, G. Wotting, Sci. Ceram. 14 (1988)

[109] M. Persoz, Ann. Chim. Phys. 44 (1830) 315.

[110] F. Lengfeld, Am. Chem. J. 21 (1899) 52.1.

[111] E. Vigoureux, C. R. Hugot, Hebd. Seances Acad. Sci. 136 (1903) 1670.

[112] M. Billy, Ann. Chim. 4 (1959) 795.

[113] D. L. Segal, Trans. J. Br. Ceram. SOC8. 5 (1986) 184.

[114] 0. Glemser, K. Beltz, P. Naumann, Z. Anorg. A&. Chem. 291 (1957) 51.

[115] M. Billy, M. Brossard, J. Desmaison, D. Giraud, P. Goersat, J. Am. Ceram. Soc. 58 (1975) 254.

[116] US 4196178 (1980), Ube Industries.

[117] T. Yamada, T. Kawahito, T. Luai in S . Somiya, E. Kanai, K. Ando (Ed.): Proc. 1st Int. Symp. Cerum. Components for Engines, KTK Scientific Publ., Tokyo 1984, p. 333.

[118] R. Riedel, M. Seher, J. Eur. Cerum. SOC. 7 (1991) 21.

[119] E. J. Jacquemij, P. J. van der Put, J. Schoonman, High Temp. High Pressures 20 (1988) 31.

[120] J. Hojo, H. Maeda, A. Kato, J. Cerum. SOC. Jpn. Int. Ed. 96 (1988) 820.

[121] Y. Kohtoku, T. Yamada, M. Migazaki, T. Iwai in W. Bunk, H. Hausner (Ed.): Proc. 2nd Int. Symp. Cerum. Comp. for Engines, Deutsche Keramische Gesellschaft 1986, p. 101

[122] G. M. Crosbie, R. L. Predmedsky, J. M. Nicholson, E. D. Stiles, Bull. Am. Cerum. SOC. 68 (1989) 1010.

[123] G. D. Ulrich, Chem. Eng. News 1984, 22.

[124] G. Franz, G. Schwier in Kursten: Proc. 5th Int. Symp. on Raw Muterids /or Nen Technologies, E. Schweizerbart'sche Verlagsbuchhandlung. Stuttgart 1990, p. 139.

[125] B. Laubach, G. Franz, U. Wickel, L. Schonfelder, DE 3536933 (1985). Bdyer AG.

[126] W. R. Cannon, S. C. Danforth, J. H. Flint, J. S. Haggerty, R. A. Marra, J. Am. Cerum. SOC. 65 (1982) 324.

[127] W. R. Cannon, S . C. Danforth, J. S. Haggerty, R. A. Marra, J. Am. Ceram. Soc. 65 (1982) 330.

[128] Y. Kizaki, T. Kandori, Y. Fujitami, Jpn. J. Appl. Phys. 24 (1985) 800.

[129] W. Ymons, K. J. Nilsen, S. C. Danforth in W. Bunk, H. Hausner: Proc. 2nd Int. Symp. Cerum. Muter. Comp. for Engines, Deutsche Keramische Gesellschaft, Cologne 1986, 20 (1988) 31.

[130] J. Canteloup, A. Mocellin, Proc. Br. Cerum. Soc. 6 (1975) 209.

[131] G. J. Vogt, C. M. Hollobaugh, D. E. Hull, L. R. Newkirk, J. J. Petrovic, U.S. Dept. of Energy, DOE-Report 84-003774 (1984).

[132] G. J. Vogt, R. S . Vigil, L. R. Newkirk, M. Tikula in C. J. Timmermans (Ed.): Proc. 7th Int. Symp. Plusmu Chem., Vol. i I , IUPAC 1985, p. 657ff.

[133] O. Schulz, H. Hausner, Elektrowuerme Int. Ed. 845 (1987) 174.

[134] N. Kubo, S. Futaki, K. Shiraishi in S. Somiya. M. Mitomo, M. Yoshimura: Silicon Nitride - f, Elsevier Appl. Sci., London, p. 93ff.

[135] C. Herring, J. K. Galt, Phys. Rev. 85 (1952) 1060.

[136] S. B. Hanna, F. E Abdel-Mohsen, Angew. Makromol. Chem. 133 (1985)

[137] H. Grewe, K. Dreyer, J. Kolaska, Ceram. Forum Intl., Ber. Dtsch. Kerum. Ges. 1987, 303.

[138] F. Pott, Zentrulbl. Bukteriol. Mikrobiol. Hyg. Abt. Orig. Bf84 (1987) 1 .

[139] Grimm, Zentrulbl. Arbeitsmed. Arbeitsschutz Prophyl. Ergon. 38 (Suppl. 1) (1988) 2.

[140] A. L. Cunningham, L. G. Davis, SAMPE J. 15 (1969) 120.

[141] R. C. Johnson, J. K. Alley, W. H. Warwick, R. H. Shell, US 3244480 (1966).

[142] M. Tanaka, T. Kawabe, JP 1324479 (1986).

[143] K. Niwdno in S . Somiya, M. Mitomo, M. Yoshimura (Eds.): Silicon Nitride - 1, Elsevier Appl. Sci., London 1989, p. 117ff.

[144] Techno Japan 22 (1979) 79.

[145] S. Motojima, H. Iwanaga, Kinroku 59 (1989) 47.

[146] G. Ziegler, Cerum. Forum lntl., Ber. Dtsch. Kerum. Ges. 68 (1991) 72.

[147] P. Greil, M. J. Hoffmann, K. L. Weisskopf, G. Petzow, Fortschrittsber. Dtsch. Kerum. Ges. 2 (1986/87) 27.

[148] G. R. Terwilliger, F. F. Langer, J. Muter. Sci. 10 (1975) 1169.

[149] S. Prochazka, C. D. Greskovich, U.S. Army Muter. and Mech. Res. Center Technical Report 78-32 [1978), SRD-77-178.

[150] J. T. Smith, C. L. Quackenbush in S . Somiya, S. Saito (Eds.): Proc. Int. Svmp. Factors in Densijkution and Sintering of Oxide and Nonoxide Ceramics, Hakone 1978, p. 426ff. ra: Silicon Nitride - f, Elsevier Appl. Sci., London, p. 93

[151] M. Mitomo, 1 Muter. Sci. 11 (1976) 1103.

[152] M. Mitomo in S. Somiya, M. Mitomo, M. Yoshimura (Eds.): Silicon Nitride - 1, Elsevier Appl. Sci., London 1990, p. 1 ff.

[153] G. Wotting, Dissertation, TU-Berlin 1983.

[154] G. Wotting, G. Ziegler in S. Somiya (Ed.): Proc. fst Int. Symp. Cerum. Comp. for Engins, KTK Scientific Publ., Tokio 1983, p. 412ff.

[155] F. F. Lange, J. Am. Cerum. SOC. 62 (1979) 428.

[156] G. Himsoldt, H. Knoch, H. Hubner, F. W. Kleislein, J. Am. Ceram. SOC. 62 (1979) 29.

[157] M. Mitomo, J. Am. Cerum. Soc. 73 (1990) 2441.

[158] G. Wotting, G. Ziegler, Fortschrittsber. Dtsch. Kerum. Ges. 1(1985) 33.

[159] D. R. Clarke in F. L. Riley (Ed.): Progress in Nitrogen Ceramics, Nijhoff, Leyden 1983, p. 341 ff.

[160] P. Greil, Sci. Cerum. 14 (1988) 645.

[161] S . Hampshire, Proc. Br. Cerum. Soc. 31 (1981) 37.

[162] K. H. Jack in F. L. Riley (Ed.): Progress in Nitrogen Ceramics, Nijhoff, Brighton 1981, p. 109ff.

[163] Z.-K. Huang, P. Greil, G. Petzow, J. Am. Cerum. Soc. Commun. 1983, C 69.

[164] V. K. Sarin, Mater. Sci. Eng. Af05/106 (1988) 151.

[165] G. Wotting, G. Ziegler, Powder Met. Int 18 (1984) 18.

[166] M. Peuckert, P. Greil, J. Muter. Sci. 22 (1987) 3717.

[167] G. Nietfeld, U. Wickel, G. Wotting in H. Hausner, G. L. Messing, S. Hirano (Ed.): Proc. 2ndint. Conf. Ceram. Powder Process. Sci., Deutsche Keramische Gesellschaft 1989, p. 795 ff.

[168] G. Nabert, G. Ziegler, WF-Kolloquium, Werkstoff-Kolloquim des Instituts fur Werkstoff-Forschung der Dtsch. Forschungsanstalt fur Luft- u.Raumfahrt (DLR), Koln, 1990. Leyden 1983, p. 341 ff. Brighton 1981, p. 109ff. C 69.

[169] H. Knoch, G. E. Gazza, .l Am. Cerum. SOC. 62 (1979) 634.

[170] J. T. Neil, A. E. Pasto, L. J. Bowen, Adv. Cerum. Mater. 3 (1988) 225.

[171] D. Munz, 0. Rosenfelder, K. Goebbels, H. Reiter in W. Bunk (Ed.): Kerumische Komponenten fur Fuhrreug-Gasturbinen I l l , Springer, Berlin 1984, p. 513.

[172] R. A. Bauer, R. van Weeren, P. J. van der Put, F. E. Kruis, B. Scarlett. J. Schoonman in G. L. Messing, H. Hausner, S. Hirano (Ed.): Proc. 3rdlnt. Con5 Ceram. Powder Process. Sci., Am. Ceram. SOC., Westerville 1990, p. 259ff.

[173] J.-S. Kim, H. Schubert, G. Petzow, J. Eur. Cerum. Soc. 1991, in press.

[174] M. Kulig, W. Oroschin, P. Greil, J. Eur. Ceram. SOC. 5 (1989) 209.

[175] R. de Jong, R. A. McCandey in G. de With, R. A. Terpstra, R. Metselaar (Ed.): Proc. 1st Eur. Cerum. SOC. (ECerS) Canf., Elsevier Appl. Sci., London 1989, p. 1150-1154.

[176] M. J. Edirisinghe, J. R. G. Evans, Int. J. High Tech. Cerum. 2 (1986) 249.

[177] S . J. Stedmeyer, J. R. G. Evans, J. Woodthorpe, Cerum. Int. 16(1990) 107.

[178] U. Becker, Kunststoffe 80 (1990) 575.

[179] B. Oberacker, A. Kuhne, F. Thummler, Powder Met. Int. 19 (1987) 43.

[180] K. Hunold, Ceram. Forum lntf., Ber. Dtsch. Keram. Ges. 60 (1983) 182.

[181] S. Kume, H. Yoshida, M. Machida, J. Cerum. Soc. Jpn. Int. Ed. 95 (1987) 205.

[182] I. Tanaka, G. Pezzotti, T. Okamoto, Y. Miyamoto, J. Am. Cerum. SOC. 72 (1989) 1656.

[183] W. Konig, M. Popp, J. Wemhoner in J. Kriegesmann (Ed.): Technische Kerumische Werkstofle, Deutscher Wirtschaftsdienst, Cologne 1989, Chapter 3.7.3.

[184] G. Spur, I. Subotka, T. H. Tio, U. E. Wunsch, FBM-Fertigungstechnologie 64 (1987) 31; ibid. 65 (1988) 28.

[185] E. Gugel, G. Leimer in W. Bunk (Ed.): Keramische Komponenten fir Fuhrzeugguscurbinen I l l , Springer, Berlin 1984, p. 133.

[186] K. D. Morgenthaler in W Bunk (Ed.): Kerumische Komponenten fir Fuhrreuggusrurbinen I l l , Springer, Berlin 1984, p. 389.

[187] G. Ziegler, J. Heinrich, G. Wotting, J. Muter. Sci. 22 (1990) 3041.

[188] K. Ueno, J. Cerum. Soc. Jpn. Int. Ed. 97 (1989) 80.

[189] K. Komeya, Proc. 7fh CIMTEC, Montecatini 1990, in press.

[190] Y. Tajima, K. Urashima, M. Watanabe, Y. Matsuo in G. L. Messing, F. Fuller, H. Hausner (Ed.): Ceramic Transactions 1, Am. Ceram. SOC., Westerville 1988, p. 1034.

[191] G. Wotting, G. Schwier, H. Lange in S . Hirano, H. Hausner, G. L. Messing: Proc. 4th Int. Conf. Ceram. Powder Process. Sci., Nagoya 1991, in press.

[192] P. D. Stralek, Am. Ceram. SOC. BUN. 65 (1986) 351.

[193] H. Kodama, T. Miyoshi, Cerum. Eng. Sci. Proc. 10 (1989) 1072.

[194] G. D. Quinn, J. Muter. Sci. 25 (1990) 4361.

[195] A. Rabenau, Ber. Dtsch. Keram. Ges. 40 (1963) 6.

[196] G. Wotting, G. Ziegler, Sprechsaalf23 (1990) 1102.

[197] H. Feld, E. Gugel, H. G. Nitzsche, Werkst. and Korrosion 1969, 671.

[198] R. E. Tressler, M. McNallun (Ed.): Proc. Symp. Corrosion and Corrosive Degradation of Ceramics, Am. Ceram. SOC., Westerville 1989. I1991 J. T. Smith, C. L. Quackenbush, Am. Cerum. Soc. Bull. 59 (1980) 529.

Chapter 2. Synthesis of Si_3N_4 Powder

2.1 Introduction

Silicon nitride has been used in various applications under extreme conditions, including component of valves in internal combustion engines, heat exchangers, cutting tools, and gas turbines [1–4], because of good chemical durability, low density, excellent hardness, and high mechanical strength at high temperature. The combination of thermal, dielectric, and superior high-temperature mechanical properties has led to the implementation of silicon nitride in electronic applications including electronic substrates, heat sinks, RF waveguides, windows, and radomes.[5] As an indispensable raw material used to prepare silicon-nitride-based ceramics, except for the reaction sintering method, the demands for silicon nitride powder are constantly increasing. [6–8]

The quality of the silicon nitride powder can directly affect the performance of silicon nitride ceramic products. [9] At present, several methods are used to produce silicon nitride powder, including (1) direct nitridation of silicon powder, (2) carbothermal reduction and nitridation of SiO_2, (3) self-propagation high-temperature combustion synthesis, (4) chemical vapor-phase reaction method, and (5) thermal decomposition of silicon diimide.[10–13] The first two methods are characterized by long production time, high-energy consumption, and low quality of the silicon nitride powder.[9] The self-propagation high-temperature combustion synthesis technology has been applied to the synthesis of various high-temperature materials including ceramics, intermetallic compounds, and composites. It was

reported that the silicon nitride powder synthesized by this method was mainly β-Si_3N_4, and it was difficult to control the α/β ratio in the product. [14–16] Sintering mechanism of Si_3N_4 has been reported. Sintering additives such as MgO, Al_2O_3, and Y_2O_3 can react with SiO_2 to form silicates, which can exist in the liquid phase at the sintering temperature. α-Si_3N_4 powder melts in the liquid phase; β-Si_3N_4 is precipitated; and finally β-Si_3N_4 sintered body is formed by the Ostwald ripening mechanism[17–21] The nanosize powder synthesized by the chemical vapor-phase reaction in RF plasma is mainly amorphous.[22–25]. Nanosize amorphous silicon nitride powder with a high surface energy offers significant advantages in terms of the sintering rate [13,26,27]. In spite of its advantages, the chemical vapor-phase reaction in RF plasma is not suitable for industrial applications, because it is not cost-effective for mass production.[9,28]

The imide decomposition method is a well-established technology. The imide synthesis reaction takes place at -50–0 °C using liquid-phase reactants.[13,29,30] Most silicon nitride powders, which are industrially used, are produced by this method. The process, however, consumes a considerable amount of energy. The imide synthesis reaction occurs at extremely low temperature because it uses liquid NH_3, which has very low boiling point of -33 °C. The organic solvent, which is used to dissolve $SiCl_4$, must be removed from the reaction product. Furthermore, the handling of liquid ammonia can be very difficult and dangerous as well.

One promising method for the synthesis of silicon nitride powder is the vapor-phase reaction of $SiCl_4$ with NH_3 [31,32]. It is not necessary to use organic solvent and easy to handle the gaseous reactants using this method. Lange *et al*. reported that the investigations of the vapor-phase reaction between $SiCl_4$ and NH_3 at the

temperatures in the range 300–1700 °C showed the formation of extremely fine, spherical, and amorphous particles with surface areas up to 300 $m^2 g^{-1}$[32]. The method, however, has not been industrially used to produce silicon nitride powder, because the products grow on the nozzle and are deposited on the reactor wall. It is very difficult to collect the products, which have been deposited on the reactor wall and grown on the nozzle. The nozzle can be blocked by the solid products as well [33,34]. The vapor-phase reaction method can be used to produce silicon nitride powder once the problems associated with the reaction products growing on the nozzle and being deposited on the reactor wall are solved. Those problems can be overcome by optimizing the processing conditions. The process parameters of the vapor-phase reaction method, however, have not been systematically investigated or optimized.

In this study, in order to investigate the reaction phenomena and parameters of the vapor-phase reaction, the synthesis and decomposition temperatures of diimide were studied, and the effects of the flow rates of the reactants and carrier gas on the reaction temperature, yield, and the particle size were investigated. The heat of the reaction, which can affect the reaction temperature, was calculated. Under the optimized conditions, 87% yield was.

2.2 Experimental Procedure

The reaction between $SiCl_4$ and NH_3 was carried out at room temperature in a quartz reactor (D100 mm x H500 mm, 4L). 0.1 mole of $SiCl_4$ and 0.6 mole of NH_3 were introduced into the reactor with separate nozzles, and the reactants were

supplied from the bottom to the top of the reactor. Solid products were collected at the bottom of the reactor. The off gas escaped from the top of the reactor. Liquid $SiCl_4$ was vaporized at 150 °C before entering the reactor. Ar was flowed with $SiCl_4$ to prevent the condensation of $SiCl_4$, which is necessary to ensure the vapor-phase reaction at room temperature.

The synthesized solid products went through a two-step thermal process to remove the NH_4Cl by-product and decompose diimide to produce amorphous Si_3N_4 in the quartz reactor. The two-step thermal process was carried out immediately after the reaction in the reactor with an electrical tube furnace to prevent the exposure of highly hygroscopic diimide to moisture. The first thermal process to remove the by-product was carried out at 500 °C for 2 h, followed by a second thermal process for the decomposition of diimide at 1000 °C for 2 h.

The prepared powder was characterized by thermogravimetric analysis (TGA; Mettler Toledo, STAR), particle size analysis (PSA; BECKMAN COULTER, LS13), and scanning electron microscopy (SEM; FEI, NanoSEM200). The reaction yield was calculated by the following equation.

$$\text{Yield} = \frac{\text{weight of the synthesized amorphous silicon nitride}}{\text{weight of the theoritical amorphous silicon nitride}} \times 100$$

The weight of the amorphous Si_3N_4 produced from the decomposition of diimide was used to calculate the reaction yield. No weight loss observed during the decomposition of diimide.

2.3 Results and Discussion

2.3.1 Reaction Phenomena

Reaction between $SiCl_4$ and NH_3 was carried out at room temperature in a 5L four-neck flask reactor. Reactants were introduced from the double and triple nozzle. NH_3 was introduced from the 1/8-inch inner tube of the double nozzle, and $SiCl_4$ was introduced from the 1/4 inch outer tube of the double nozzle. The nozzle was placed in the middle of the reactor so that the reaction is carried out near the bottom of the reactor and the product can be collected at the bottom of the reactor. The off gas escaped from the reactor through the vent line placed on the top of the reactor. The nozzle designs are presented in Fig. 2-1. Fig. 2-2 shows the result of the reaction between $SiCl_4$ and NH_3. The reaction occurred near the bottom of the reactor, producing white solid powder. With the progress of the reaction, the product was deposited around the nozzle as shown in Fig. 2(c) and white powder was not produced. The deposition of the product around the nozzle would cause flogging of the nozzle. The deposited product should be pulverized to get powder, thus increasing the manufacturing cost. In order to solve the deposition of the product around the nozzle, inert gas stream between $SiCl_4$ and NH_3 gas was introduced with a triple nozzle. The inert gas stream will play a barrier between $SiCl_4$ and NH_3 gas, and thus the reaction can occur far from the nozzle. The reaction between $SiCl_4$ and NH_3 using triple nozzle occurred in the 5L four-neck flask reactor. The product was deposited around the nozzle. The inert gas stream did not play a barrier to prevent the deposition of the product. The schematic of reaction phenomena is presented in Fig. 2-3. The reactants were introduced into the reactor with top-down flow, and the off gas flowed to the top of the reactor to

escape from the reactor through the vent line. The sprayed reactants flowed from the bottom of the reactor towards the top of the reactor, and thus the reaction occurred around the nozzle. Furthermore, the natural convection caused by the heat of reaction made the reactants to flow from the bottom of the reactor towards the top of the reactor. Reaction occurred around the nozzle because of the reactants stream from bottom towards the top along the nozzle. Therefore, the reaction product was produced around the nozzle, and the product deposited on the nozzle.

2.3.2 Nozzle and Reactor Design

In order to prevent deposition from the nozzle, various nozzles and reactors were designed to make the stream of reactant gases not to flow along the nozzle. The nozzles and reactors are presented in Fig. 4. D150 mm × H350 mm size of inside wall was placed in the D180 mm × H400 mm size of reactor. The separated nozzle was placed on the top (No. 1) or middle (No. 2) of the reactor and reactants flowed from the top to bottom. When reactors No. 1 and 2 were used, the product of the reaction did not deposit around the nozzle; however, it deposited on the top of the reactor. The temperature of the top of the reactor was higher than that of the bottom of the reactor. The natural convection caused by the heat of reaction made the heat accumulated on the top of the reactor. The heated reactant gases by heat of reaction flowed towards the top of the reactor, and the reaction occurred on the top of the reactor, leading to the deposition of the product on the top of the reactor. Considering the natural convection, the reactor was turned upside down (No. 3), thus the reactants gas stream flow from down towards the top of the reactor. Off

gas heated by the heat of reaction escaped from the reactor through the top of the reactor, and thus the heat of reaction was not accumulated in the reactor. As a result of the reaction using reactor No. 3, product was not deposited around the nozzle or any part of the reactor. From the results of the experiments using the reactors No. 1–3, the optimized reactor was designed (No. 4). When optimized reactor (D100 mm × H500 mm) with a down-top flow of reactants was used, the product of white solid powder, which is mixture of diimide and NH_4Cl, was obtained in 97% yield.

2.3.3 Effect of the Reactant Flow Rate

The yields, tap-densities, and mean particle sizes at different flow rates are listed in Table 2-1. The tap density of the reaction product increased with increasing flow rate of the reactants (numbers 1–6 in Table 2-1). The tap densities of the reaction product (diimide and NH_4Cl mixture) were 0.21 and 0.58 g cm^{-3} at the $SiCl_4$ flow rates of 6 and 48 mL h^{-1}, respectively. The particle sizes of the amorphous Si_3N_4 at the $SiCl_4$ flow rates of 12, 24, and 48 mL h^{-1} were measured by PSA, and the results are listed in Table 2-1 and Fig. 2-5. The SEM images of amorphous Si_3N_4 particles are shown in Fig. 2-6. When the $SiCl_4$ flow rate was 12, 24, and 48 mL h^{-1}, the mean particle size was 3.9, 5.3, and 9.9 μm, respectively. Amorphous Si_3N_4 particles with spherical shapes were observed in the SEM analysis as shown in Fig. 2-6, and the size of the particle observed in the SEM images was consistent with that of the PSA result. The particle size increased and the particle size distribution became broader as the reactants' flow rates increased, as shown in Fig. 2-5. A wide particle size range can help to obtain homogeneous packing, which can increase the

tap density. As the flow rates of the reactants increase, the particle size increased. The particle size of the reaction product increased as the flow rate of the reactants increased, which can be explained using two reaction parameters - the higher Ar flow rate and the higher concentration of the reactants. Solid-phase products are formed as a result of the vapor-phase reaction. The reactants are adsorbed on the surface of the solid product, and the reaction occurs on the surface in the reaction zone where the vapor-phase reactants and the solid-phase product coexist. The particle grows because the reaction occurs on the surface of the particle. When the Ar flow rate is increased, the sedimentation time of the particle can increase, and the particle can have an increased number of chances to react on its surface due to the longer sedimentation time. For this reason, the particle size can increase during the reaction. If the concentrations of the reactants are high, the number of produced particles per unit area can increase. Reactants then have additional chances to adsorb on the surface of the particles at a higher concentration. The adsorbed reactants react on the surface of the particles, leading to larger particle size. Experiments 6–9 in Table 2-1 show that the increase in the concentrations of the reactants decreases the Ar flow rate. The tap density increased as the concentrations of the reactants increased, whereas it decreased with increasing Ar flow rate. The tap density, which is affected by the particle size and the size distribution, was affected more by the concentration of the reactants than by the Ar flow rate. The reaction yield decreased with increasing Ar flow rate. 97.9% and 87.3% yields were observed when the Ar flow rate was 125 and 1000 mL min^{-1}, respectively. Fine particles, which do not settle on the bottom of the reactor, can escape from the reactor with the off gas stream. When the Ar flow rates were 1250 and 1750 mL

min^{-1}, the yields were 78.7% and 48.0%, respectively. The reaction yield rapidly decreased when the Ar flow rate exceeded 1000 mL min^{-1}. An Ar flow rate >1000 ml min^{-1} was too fast for the reaction; thus not only fine particles, but also unreacted reactants can escape from the reactor, lowering the reaction yield.

2.3.4 Effect of the Reaction Temperature

The reactions carried out at 50, 100, 150, 200, and 300 °C afforded the product in reasonable yields, as shown in Fig. 2-7. The reaction yields were 87%, 87%, and 82% at 25, 100, and 150 °C, respectively. The reaction yield decreased dramatically when the temperature exceeded 200 °C and no product was obtained at 200 and 300 °C, indicating that diimide is not obtained at temperatures >200 °C. The reaction did not occur at temperatures >150 °C, because $Si(NH)_2$ decomposed into Si_3N_4 and NH_3 at temperatures >150 °C. In order to investigate the imide decomposition temperature, TGA of the reaction product and the NH_4Cl reagent was carried out. The results of the TGA are shown in Fig. 2-8.

As shown in Fig. 2-8, 4.4 and 80 wt% of weight loss of the reaction product were observed at ~100 °C and 200 °C, respectively. 100% weight loss of the NH_4Cl reagent was observed at temperatures >250 °C. The first weight loss of the reaction product at ~100 °C was the result of the release of NH_3 during the $Si(NH)_2$ decomposition process. The second weight loss at a temperature close to 200 °C was the result of NH_4Cl decomposition. The TGA results show that $Si(NH)_2$ is completely decomposed at ~150 °C. Mazdiyasni *et al*. reported that diimide ($Si(NH)_2$) formed by the reaction between $SiCl_4$ and NH_3 is polymerized to

$[Si(NH)_2]_n$ at 360 °C, after which its pyrolysis to two intermediate species, $2[Si_3(NH)_3N_2]n$ at 400 °C and $3[Si_2(NH)N_2]_n$ at 650 °C, yields α-Si_3N_4 at 1200 °C [35]. Lange *et al*. reported that $Si(NH)_2$ is stable up to 200 °C and gradually loses NH_3 with increasing temperature until amorphous Si_3N_4 is formed. Thermal decomposition in the reaction of $Si(NH)_2$ and HCl in the presence of NH_4Cl affords $Si_2N_3H_2Cl$, which is decomposed into amorphous Si_3N_4 at >800 °C [32]. In this study, nearly all $Si(NH)_2$ decomposed at ~100 °C. As shown in Fig. 2-7, 85% yield was obtained at temperatures <150 °C, and no reaction was observed at temperatures >200 °C, which is the decomposition temperature of $Si(NH)_2$. The vapor-phase reaction is given by the following equations [32].

$$SiCl_4 + 6NH_3 \rightarrow Si(NH)_2 + 4NH_4Cl \quad (2\text{-}1)$$

$$SiCl_4 + 2NH_3 \rightarrow Si(NH)_2 + 4HCl \quad (2\text{-}2)$$

$$3SiCl_4 + 4NH_3 \rightarrow Si_3N_4 + 12HCl \quad (2\text{-}3)$$

By controlling the molar ratio of the reactants and the reaction temperature, only $Si(NH)_2$ or Si_3N_4 as the solid product can be obtained. However, it is difficult to realize reaction (2-2), because the decomposition temperature of $Si(NH)_2$ is higher than that of NH_4Cl. Amorphous Si_3N_4 can be formed directly by reaction (2-3) at temperatures >300 °C, but the formation of NH_4Cl cannot be avoided in the reaction between NH_3 and HCl. In this study, a mixture of $Si(NH)_2$ and $SiCl_4$ was formed by reaction (2-1) at temperatures <150 °C. To yield Si_3N_4, the separation of NH_4Cl by sublimation during the decomposition process of $Si(NH)_2$ must be

carried out. It can be more economical to produce Si_3N_4 powder by reaction (2-1) owing to the low reaction temperature compared to that of reaction (2-3). The formation of a large amount of NH_4Cl by-product, however, has to be taken into account when upscaling is considered.

2.3.5 Heat of the Reaction

The control of the reaction temperature is important for the synthesis of $Si(NH)_2$ because the reaction is temperature sensitive. $Si(NH)_2$ was not formed at 200 C and 300 °C, as shown in Fig. 2-7. The reaction temperature has to be <200 °C to ensure that the reaction takes place. The temperature, however, will increase during the reaction because of the vigorous exothermic reaction. The heat of this reaction remains unknown. The standard enthalpy of the reaction from the standard enthalpy of the formation of each reactant and product was calculated and is as follows: $\Delta_f H°_{SiCl4(g)} = -662.7$ kJ mol^{-1}, $\Delta_f H°_{NH3(g)} = -46.1$ kJ mol^{-1}, and $\Delta_f H°_{NH4Cl(s)} = -314.5$ kJ mol^{-1} at 298 K and 1 atm. [36] The thermodynamic properties of $Si(NH)_2$ have not been reported, and thus the standard enthalpy of the formation of $Si(NH)_2$ was calculated by the ASPEN plus. The method of Benson and Joback was used for the calculation. The calculated standard enthalpy of the formation of $Si(NH)_{2(s)}$ was 97.1 kJ mol^{-1}.

$SiCl_4 + 6NH_3 \rightarrow Si(NH)_2 + 4NH_4Cl \qquad \Delta H = -221.6$ kJ mol^{-1}

The calculation of the standard enthalpy of the reaction using the standard enthalpy of the formation of each component ($\Delta H = -221.6$ kJ mol^{-1}) is reasonable, as the

reaction was carried out at the standard ambient temperature and pressure levels (298 K and 1 atm). If the heat of the reaction between 0.1 mole of $SiCl_4$ and 0.6 mole of NH_3 is transferred only to NH_4Cl under an adiabatic condition, the temperature of NH_4Cl will increase to 587.2 °C, if the heat capacity of NH_4Cl is assumed to be constant as the temperature changes. Therefore, $Si(NH)_2$ will not be produced. The temperature has to be decreased by cooling during the reaction. In this study, Ar gas was used to prevent the condensation of $SiCl_4$. The heat of the reaction can be transferred to the Ar gas, lowering the reaction temperature. The heat of the reaction between 0.1 mole of $SiCl_4$ and 0.6 mole of NH_3 increased the temperature of NH_4Cl to 428.7 and 338.4 °C at the Ar flow rates of 250 and 500 mL min^{-1}, respectively, assuming that the heat is transferred only to NH_4Cl and Ar under an adiabatic condition and that the heat capacities of NH_4Cl and Ar are constant as the temperature changes.

Table 2-2 shows the temperatures at the end of the reaction between 0.1 mole of $SiCl_4$ and 0.6 mole of NH_3 at different Ar flow rates. The temperatures were measured at the top, middle, and bottom of the reactor.

The temperature in the middle point of the reactor was higher than those of the top and bottom, except for experiment number 10 in Table 2-2. A reaction zone was formed in the middle of the reactor. When the Ar flow rate was 250 mL min^{-1}, the temperature increased with increasing flow rates of the reactants. In contrast, the temperature decreased as the Ar flow rate increased when the $SiCl_4$ and NH_3 flow rates were 24 and 500 mL min^{-1}, respectively. The heat of the reaction was transferred to the air-cooled reactor. The heat exchange rate between the reactor and the air was lower than that of the heat release from the reaction with increasing

flow rates of the reactants. In addition, the temperature at the middle point in the reactor increased to 126 °C in experiment number 12, whereas it increased to 45 °C in experiment number 10, as shown in Table 2-2. Experiments 12–14 in Table 2-2 demonstrate that the temperatures at the middle point decreased as the Ar flow rate increased. The flow of Ar gas was effective in cooling down the reactor, but the yield decreased as the Ar flow rate increased, as listed in Table 2-1.

An increase in the flow rate of the reactants is beneficial to productivity but the temperature increased as the reactant flow rate increases, decreasing the yield. Increasing the Ar flow rate for cooling can lead to a loss of the reactants, which can eventually lower the yield. Both the productivity and the yield can be improved by optimizing the process conditions of the reaction.

2.4 Conclusions

To investigate the reaction phenomena and parameters of low-temperature vapor-phase reaction for the synthesis of $Si(NH)_2$, the synthesis and decomposition temperatures of $Si(NH)_2$ were studied. In addition, the effects of the flow rates of the reactants and the carrier gas on the particle size, the reaction temperature, and the yield were investigated. The reaction product was grown on the nozzle because the reaction zone was formed near the nozzle. The convection caused by the heat of reaction played an important role of product growing phenomenon. Down-top flow reaction was the best way to prevent the product from the deposition. The concentration of the reactant affected the particle size of the product. No reaction was observed at temperatures >200 °C because of the decomposition of $Si(NH)_2$.

The reaction temperature increased as the reactant flow rates increased because of the exothermic nature of the reaction, which lowered the yield. The reaction yield decreased with increasing Ar flow rate; this process can be used to cool the reactor. The flow rates of $SiCl_4$, NH_3, and Ar were increased to 48, 1000, and 1000 mL min^{-1}, respectively, for the optimization, affording 87% yield in the reactor used in this study (D100 mm × H500 mm, 4L).

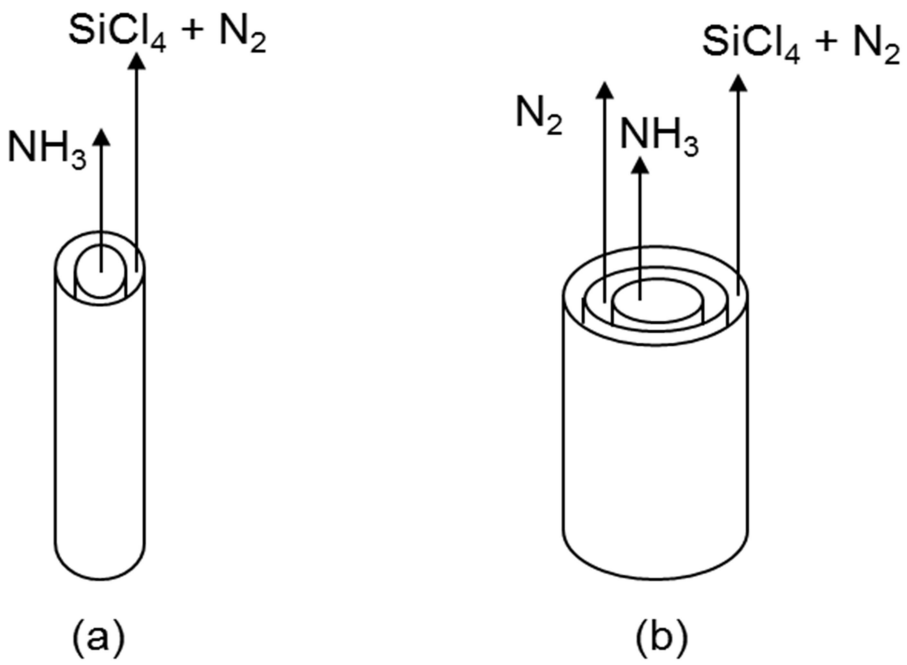

Fig. 2-1. Nozzle design; (a) double nozzle and (b) triple nozzle.

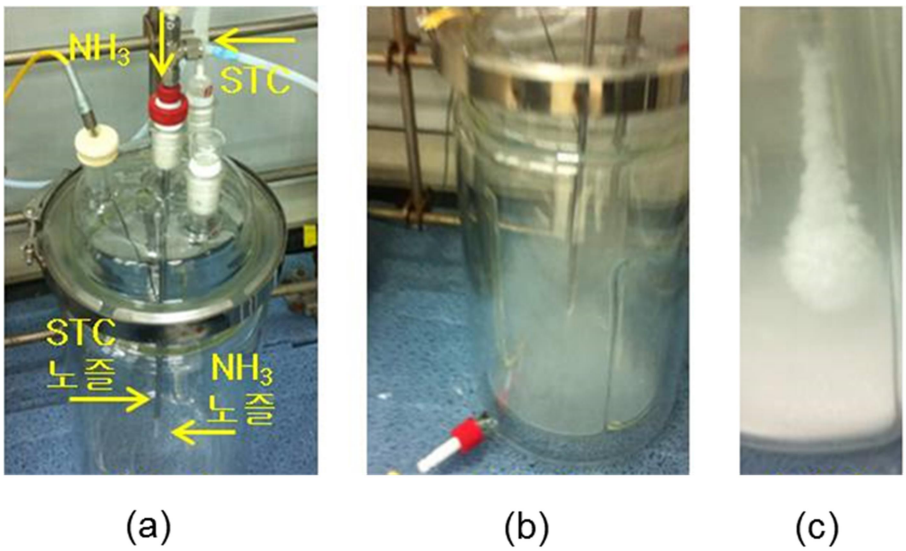

Fig. 2-2. Reaction between $SiCl_4$ and NH_3 with 5L 4 neck flask reactor; (a) before the reaction, (b) during the reaction, and (c) after the reaction.

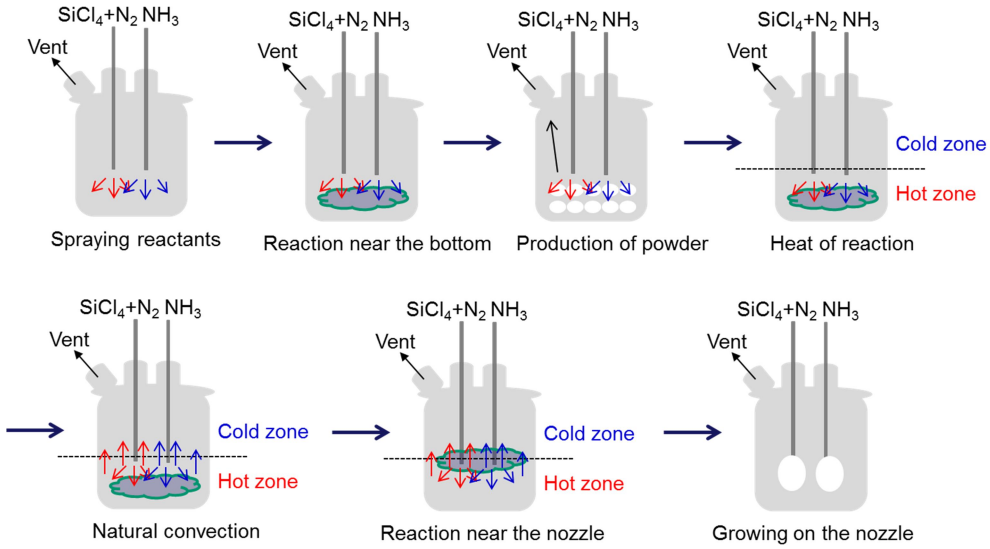

Fig. 2-3. Scheme of reaction phenomena.

No.	Dimension (mm)	Volume (L)	Location of Nozzle	Schematic	Before rxn	After rxn
1	D150 x H350 (Inside wall)	6	Top	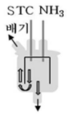	-	
2			Middle	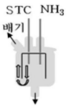		Grown on the nozzle
3			Bottom			Grown on the nozzle
4	D100 x H500	4	Bottom	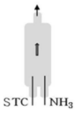		

Fig. 2-4. Nozzle and Reactor design

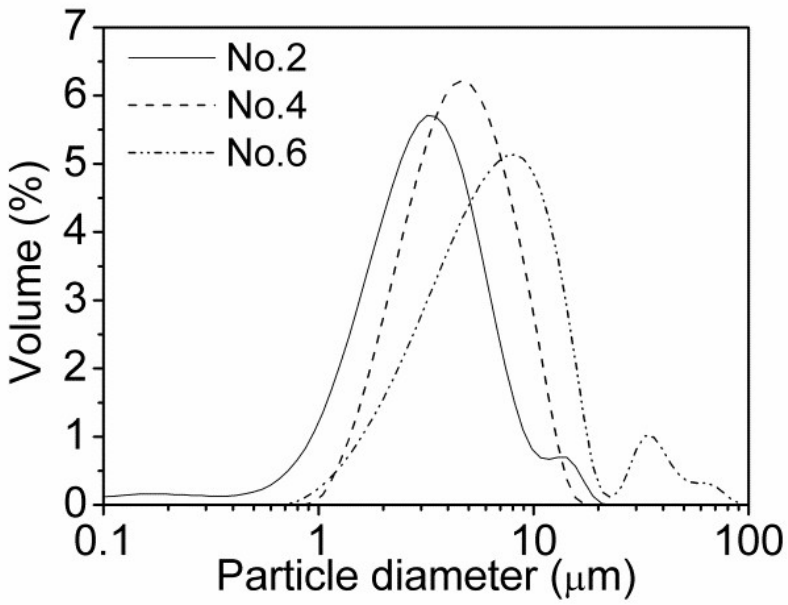

Fig. 2-5. Particle size distribution when different flow rates of the reactants were used (No. 2; $SiCl_4$ 12 ml h^{-1}, NH_3 250 ml min^{-1}, and Ar 250 ml min^{-1}, No. 4; $SiCl_4$ 24 ml h^{-1}, NH_3 500 ml min^{-1}, and Ar 500 ml min^{-1}, No. 6; $SiCl_4$ 48 ml h^{-1}, NH_3 1000 ml min^{-1}, and Ar 1000 ml min^{-1})

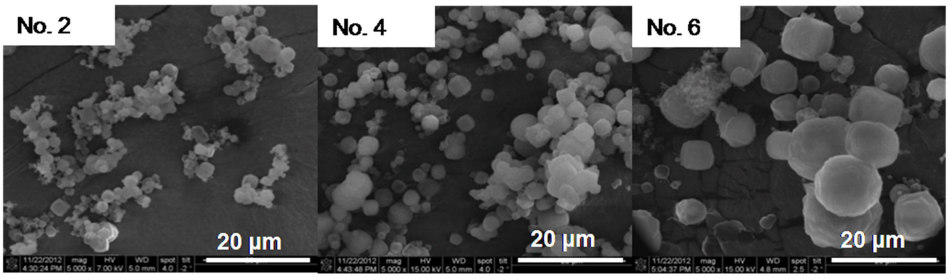

Fig. 2-6. SEM image of amorphous Si_3N_4 when different flow rates of the reactants were used (No. 2; $SiCl_4$ 12 ml h^{-1}, NH_3 250 ml min^{-1}, and Ar 250 ml min^{-1}, No. 4; $SiCl_4$ 24 ml h^{-1}, NH_3 500 ml min^{-1}, and Ar 500 ml min^{-1}, No. 6; $SiCl_4$ 48 ml h^{-1}, NH3 1000 ml min^{-1}, and Ar 1000 ml min^{-1})

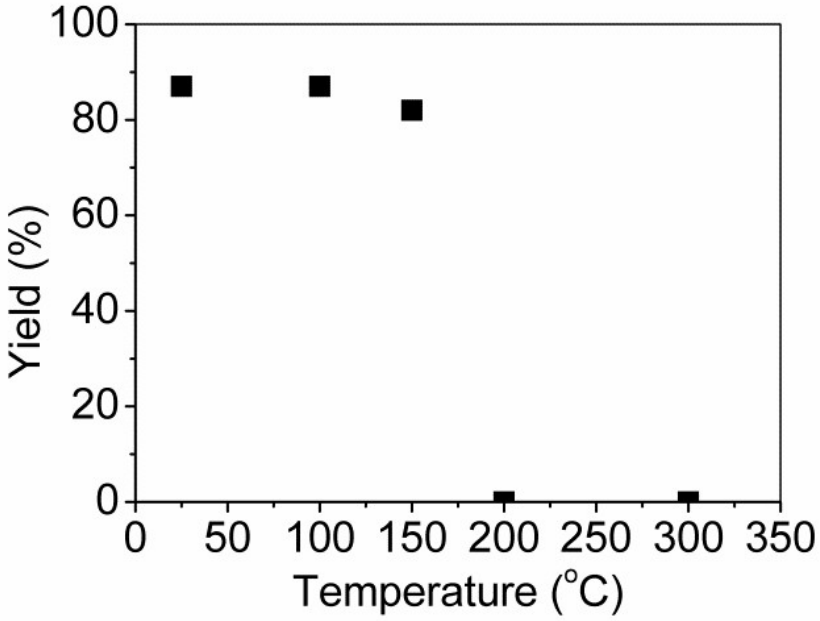

Fig. 2-7. Reaction yields at different reaction temperatures

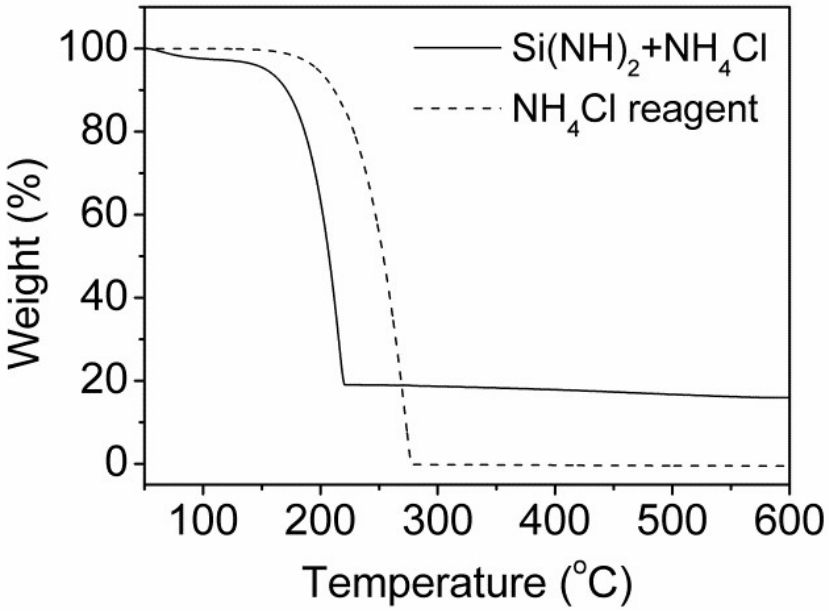

Fig. 2-8. TGA results from the reaction product and the NH_4Cl reagent (black line; the reaction product (mixture of $Si(NH)_2$ and NH_4Cl) and dashed line; the NH_4Cl reagent)

Table 2-1 The yields, tap-densities and mean particle sizes when different flow rates were used

No.	$SiCl_4$ (ml h^{-1})	NH_3 (ml min^{-1})	Ar (ml min^{-1})	Yield (%)	Tap density (g cm^{-3})		Mean particle size (μm)
					Diimide + NH_4Cl	a-Si_3N_4	
1	6	125	125	97.9	0.21		
2	12	250	250	95.8	0.21	0.11	3.9
3	18	375	375	94.4	0.20		
4	24	500	500	94.1	0.36	0.10	5.3
5	36	750	750	87.3	0.46		
6	48	1000	1000	87.3	0.58	0.12	9.9
7	12	250	1750	48.0	0.28		
8	24	500	1500	74.7	0.49		
9	36	750	1250	78.7	0.59		

Table 2-2 The temperatures at the top, middle, and bottom of the reactor at the end of the reaction with different flow rates of reactants and Ar gas

No.	$SiCl_4$ (ml h^{-1})	NH_3 (ml min^{-1})	Ar (ml min^{-1})	Temperature in the reactor (°C)		
				Top	Middle	Bottom
10	12	250	250	47	45	58
11	24	500	250	35	70	28
12	48	1000	250	41	126	36
13	24	500	500	58	70	30
14	24	500	1000	25	54	25

Reference

[1] F. L. Riley (2000) Silicon nitride and related materials, J Am Ceram Soc 83:245-265.

[2] R. N. Katz (1997) Applications of silicon nitride based ceramics, Ind Ceram (Italy) 17:158-164.

[3] A. Okada (2008) Automotive and industrial applications of structural ceramics in Japan, J Eur Ceram Soc 28:1097-1104.

[4] J. Liang, L. Topor, A. Navrotsky, M. Mitomo (1999) Silicon nitride: Enthalpy of formation of the α- and β-polymorphs and the effect of C and O impurities, J Mater Res 14:1959-1968.

[5] D. Faoite, D. J. Browne, F. R. Chang, K. T. Stanton (2012) A review of the processing, composition, and temperature-dependant mechanical and thermal properties of dielectric technical ceramics, J Mater Sci 47:4211-4235.

[6] G. Ling, H. Yang (2005) Pressureless sintering of silicon nitride with Magnesia and Yttria, Mater Chem Phys 90:31-34.

[7] S. K. Biswas, F. L. Riley (2001) Gas pressure sintering of silicon nitride-current status, Mater Chem Phys 67:175-179.

[8] J. Jiang (2009) A new synthesis method of α-silicon nitride powder-reductive combustion synthesis from silicon and silicon dioxide, J Am Ceram Soc 92:3095-3097.

[9] Y. Li, L. Wang, S. Yin, F. Yang (2013) Crystallization behavior of amorphous silicon nitride added with silicon powder, Mater Chem Phys 141:874-881.

[10] A. Atkinson, A. J. Moulson, E. W. Roberts (1976) Nitridation of high-purity silicon, J Am Ceram Soc 59:285-289.

[11] T. Licko, V. Figusch, J. Puchyova (1992) Synthesis of silicon nitride by carbothermal reduction and nitriding of silica: Control of kinetics and morphology, J Eur Ceram Soc 9:219-230.

[12] G. Petzow, M. Herrmann (2002) Silicon nitride ceramics: Structure and Bonding, Springer-Verlag Berlin Heidelberg 102:50-167.

[13] M. Nakamura, Y. Kuranari, Y. Imamura (1987) Characterization and synthetic process of Si_3N_4 material powder. In: S. Somiya, et al Silicon nitride 1. Elsevier, London, pp 40.

[14] A. G. Merzhanov, I. P. Borovinskaya (1972) Self-propagating high-temperature synthesis of refractory inorganic compounds, Dokl Chem 204:429.

[15] M. A. Todriguez, N. S. Makhonin, J. A. Escrina (1995) Single crystal β-Si_3N_4 fibers obtained by self-propagating high temperature synthesis, Adv Mater 7:745-747.

[16] I. G. Cano, M. A. Rodriguez (2004) Synthesis of β-silicon nitride by SHS: fiber growth, Scripta Mater 50:383-386.

[17] I. Amato, D. Martorana, B. Silengo (1977) Some considerations on the kinetics of hot-pressing alpha-silicon nitride powder, Mater Sci Eng 28:215-220.

[18] T. Y. Tien (1995) In phase diagrams in advanced ceramics, Academic press limited, London, pp 127-156.

[19] X. Liu, Z. Huang, Q. Ge, X. Sun, L. Huang (2005) Microstructure and mechanical properties of silicon nitride ceramics prepared by pressureless sintering with MgO-Al_2O_3-SiO_2 as sintering additives, J Eur Ceram Soc 25:3353-3359.

[20] L. Junting, L. Riping (2009) Effect of additives on the sintering of amorphous nano-sized silicon nitride powders, J Wuhan Univ Technol Mater Sci Ed 24:537-539.

[21] G. Petzow and W. A. Kaysser (1984) Basic Mechanisms of liquid Phase Sintering, in Sintered Metal-Ceramic Composites, ed. G. S. Upadhyaya, Elsevier Science Publishers, Amsterdam, pp. 595

[22] J. Szepvolgyi, I. mohai-Toth (1995) Experimental investigation into the synthesis of silicon nitride powder in an RF thermal plasma reactor using a factorial design approach, J mater chem 5:1227-1232.

[23] L. Shuquan, H. Baiyun, Z. Ziqiao (1996) Silicon nitride powder synthesized by thermal plasma method, Trans Nonferrous Met Soc China 6:103-107.

[24] J. Szepvolgyi, I. mohair (1999) Crystallization of an amorphous silicon nitride powder produced in a radiofrequency thermal plasma, Ceram Int 141:874-881.

[25] G. Soucy, J. W. Jurewicz, M. I. Boulos (1996) Parametric study of the plasma synthesis of ultrafine silicon nitride powders, J mater Sci 30:2008-2018.

[26] G. Ziegler, J. Heinrich, G. Wotting (1987) Relationship between processing, microstructure and properties of dense and reaction-bonded silicon nitride, 22:3041-3086.

[27] J. Szepvolgyi, F. L. Riley, I. Mohai (1996) Composition and microstructure of nanosized, amorphous and crystalline silicon nitride powders before, during and after densification, J Mater Sci 6:1175-1186.

[28] Y. Li, L. Wang, S. Yin, F. Yang (2012) Rapid crystallization of amorphous silicon nitride powder accelerated by liquid Si, Ceram Int 38:5311-5314.

[29] G. Schwier, G. Nietfeld, G. Franz (1989) Production and characterization of silicon nitride powders, Mat Sci Forum 47:1-20.

[30] T. Yamada, T. Kawahito, T. Iwai (1983) Crystallization of amorphous Si_3N_4 prepared by the thermal decomposition of $Si(NH)_2$, J mater Sci Lett 2:275-278.

[31] F. W. Dorn, W. Krause, F. Schroder (1992) Particle size control during production of ceramic nitride powders, Adv Mater 4:221-224.

[32] H. Lange, G. Wotting, G. Winter (1991) Silicon nitride-from powder synthesis to ceramic materials, Chem Ind Ed Engl 30:1579-1597.

[33] T. Iwai, T. Kawahito, T. Yamada (1983) Process for producing silicon nitride powder, US patent 4,405,589.

[34] L. Marosi (1989) Preparation of silicon nitride powder, US patent 4,859,443.

[35] K. S. Mazdiyasni, C. M. Cooke (1973) Synthesis, characterization, and consolidation of Si_3N_4 obtained from ammonolysis of $SiCl_4$, J Am Ceram Soc 56:628-633.

[36] H. J. Himmel, N. Schiefenhovel, M. Binnewies (2003) Identification and characterization of monomeric, volatile $SiCl_3NH_2$ as product of the reaction between $SiCl_4$ and NH_3: An important intermediate on the way to silicon nitride, Chem Eur J 9:1387-1393.

Chapter 3. Crystallization Behavior

3.1 Introduction

Silicon nitride ceramics have been widely used in energy, metallurgy, machinery, and aerospace industries.[1,2,3] The performance of the silicon nitride ceramics are directly affected by the quality of the silicon nitride powder. Among the various methods to produce silicon nitride powder, such as direct nitridation, carbothermal reduction, gas-phase reaction, and imide decomposition[4,5,6,7], the latter is considered suitable for the production of Si_3N_4 powder with high quality.[8] The thermal decomposition of imide has been used for decades to produce silicon nitride powder via a relatively simple liquid-phase process[9]; however, it is an expensive technique. A promising method to produce silicon nitride powder, which can be more cost-effective while maintaining a high quality of the powder, is the vapor-phase reaction of silicon tetrachloride with ammonia.[10,11] We have reported the optimized conditions of the reaction parameters for the synthesis of the amorphous silicon nitride powder by using the low-temperature vapor-phase reaction method.[12] The synthesized amorphous silicon nitride powder needs to be crystallized to the α-phase for the sintering process to manufacture the silicon nitride ceramics.[7]

In the past two decades, several studies on the crystallization process of the amorphous silicon nitride powder have been performed.[13,14,15,16] Micro amorphous silicon nitride powder was prepared by pyrolysis of polysilazane under flowing NH_3 atmosphere and by thermal decomposition of $Si(NH)_2$; nanosized amorphous

silicon nitride powder was prepared by the vapor-phase reaction of silicon tetrachloride with ammonia.[17] Morgan[18] and Prochazka et al.[19] reported that the amorphous-crystalline transition, which occurred at approximately 1480–1490 °C, was strongly exothermic, and was accelerated by the heat evolved during the phase transition. Janos et al. reported that a crystallization temperature range of approximately 1420–1480 °C was recommended for the thermal plasma silicon nitride powders.[16] Allaire et al. suggested a low temperature limit of ~1500 °C for the complete crystallization of the amorphous silicon nitride powder.[13] The ammonium chloride impurities in the silicon nitride powder and the nitrogen in the furnace atmosphere cause the formation of whiskers[13]. Powders with approximately 80% of crystalline phase content and an α/β ratio of roughly 6 were produced by annealing amorphous silicon nitride powder at 1450 °C for 6 h under nitrogen flow.[16] The X-ray diffraction (XRD) results of an early study show that a small amount of β-SiC was formed, and the transformation of α- to β-Si_3N_4 also occurred in the powders after heating at 1700 °C under nitrogen atmosphere.[20] At high temperature, generally in the range of approximately 1600–1700 °C, the transformation from α- to β-phase occurs, usually assisted by impurities, but the reverse transformation from β to α has not been observed.[21,22] Early studies showed that the crystallization behavior of the amorphous silicon nitride strongly depends on the processing history of the amorphous structure. The crystallization temperature was found to vary from 1200 °C to 1500 °C depending on the synthesis method and the characteristics of the amorphous materials, such as the kinds and amounts of impurities contained as well as the particle size;[14,15,20,23] however, to the best of our knowledge, there is no report on the crystallization of

amorphous silicon nitride powder synthesized by low-temperature vapor-phase reaction method.

The aim of this work is to establish the process conditions for the crystallization of amorphous silicon nitride powder synthesized by low-temperature vapor-phase reaction method. To examine the crystallization behavior, the amorphous silicon nitride powder was heat treated at various temperatures for different periods of time. The effects of the heat-up rate on the particle size of the α-phase silicon nitride powder were investigated, and were then used to explain the variation of the particle size and size distribution.

3.2 Experimental Procesure

The amorphous silicon nitride powder was prepared by low-temperature vapor-phase reaction method. The details of the process were previously reported elsewhere.[12] The reaction between $SiCl_4$ and NH_3 was conducted at room temperature, and the solid product (imide + NH_4Cl by-product) went through a two-step thermal process to obtain the amorphous silicon nitride powder. The first thermal process to remove the NH_4Cl was conducted at 500 °C for 2 h, followed by a second thermal process for the decomposition of diimide at 1000 °C for 2 h. Two grams of the amorphous silicon nitride powder was loaded in a graphite crucible, and then heat treated in an alumina tube furnace under nitrogen atmosphere using various temperature profiles, namely, different heat-up rates, temperatures, and durations.

The prepared samples were characterized by particle size analysis (PSA; BECKMAN COULTER, LS13), X-ray diffraction (XRD; PANalytical, EMPYREAN), and scanning electron microscopy (SEM; FEI, NanoSEM200).

3.3 Results and Discussion

3.3.1 Effect of Crystallization Temperature

The XRD patterns of the products obtained after heat treating the amorphous silicon nitride powder for 3 h at (a) 1300 °C (A), 1400 °C (B) and (b) 1450 °C (C), 1500 °C (D), 1550 °C (E), and 1600 °C (F) are shown in Fig. 3-1. Peaks with very small intensities, which can be assigned to α-Si_3N_4, were observed in sample B, indicating that a small degree of crystallization occurs at 1400 °C. Clearly, compared to the sample heat treated at 1400 °C, the diffraction intensities of the peaks corresponding to the crystalline phase (α-Si_3N_4) substantially increased when the powder was heat treated at 1450 °C; notably, the intensities did not change as the heat-treatment temperature further increased above 1500 °C and up to 1600 °C. This trend indicates that the crystallization to α-Si_3N_4 occurs at temperatures above 1450 °C. Janos et al. reported that the crystallization temperature and duration affected the formation of the β-phase.[16] Allaire et al. reported that a nitrogen atmosphere promoted the formation of the β-phase.[13] In Fig. 3-1, however, the diffraction peaks of the β-phase were not observed for all the samples. In this study, the absence of the diffraction peaks from the β-phase is

consistent with the assumption that metal impurities can assist the formation of the β-phase,[21,22] as no metal impurities were present in the synthesized powder.

The SEM images of the powders obtained after heat treating the amorphous silicon nitride powder for 3 h at 1300 °C (A), 1400 °C (B), 1450 °C (C), 1500 °C (D), 1550 °C (E) and 1600 °C (F) are shown in Fig. 3-2. Spherical amorphous silicon nitride particles with a size of ~10 μm were observed in the samples heat treated at 1300 °C (A) and 1400 °C (B). Well-defined crystals with an average size of approximately 1–1.5 μm were observed in the sample heat treated at temperatures above 1450 °C. The size of the hexagonal crystals slightly increased when the temperature increased from 1500 °C to 1600 °C, reaching a value of approximately 2 μm for the sample heat treated at 1600 °C for 3 h (F); the increase in size indicates that the crystal growth occurred after the completion of the crystallization. Crystals on the surface of the residual amorphous silicon nitride particles were observed in the sample heat treated at 1450 °C for 3 h (C), which can be considered as an intermediate state during the phase transition from amorphous to α-phase. Partial crystallization occurred in sample C. From the results of the XRD and SEM images, although a certain degree of crystallization occurred at 1400 °C and 1450 °C, the lowest temperature needed for the complete crystallization of the amorphous silicon nitride powder synthesized by low-temperature vapor-phase reaction appear to be close to 1500 °C.

3.3.2 Effect of Crystallization Duration

The amorphous silicon nitride powder was completely crystallized to α-Si_3N_4 when heat treated at 1500 °C for 3 h, as confirmed by the results of the XRD and SEM analyses shown in Figs. 3-1 and 3-2. To investigate the effect of the heating duration, the amorphous silicon nitride powder was heat treated at 1500 °C and 1550 °C for periods of time ranging from 1 to 4 hours at a heat-up rate of 10 °C/min. The diffraction patterns of the samples obtained after heat treating the amorphous silicon nitride powder at (a) 1500 °C for 1 h (G), 2 h (H), 3 h (I), 4 h (J), and at (b) 1550 °C for 1 h (K), 2 h (L), and 3 h (M) are shown in Fig. 3-3. The intensities of the diffraction peaks of the samples heat treated at 1500 °C increased when the heating duration increased, suggesting that the degree of crystallinity was accordingly enhanced. The SEM images of the samples obtained after heat treating at 1500 °C for 1 h (G), 2 h (H), 3 h (I), and 4 h (J), and those at 1550 °C for 1 h (K), 2 h (L), and 3 h (M) are shown in Figs. 3-4 and 3-5, respectively. Crystals on the surface of the residual amorphous silicon nitride particles were observed in the samples heat treated at 1500 °C for 1 h (G) and 2 h (H), which can be considered as an intermediate state during the phase transition from amorphous to α-phase. Crystals with a size of several hundred nanometers aggregated together and formed spherical particles of 10 μm size in sample H, which seemed to be amorphous; however, the surface of the particle was transforming to the crystal phase. In samples I and J, well-defined crystals having hexagonal section and an average size of approximately 1 μm to 1.5 μm were observed. The sample heat treated at 1550 °C for 1 h (K) was completely crystallized, and further crystal growth did not

occur when the duration was increased from 1 h to 3 h (Figs. 3-3 and 3-5). Hexagonal crystals with an average size of approximately 2 μm were observed.

From these results, the heating duration at the specific treatment temperature has clearly an effect on the degree of crystallinity in the crystallization process. There is a minimum time to complete the crystallization, which can vary as the crystallization temperature changes, and, as the duration increases, the crystal growth occurs and the size of the crystals increases. No appreciable changes in the size and shape of the crystals were observed after heat treating at 1500 °C for 3 h or at 1550 °C for 1 h, suggesting that the crystallization process was completed after the heat treatment at 1500 °C for 3 h or at 1550 °C for 1 h.

3.3.3 Crystallization Behavior

The experimental results in Figs. 3-1, 3-2, and 3-4 show that the crystallization and the crystal growth occurred at a temperature above 1400 °C. The heating duration affected the crystal-growth behavior at 1500 °C. The longer the duration, the larger the extent of crystal growth occurred. Fig. 3-6 shows a schematic model for the crystallization process of the amorphous silicon nitride powder. The crystallization process starts at the surface of the amorphous particle: the outer regions of the particle become crystalline, while the inner part remains amorphous. The energy on the surface of the amorphous silicon nitride particle is higher than that inside the particle, and the re-arrangement of the atoms (needed for the transformation to the crystalline phase) at the surface can be considerably faster than that inside the particle. The silicon nitride crystals, formed by the re-arrangement of the Si and N

atoms on the surface of the large amorphous particle, are separated from the amorphous particle itself. The Si and N atoms of the amorphous phase located on the new surface of the amorphous particle after the separation of the crystals can re-arrange and form crystals, which in turn separate from the host amorphous particle; this process continues until the whole amorphous particle is converted into crystals. The formation of the nuclei for the crystallization is controlled by the nucleation barrier shown in Equation 1 (ΔG^* = nucleation barrier);[24] the barrier is inversely proportional to the temperature

$$\Delta G^* = \left[\frac{16\pi\left(\gamma^{SL}\right)^3 T_m}{3\left(\Delta H\right)^2}\right]\frac{1}{\left(\Delta T\right)^2} \qquad (3\text{-}1).$$

The increase of the temperature leads to the decrease of the nucleation barrier, which means that more nuclei for the crystallization can be formed. The newly formed nuclei can then grow in size.

3.3.4 Effect of Heat-up Rate

From Equation 3-1, the formation of the nuclei for the crystallization can be controlled by tuning the temperature. The phase transition occurred at a temperature above 1400 °C (Fig. 3-1). The relative extent of nucleation and growth (which will determine the crystal size and its distribution) can be controlled by tuning the heat-up rate during the nucleation

When the heat-up is slow, there is plenty of time for nucleation before the growth starts. When the growth starts, there are already a number of nuclei that are ready to grow, leading to a relatively uniform size of the crystals. When the heat-up is

fast, intensive nucleation can still occur when the growth starts. The crystals grown from the nuclei formed during the heat-up (with the "early crystals") can grow and become larger than the crystals grown from the nuclei formed after that the growth of the "early crystals" occurred. In this case, the particle size can be relatively not uniform.

To control the particle size of the α-Si_3N_4 powder, the amorphous silicon nitride powder was heat treated at 1550 °C for 1 h; heat-up rates of 0.7 °C/min, 2 °C/min, 4.5 °C/min, and 10 °C/min were adopted from 1100 °C up to 1400 °C; then, the temperature was increased with a heat-up rate of 10 °C/min from 1400 °C to 1550 °C. The temperature profile is shown in Fig. 3-7. Table 3-1 and Fig. 3-8 show the particle size and its distribution for the samples heat treated with the temperature profile shown in Fig. 3-7. The mean particle sizes of the amorphous silicon nitride powder heat treated at 1550 °C for 1 h with heat-up rates of 0.7 °C/min, 2 °C/min, 4.5 °C/min, and 10 °C/min were 1.25 μm, 1.28 μm, 1.28 μm, and 1.10 μm, respectively. Two clear peaks at ~0.3 and ~2 μm were observed for the P and Q samples, while only one peak at ~1.5 μm was observed for the N and O samples (Fig. 3-8). When the heat-up is slow, the growth starts after that the nucleation is almost completed, which leads to the singlet particle size distribution (N and O in Fig. 3-8). On the other hand, a bimodal particle size distribution was observed (P and Q in Fig. 3-8) when the heat-up rate was increased, indicating that the nucleation was not completed when heating from 1100 °C to 1400 °C, and that the nucleation and crystal growth occurred simultaneously during the heating step from 1400 °C to 1550 °C.

We investigated the effect of the heat-up rate in the temperature range of 1400–1550 °C on the particle size and its distribution. The amorphous silicon nitride powder was heat treated at 1550 °C for 1 h; a heat-up rate of 10 °C/min was adopted up to 1400 °C, and then the temperature was increased with heat-up rates of 0.7 °C/min, 2 °C/min, 4.5 °C/min, and 10 °C/min from 1400 °C to 1550 °C. The temperature profile is shown in Fig. 3-9. The particle size distributions of the prepared samples are shown in Fig. 3-10.

All the samples exhibited a bimodal particle size distribution. The heat-up to 1400 °C with the rate of 10 °C/min was too fast to allow a complete nucleation; thus, the nucleation and crystal growth occurred simultaneously during the heat-up from 1400 °C to 1550 °C, even when the heat-up was very slow (0.7 °C/min, R in Fig. 3-10). Clearly, most of the nucleation occurred at a relatively low temperature below 1400 °C and, therefore, decreasing the heat-up rate led to a uniform particle size (O and N in Fig. 3-7). The bimodal particle size distribution could be achieved by adopting a fast heat-up rate during the crystallization process. The bimodal particle size distribution can help increase the packing density before the sintering process for the fabrication of silicon nitride ceramics, in turn contributing to increase the sintering density of the ceramics.

3.4 Conclusions

Amorphous silicon nitride powder was heat treated at various temperatures for different periods of time to examine the crystallization behavior. The effects of the heat-up rate on the particle size, and its distribution, of the α-phase silicon nitride

powder were investigated. A phase transition from amorphous to α-phase occurred at temperatures above 1400 °C. The crystallization process was completed after heat treatment at 1500 °C for 3 h or at 1550 °C for 1 h. The crystallization process starts at the surface of the amorphous particle: the outer regions of the particle become crystalline, while the inner part remains amorphous. The re-arrangement of the Si and N atoms on the surface of the amorphous particle leads to the formation of hexagonal crystal structures that are separated from the host amorphous particle. The nucleation occurred at temperatures below 1400 °C.

The particle size and its distribution can be tuned by varying the heat-treatment profile (namely, the heat-treatment temperature, heating rate, and heating duration at the specified treatment temperature), which can be used to control the relative extent of nucleation and growth. The completion of most of the nucleation by lowering the heat-up rate can be used to achieve a singlet particle size distribution. Conversely, a bi-modal particle size distribution can be achieved by adopting a fast heat-up rate during the crystallization process.

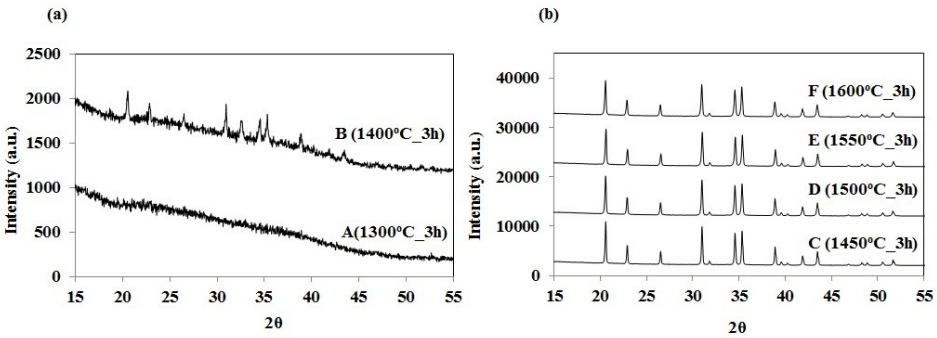

Fig. 3-1. XRD patterns of the amorphous silicon nitride powders heat-treated for 3 h at (a) 1300°C (A), 1400°C (B) and (b) 1450°C (C), 1500°C (D), 1550°C (E), 1600°C (F)

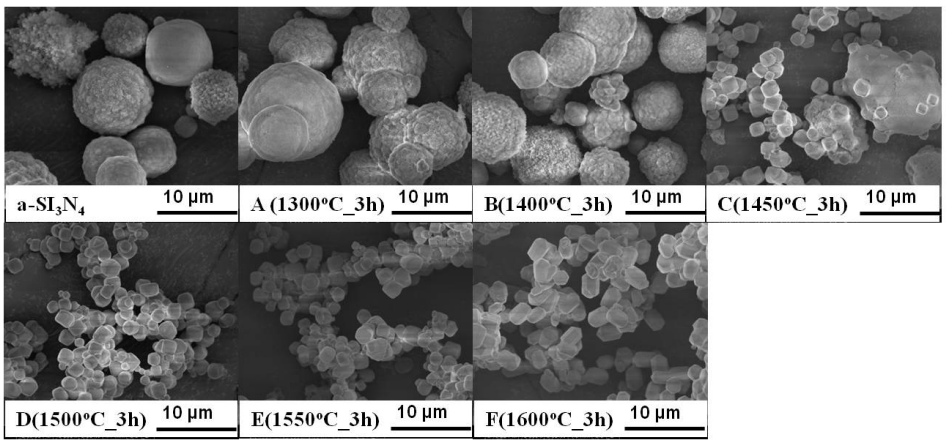

Fig. 3-2. SEM images of the amorphous silicon nitride powder and the samples heat-treated for 3 h at 1300°C (A), 1400°C (B), 1450°C (C), 1500°C (D), 1550°C (E), and 1600°C (F)

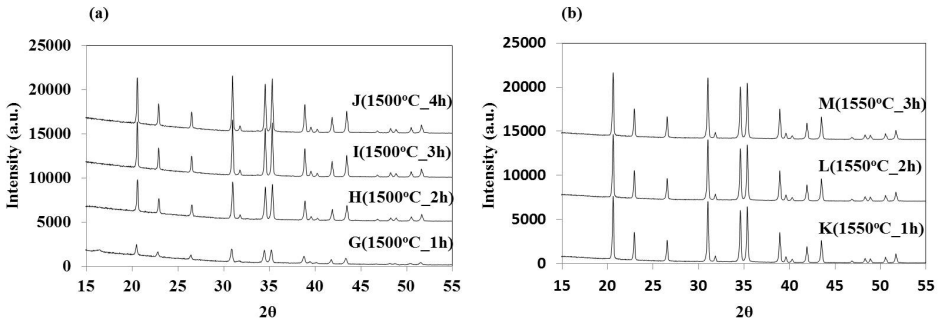

Fig. 3-3. XRD patterns of the amorphous silicon nitride powders heat-treated at (a) 1500°C for 1 h (G), 2 h (H), 3 h (I), 4 h (J) and (b) 1550°C for 1 h (K), 2 h (L), 3 h (M)

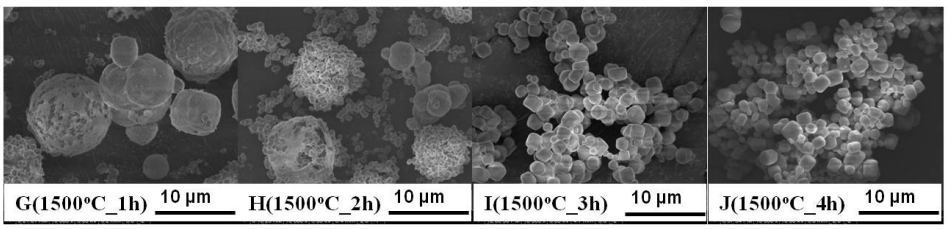

Fig. 3-4. SEM images of the amorphous silicon nitride powders heat-treated at 1500°C for 1 h (G), 2 h (H), 3 h (I) and 4 h (J)

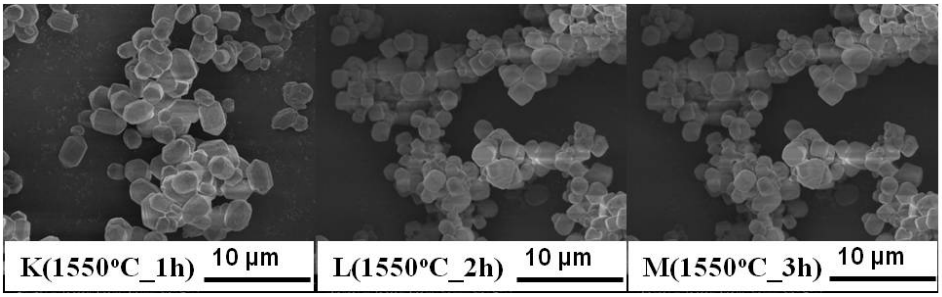

Fig. 3-5. SEM images of the amorphous silicon nitride powders heat-treated at 1550°C for 1 h (K), 2 h (L) and 3 h (M)

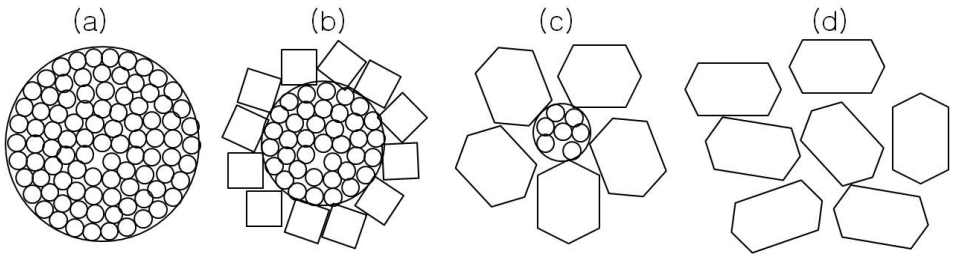

Fig. 3-6. Schematic model for crystallization behavior

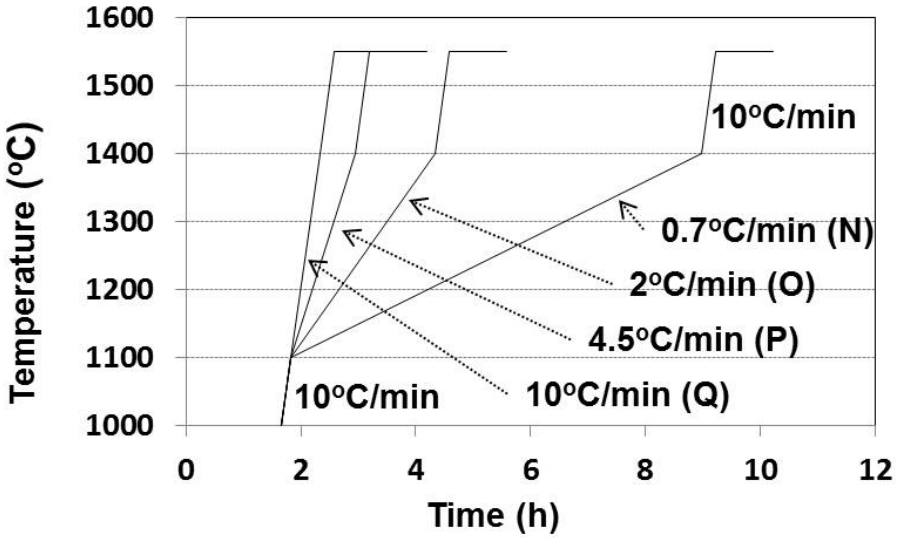

Fig. 3-7. Temperature profile of the samples heat treated at 1550°C for 1 h with heat-up rate of 0.7 °C/min (N), 2 °C/min (O), 4.5 °C/min (P) and 10 °C/min (Q) at the temperature from 1100°C to 1400°C, and then the temperature was increased with heat-up rate of 10 °C/min from 1400°C to 1550°C

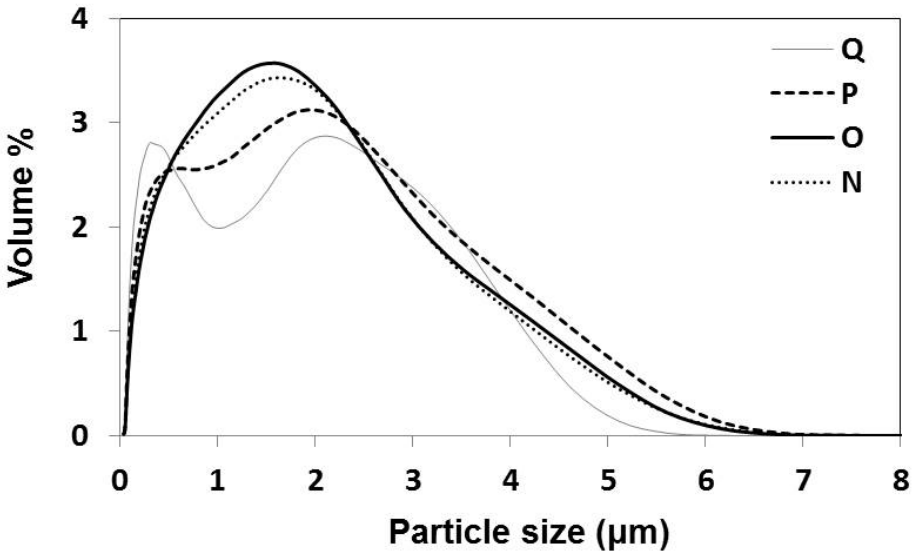

Fig. 3-8. Particle size analysis of the amorphous silicon nitride powders heat-treated at 1550°C for 1 h with heat-up rate of 0.7 °C/min (N), 2 °C/min (O), 4.5 °C/min (P), and 10 °C/min (Q) at the temperature from 1100°C to 1400°C, and then the temperature was increased with heat-up rate of 10 °C/min from 1400°C to 1550°C

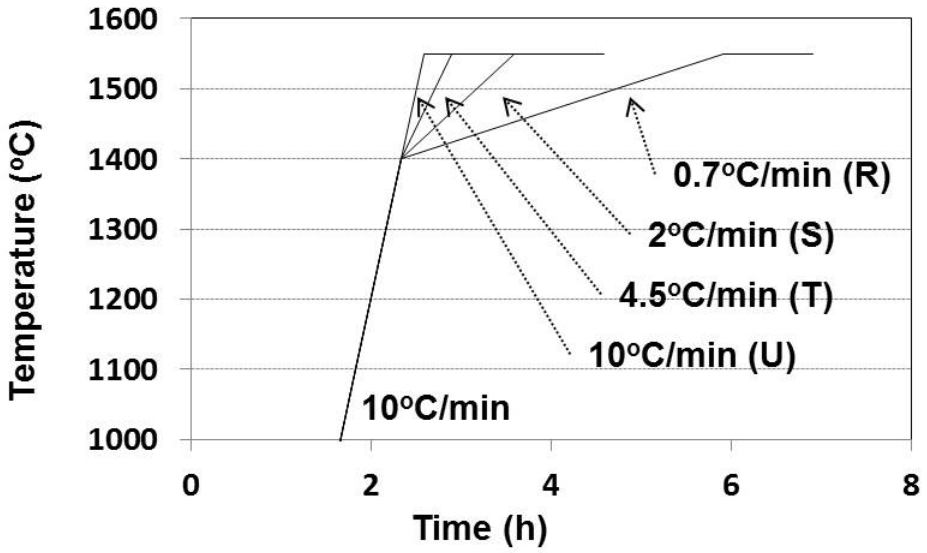

Fig. 3-9. Temperature profile of the samples heat treated at1550°C for 1 h with heat-up rate of 10 °C/min to 1400°C, and then temperature was increased with heat-up rate of 0.7 °C/min (R), 2 °C/min (S), 4.5 °C/min (T), and 10 °C/min (U) from 1400°C to 1550°C

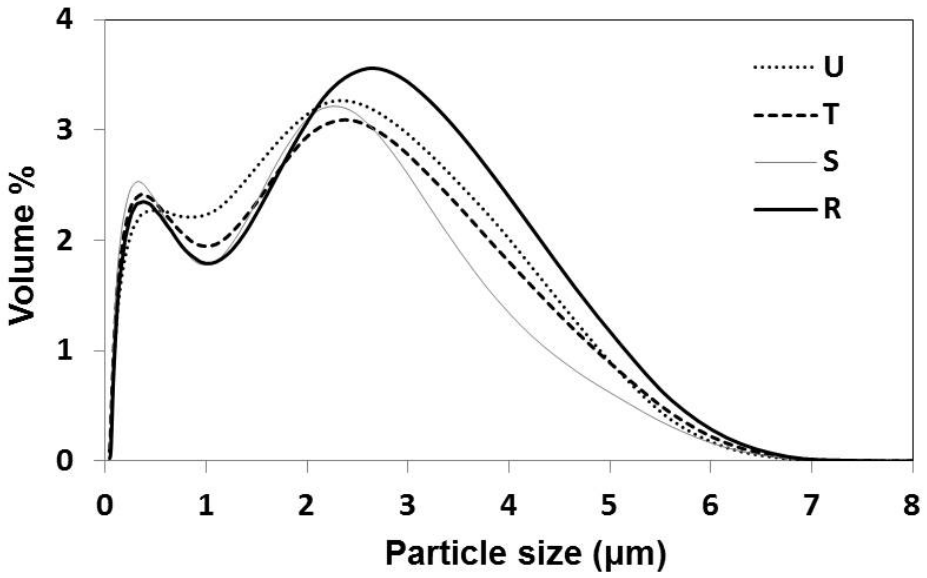

Fig. 3-10. Particle size analysis of the amorphous silicon nitride powders heat-treated at 1550°C for 1 h with heat-up rate of 10 °C/min to 1400°C, and then temperature was increased with heat-up rate of 0.7 °C/min (R), 2 °C/min (S), 4.5 °C/min (T), and 10 °C/min (U) from 1400°C to 1550°C

Table 3-1. Particle size analysis of amorphous silicon nitride powder heat-treated at 1550°C for 1 with heat-up rate of 0.7 °C/min (N), 2 °C/min (O), 4.5 °C/min (P), and 10 °C/min (Q) at the temperature from 1100°C to 1400°C, and then the temperature was increased with heat-up rate of 10 °C/min from 1400°C to 1550°C. The heat-up temperature profile is shown in Fig. 7.

Materials	Mean (μm)	d10 (μm)	d50 (μm)	d90 (μm)
N (0.7 °C/min)	1.25	0.10	0.88	0.34
O (2 °C/min)	1.28	0.19	0.93	0.39
P (4.5 °C/min)	1.28	0.16	0.82	0.38
Q (10 °C/min)	1.10	0.14	0.60	0.43

References

[1] F. L. Riley, *J. Am. Ceram. Soc.* 83, 245 **(2000).**

[2] R. N. Katz, *Ind. Ceram. (Italy)* 17, 158 **(1997).**

[3] A. Okada, *J. Eur. Ceram. Soc.* 28, 1097 **(2008).**

[4] A. Atkinson, A. J. Moulson, and E. W. Roberts, *J. Am. Ceram. Soc.* 59, 285 **(1976).**

[5] T. Licko, V. Figusch, and J. Puchyova, *J. Eur. Ceram. Soc.* 9, 219 **(1992).**

[6] G. Petzow, and M. Herrmann, Silicon nitride ceramics: Structure and Bonding, Springer-Verlag Berlin Heidelberg 102, 50 **(2002).**

[7] M. Nakamura, Y. Kuranari, and Y. Imamura, Characterization and synthetic process of Si_3N_4 material powder. In: S. Somiya, et al Silicon nitride 1, Elsevier, London, 40 **(1987).**

[8] T. Yamada, T. Kawahito, and T. Iwai, *J. mater. Sci. Lett.* 2, 275 **(1983).**

[9] T. Iwai, T. Kawahito, and T. Yamada, US patent 4,859,443 **(1983).**

[10] F. W. Dorn, W. Krause, and F. Schroder, *Adv. Mater.* 4, 221 **(1992).**

[11] H. Lange, G. Wotting, and G. Winter, *Angew. Chem. Int. Ed. Engl.* 30, 1579 **(1991).**

[12] Y. K. Chung, J. H. Koo, S. A. Kim, E. O. Chi, J. H. Hahn, and C. Park, *Ceram. Int.* 40, 14563 **(2014).**

[13] F. Allaire, and R. Langlois, *J. Mater. Sci.* 7, 1265 **(1992).**

[14] R. Riedel, and M. Seher, *J. Eur. Ceram. Soc.* 7, 21 **(1991).**

[15] M. Seher, J. Bill, F. Aldinger, and R. Riedel, *J. Cryst. Growth* 137, 452 **(1994).**

[16] J. Szepvolgyi, and I. Mohai, *Ceram. Int.* 25, 711 **(1999).**

[17] Y. Li, L. Wang, S. Yin, and F. Yang, *Mater. Chem. Phys.* 141, 874 **(2013).**

[18] P. E. D. Morgan, Final Annual Report A-C 3316, Contract No. N00014-72-C-0262, Franklin Institute Research Laboratoies, Philadelphia, Pennsylvania **(1974).**

[19] S. Prochazka, and C. Greskovich, *Amer. Ceram. Soc. Bull.* 57, 579 **(1978).**

[20] Y. Li, Y. Liang, F. Zheng, X. Shong, and Z. Hu, *J. Mater. Sci. Lett.* 13, 1588 **(1994).**

[21] C. Greskovich, and S. Prochazka, *J. Am. Ceram. Soc.* 60, 170 **(1977).**

[22] L. J. Bowen, R. J. Weston, T. G. Garruthers, and R. J. Brook, *J. Mater. Sci.* 13, 341 **(1978).**

[23] S. T. Sawbill, and J. S. Haggerty, *J. Am. Ceram. Soc.* 65, C-131 **(1982).**

[24] B. Chalmers, Principles of Solidification, John Wiley & Sons, Inc., **(1964),** pp. 62-76**.**

Chapter 4. Si_3N_4 Nanowires

4.1 Introduction

One-dimensional (1D) nanostructures such as nanowires, nanotubes, and nanobelts have attracted considerable attention due to their unique morphologies/properties and potential applications in nano-optoelectronic devices and nanocomposites.[1-5] Silicon nitride which is one of the most important high temperature structural ceramics[6-8], is well known for its excellent mechanical properties and thermal stability such as high strength, high hardness, and good resistance to thermal shock and oxidation. Moreover, a wide energy band (5.0-5.3 eV) of Si_3N_4 makes it possible to tailor its electro-optic properties by proper doping.[9] Si_3N_4 with 1D nanostructure is a promising material for manufacturing of composites and for optical and electronic nanodevices operating in severe environments. As a result, a variety of synthesis methods have been attempted to prepare Si_3N_4 1D nanostructures with various morphologies.[10-16] Yang et al. synthesized Si_3N_4 nanobelts by the catalyst-assisted (e.g., $FeCl_2$, $NiCl_2$, and Al powder) pyrolysis of polysilazane.[12,15,17] Huo et al. reported the direct nitridation of Fe-Si alloy particles.[14] Shuyue et al.[18] and Juntong et al.[19] used catalytic thermal-CVD method. Yin et al. reported the vapor-solid reaction of NH_3 with SiO.[20] Zhang et al.[21] and Wang et al.[13] prepared Si_3N_4 nanowires through the reaction of silica gel and carbon nanoparticles. Zhang et al. synthesized Si_3N_4 nanowires by heating Si powders or Si/SiO_2 powder mixture in N_2 or NH_3 atmosphere with or without Fe or Ni powders.[22] Kim et al.[23] and Xie et al.[24] synthesized Si_3N_4 nanowires through the

reaction of silicon substrate and NH_3 with Fe nanoparticles as the catalyst. Zhang et al. synthesized Si_3N_4 nanowires via direct crystallization of amorphous Si_3N_4 (a-Si_3N_4) powder under high temperature in N_2 flow[25], which is not consistent with most literatures in which Si_3N_4 powders (not nanowires) were synthesized from the crystallization of a-Si_3N_4 powder under high temperature in N_2 atmosphere.[26-28] Zou et al.[29] and Xu et al.[30] synthesized Si_3N_4 nanorods in solvent thermal route at low temperature. Although many of these methods produced high-yield Si_3N_4 nanowires, difficulties in the preparation were also reported. For instance, it is difficult to separate high-quality nanowires from the remaining powder in vapor-solid reactions. For the pyrolysis, the liquid polysilazane has to be solidified by heat treatment before the pyrolysis, and the residual carbon derived from the reaction still remains in the product. In the case of using any catalyst, separation of the catalyst and the nanowires is needed. For the direct nitration of Si or carbothermal reduction of SiO_2 with C, the unreacted Si, SiO_2 or C and byproduct such as SiC can still remain in the product. The use of Si/SiO_2 and C as raw material and any metallic catalysts should be avoided to produce high-quality Si_3N_4 nanowires.

In the meantime, the growth mechanism of Si_3N_4 nanowires has also been extensively discussed. Catalytic growth of Si_3N_4 nanowires has been explained by the vapor-liquid-solid (VLS) mechanism which Wagner et al. proposed.[31] There still exist different descriptions in details on the formation of Si_3N_4 nanowires prepared from different routes. Chen et al. explained the growth mechanism of rod-like β-Si_3N_4 crystals from combustion synthesis by a synergy of VLS and Vapor-Solid (VS).[32] Kim et al. found that the Si_3N_4 nanowires grown directly from silicon

substrate resulted from a combination of Solid-Liquid-Solid (SLS) and VLS.[23] Yang et al. reported that the growth of plate-like and branched Si_3N_4 whiskers which were obtained from catalyst-assisted pyrolysis of polymeric precursors followed a Solid-Liquid-Gas-Solid (SLGS) mechanism.[12,15,17] Lin et al. reported that the Si_3N_4 nanotubes prepared from a thermal heating CVD method were formed via the VLS mechanism.[33] Zhang et al. prepared Si_3N_4 nanowires by heating Si or Si/SiO_2 powder in N_2 or NH_3 atmosphere with or without catalysts and suggested that the growth was a VS process.[22] It is obvious that SiO vapor as the Si source of nanowire plays an important role in the growing of Si_3N_4 nanowires no matter what the growth mechanism is.

To the best of our knowledge, there was no report on the synthesis of Si_3N_4 nanowires from the a-Si_3N_4 powder which was synthesized by low-temperature vapor-phase reaction method. The aim of this work is to establish the synthesis process of Si_3N_4 nanowires from a-Si_3N_4 powder and the growth mechanism. High-quality nanowires without any impurities such as Si, SiC, C or metallic catalysts can be produced from the high-quality a-Si_3N_4 powder which was synthesized by low-temperature vapor-phase reaction method. Si_3N_4 nanowires were synthesized from the reaction of SiO with N_2. To supply SiO vapor which is needed to grow nanowires, ammonia gas was introduced during the heat treatment of a-Si_3N_4 powder. The SiO which was formed by the reduction of SiO_2 on the surface of a-Si_3N_4 powder, reacted with N_2, which leads to the growth of Si_3N_4 nanowires. To understand the growth mechanism of nanowires from the a-Si_3N_4 powder, Fe or Ni as a catalyst was added to the a-Si_3N_4 powder. The growth of nanowires followed Vapor-Solid-Solid (VSS) mechanism. The Ni promoted the production of SiO,

which helped the synthesis of the nanowires at 1400 ^{o}C while it was produced at 1550 ^{o}C without Ni catalyst.

4.2 Experimental Procedure

Si_3N_4 nanowires were synthesized from the amorphous Si_3N_4 (a-Si_3N_4) powder which was prepared by low temperature vapor-phase reaction method. The details of the process were previously reported.[34] The reaction between $SiCl_4$ and NH_3 was conducted at room temperature, and the solid product (imide + NH_4Cl by-product) went through a two-step thermal process to obtain the a-Si_3N_4 powder. The first thermal process to remove the NH_4Cl was carried out at 500 °C for 2 h, which was followed by the second thermal process for the decomposition of diimide at 1000 °C for 2 h. Two grams of the a-Si_3N_4 powder was loaded in a graphite crucible, and then heat treated in an alumina tube furnace under nitrogen or ammonia atmosphere at 1550 ^{o}C for 1 h. Fe (99%, Sigma-Aldrich) or Ni (99%, Sigma-Aldrich) was added to the a-Si_3N_4 powder, and the mixture was heat treated at 1400°C for 3 h or 1550 ^{o}C for 1 h under ammonia atmosphere.

The prepared samples were characterized by X-ray diffraction (XRD; PANalytical, EMPYREAN), transmission electron microscopy (TEM; JEOL, JEM-2100F), N/O analysis (LECO, ONH836), and scanning electron microscopy (SEM; FEI, NanoSEM200).

4.3 Results and Discussion

4.3.1 Characterization of Silicon Nitride Nanowires

Si_3N_4 nanowires were synthesized from the amorphous Si_3N_4 (a-Si_3N_4) powder. The a-Si_3N_4 powder was heat-treated at 1550 ^oC for 1 h under 20% NH_3/N_2 atmosphere. The XRD pattern of the nanowire is presented in Fig. 4-1. All the diffraction peaks could be indexed to the hexagonal α-Si_3N_4, which was consistent with the reported data (PDF 41-0360, a = 0.77541 nm and c = 0.56217 nm). The sharp peaks indicate that the nanowires are composed of highly crystallized hexagonal Si_3N_4 phase. The morphology of the Si_3N_4 nanowires was further investigated by SEM. The low-magnification SEM image in Fig. 4-1 shows the synthesized Si_3N_4 nanowires. The high-magnification SEM image shown in Fig. 4-1 indicates that the surface of the nanowires is smooth and clean without any attached particles. The thickness of the nanowire is in the range of 200 ~ 300 nm with lengths of tens of micrometers. The tip of the nanowire has attracted much attention because it can give information on the growth mechanism of the nanowires. No liquid droplets were found on the tips of nanowires, suggesting that the nanowires in the present process were not grown by the VLS mechanism.[31]

The structure of the Si_3N_4 nanowires was further investigated by HR-TEM. Typical HR-TEM images of single crystalline α-Si_3N_4 nanowires are shown in Fig. 4-3 and 4-4. The clear lattice fringes show that the nanowires are highly crystallized. Moreover, lattice-fringe spacings of 0.67 nm and 0.56 nm conformed well to the (001) and (100) planes of α-Si_3N_4, respectively. The insets of Fig. 4-3 (a) and (b) show the corresponding SAED patterns, in which regularly separated diffraction spots also show the high crystallinity of the wires. The longitudinal direction of the

α-Si_3N_4 nanowires coincided with the [100] and [101] directions of the wire. This indicates that the crystal growth directions of α-Si_3N_4 nanowires are the [100] and [101]. In addition, a few nanowires were found to have stacking faults which are clearly shown in Fig. 4-4. Ming et al. reported that the changing gas composition around the growing whisker is responsible for the change of the morphology (i.e. from whisker to knuckle).[35] Xu et al. found that plane defects and stacking faults were observed in the SiC nanowires during the solid-gas reaction of C and SiO.[36] In the present work the slight change of the gas composition around the growing nanowires can lead to the formation of stacking faults during the growth. Juntong et al. reported that stacking faults and misfit dislocations are responsible for the cathodoluminescence behavior of the α-Si_3N_4 nanobelts.[19] Cathodoluminescent behavior (not measured in this work) which can be used in photoelectric nanodevices, can be expected to occur in the nanowires with stacking faults which were synthesized in the present work from the a-Si_3N_4 powder (Fig. 4-4).

4.3.2 Effect of the Ammonia Concentration

Si_3N_4 nanowires were synthesized from a-Si_3N_4 powder at 1550 ^oC for 1 h under different concentration of NH_3/N_2 atmosphere. For comparison, a-Si_3N_4 powder was heat-treated at 1550 ^oC for 1 h under N_2 atmosphere. The SEM images of the samples shown in Fig. 4-5 indicate that the nanowires were not synthesized from the a-Si_3N_4 powder heat-treated under N_2 and 1% NH_3/N_2 atmosphere. This result is consistent with the data reported in the literatures.[26-28] Only few nanowires were synthesized from the a-Si_3N_4 powder heat-treated under 3% NH_3/N_2 atmosphere,

but mostly hexagonal rod-like particles were observed. Nanowires with few hexagonal rod-like particles were synthesized from a-Si_3N_4 powder at 1550 ^oC for 1 h under 5% and 10% NH_3/N_2 atmosphere. The thickness of the nanowire was in the range of 200 ~ 300 nm with lengths of tens of micrometers, and no traces of liquid droplets were found on the tips of nanowires. Fig 4-5 (f) shows that nanowires without hexagonal rod-like particles were synthesized from the a-Si_3N_4 powder at 1550 ^oC for 1 h under 20% NH_3/N_2 atmosphere. It was found from the results that the atmosphere during the heat treatment has a substantial effect on the growth of nanowires from the a-Si_3N_4 powder. There is a minimum concentration of ammonia which is needed for the nanowires to grow. No appreciable changes in the thickness and length of the nanowires were observed after heat treating at 1550 ^oC for 1 h under 5%, 10% or 20% NH_3/N_2 atmosphere.

4.3.3 Effect of the Fe or Ni Addition

It is generally recognized that the nanowires are directly produced from liquid metallic droplets if metal catalysts are involved in the synthesis process. Fe and Ni are known to be effective catalysts for the growth of Si_3N_4 nanowires from the pyrolysis of polymeric precursor or CVD method.[18,19,37] To investigate the growth mechanism from the a-Si_3N_4 powder, 1wt% of Fe or Ni was added to the a-Si_3N_4 powder and the mixture was heat-treated at 1400 ^oC for 3 h or 1550 ^oC for 1 h under 20%NH_3/N_2 atmosphere, and the SEM images of the samples are shown in Fig. 4-6 and 4-7. Fig. 4-6 shows the SEM images of nanowires obtained from a-Si_3N_4 powder with Fe which was heat-treated under 20%NH_3/N_2 atmosphere at (a)

1400 °C for 3 h and (b) 1550 °C for 1 h. Fig. 4-7 shows the SEM images of nanowires obtained from a-Si_3N_4 powder with Ni heat-treated under 20%NH_3/N_2 atmosphere at (a) 1400 °C for 3 h and (b) 1550 °C for 1 h. Fig. 4-6 (c) and Fig. 4-7 (c) show high-magnification SEM images of the nanowires with Fe and Ni, respectively, which were heat-treated at 1550 °C for 1 h. Particles with spherical shape which is similar to the shape of the a-Si_3N_4 powder, were observed in the nanowires obtained from a-Si_3N_4 powder with Fe heat-treated at 1400 °C for 3 h under 20%NH_3/N_2 atmosphere (Fig. 4-6 (a)). The a-Si_3N_4 powder with Fe was transformed to nanowires at 1550 °C for 1 h (Fig. 4-6 (b)) while the powder with Ni was transformed to nanowires at 1400 °C for 3 h under 20%NH_3/N_2 atmosphere (Fig. 4-7 (a)). The growth temperature was lowered when Ni was added to the a-Si_3N_4 powder. Traces of liquid metallic droplets in the nanowires grown from a-Si_3N_4 powder with Fe or Ni were not observed, which indicates that the growth of nanowires from a-Si_3N_4 powder with Fe or Ni catalyst does not follow VLS mechanism.

4.3.4 Growth Mechanism

The basic reactions involved in the formation of Si_3N_4 nanowires are given via the following reactions.

$$SiO_{2(s)} + C_{(s)} \rightarrow SiO_{(g)} + CO_{(g)} \quad (4\text{-}1)$$

$$6SiO_{(g)} + 4N_{2(g)} \rightarrow 2Si_3N_{4(nw)} + 3O_{2(g)} \quad (4\text{-}2)$$

$$3SiO_{(g)} + 3C_{(s)} + 2N_{2(g)} \rightarrow Si_3N_{4(nw)} + 3CO_{(g)} \quad (4\text{-}3)$$

SiO is produced from the reduction of SiO_2 by C, and it reacts with N_2 to form Si_3N_4 nanowires.[35,38-40] From the reactions above, it is obvious that SiO plays an important role in the growing of Si_3N_4 nanowires. In the present work, SiO was produced from the reduction of SiO_2 on the surface of a-Si_3N_4 powder and Si_3N_4 nanowires were formed from the reaction between SiO and N_2. Fig. 4-8 shows the SEM images and EDS results of Si_3N_4 nanowires grown at 1550 ^oC for 1 h at 10%NH_3/N_2 atmosphere. Not only nanowires but also particles were observed. EDX results indicate that oxygen remained on the surface of the particle in Fig. 4-8 (b) while oxygen was not observed on the surface of nanowire in Fig. 4-8 (a). The SiO which was formed by the reduction of SiO_2 on the surface of a-Si_3N_4 powder, reacted with N_2, which leads to the growth of Si_3N_4 nanowires (reaction No. (4-2)). Gardner[41] and Han et al.[42] have reported that SiO was produced from the reduction of SiO_2 by H_2 at the temperature range from 1115^oC to 1630^oC. In the present work, ammonia is decomposed to N_2 and H_2, and the produced H_2 leads to the reduction reaction of SiO_2 to SiO. The formation of the nanowires proceeds via the following reaction.

$$3SiO_{2(s)} + 4NH_{3(g)} \rightarrow Si_3N_{4(nw)} + 2N_{2(g)} + 4H_2O_{(g)} \quad (4\text{-}4)$$

We have investigated the oxygen contents of nanowires which were measured by N/O analyzer as the concentration of NH_3 changes, and the results are shown in Fig. 4-9. Oxygen content, was decreased when the concentration of ammonia was increased during the heat-treatment at 1550 ^oC for 1 h. Remarkable decrease of

oxygen content was observed when the a-Si_3N_4 powder was heat-treated at 1550 ^oC for 1 h under 5% NH_3/N_2 atmosphere. Further decrease of oxygen content was not observed when the a-Si_3N_4 powder was heat-treated at 1550 ^oC for 1 h under 10% or 20% NH_3/N_2 atmosphere. As shown in Fig. 4-5, nanowires were synthesized when the ammonia content was more than 5%, which is the content of ammonia where a rapid decrease of oxygen content was measured (Fig. 4-9). Ammonia as a reducing agent can affect the reduction of SiO_2 to SiO, and the SiO can react with N_2 which can lead to the growth of nanowires. Yin et al. have reported that Si_3N_4 nanowires were synthesized from the SiO powder under NH_3 atmosphere and the growth follows the VS mechanism.[20] The result of the present work is consistent with the literature.[20] There is a minimum concentration of ammonia which is needed for the nanowires to grow. The concentration of ammonia of less than 5% is not large enough for the reduction of SiO_2, which is needed for the growth of nanowires. Careful investigation of TEM results of the tips of nanowires was carried out, and the results are shown in Fig. 4-10. Any traces of liquid droplets were not observed on the tips of nanowires, which indicates that the growth of nanowires does not follow VLS mechanism. Even when any catalyst such as Fe or Ni was added to the a-Si_3N_4 powder, the traces of liquid droplets such as Fe-Si-N or Ni-Si-N were not observed. The absence of catalyst-containing particles at the tips of the nanowires indicates that the growth of nanowires was not dominated by the well-established VLS mechanism. The reduction of SiO_2 to SiO by ammonia was promoted by the presence of Ni catalyst, and so the growth was observed at lower temperature when Ni was added to the a-Si_3N_4 power than when Fe was added. Fig. 4-11 shows a schematic of growth mechanism which we propose. The

nucleation of nanowire occurs on the surface of a-Si_3N_4 powder which is covered by a thin layer of SiO_2. The Si and N atoms of the surface of the amorphous powder move to the nanowire seed formed from the reaction between SiO and N_2, and the nanowires grow from the re-arrangement of Si and N atoms of the a-Si_3N_4 powder. The difference between the surface energy of nanowires and powders can accelerate the growth of nanowires. The formation of nanowire seed follows VS mechanism, and the growth of nanowires is dominated by the solid phase diffusion of Si and N atoms. Growth of nanowires from the seed which is formed on the a-Si_3N_4 powder under NH_3 atmosphere follows VSS mechanism, and the crystal growth of α-Si_3N_4 nanowires occurs along the [100] and [101] direction. It is believed that the morphologies of 1D structure are dominated by the combined effect of surface energy and growth kinetics.[43] Liu et al. have reported that the calculated surface energy (δ) of three low-index planes of Si_3N_4 follow the order: $\delta(100) > \delta(001) > \delta(101)$.[18] Higher-energy planes constantly grow with the sufficient supply of raw materials, whereas lower-energy planes slowly grow with insufficient supply of raw materials due to their smaller surface energies. This indicates that nanowires tend to grow along the [100] direction. In the present study, nanowires were observed to grow along the [101] direction as well, in addition to the [100]. Detailed understanding of the growth kinetics which includes the effect of growth temperature and flow stream parameter on the growth is needed to explain the growth of the nanowires in two different directions.

4.4 Conclusions

The amorphous Si_3N_4 (a-Si_3N_4) powder which was synthesized by low-temperature vapor-phase reaction method was used to synthesize highly crystallized Si_3N_4 nanowires using heat-treating under ammonia atmosphere. It was the purpose of this work to establish the synthesis process of Si_3N_4 nanowires from a-Si_3N_4 powder and the growth mechanism. In order to supply SiO which is needed to grow nanowires, ammonia gas was introduced during the heat treatment of a-Si_3N_4 powder. The SiO which was formed by the reduction of SiO_2 on the surface of a-Si_3N_4 powder, reacted with N_2, which leads to the growth of Si_3N_4 nanowires. There is a minimum concentration of ammonia which is needed for the nanowires to grow, which is ~ 5%. The nucleation of nanowire occurs on the surface of a-Si_3N_4 powder which is covered by a thin layer of SiO_2. The Si and N atoms of the surface of the amorphous powder move to the nanowire seed formed from the reaction between SiO and N_2, and the nanowires grow from the re-arrangement of Si and N atoms of the a-Si_3N_4 powder. Growth of nanowires from the seed which is formed on the a-Si_3N_4 powder under NH_3 atmosphere follows VSS mechanism, and the crystal growth of α-Si_3N_4 nanowires occurs along the [100] and [101] direction. The reduction of SiO_2 to SiO by ammonia was promoted by the presence of Ni catalyst, and so the growth was observed at lower temperature when Ni was added to the a-Si_3N_4 power than when Fe was added. The process parameter to synthesize Si_3N_4 nanowires from a-Si_3N_4 powder synthesized by low-temperature vapor-phase reaction method was optimized, and its growth mechanism was investigated.

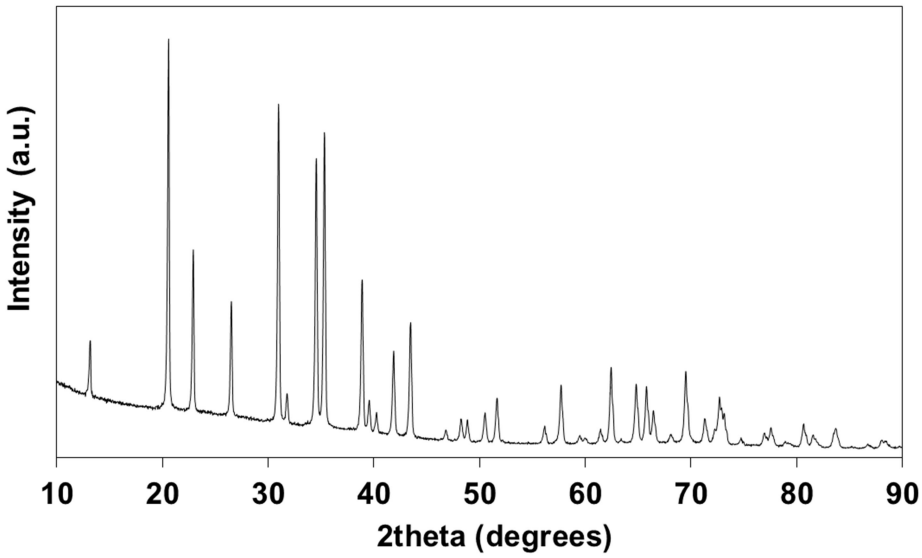

Fig. 4-1. XRD pattern of the Si_3N_4 nanowires heat-treated at 1550 ^oC for 1 h under 20% NH_3/N_2 atmosphere.

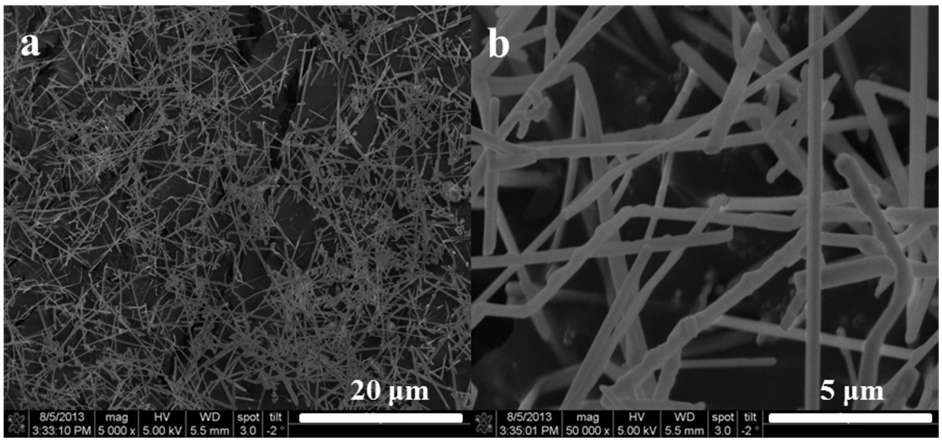

Fig. 4-2. SEM images of the Si_3N_4 nanowires heat-treated at 1550 ^{o}C for 1 h under 20% NH_3/N_2 atmosphere: (a) Low-magnification and (b) high-magnification SEM images of the sample.

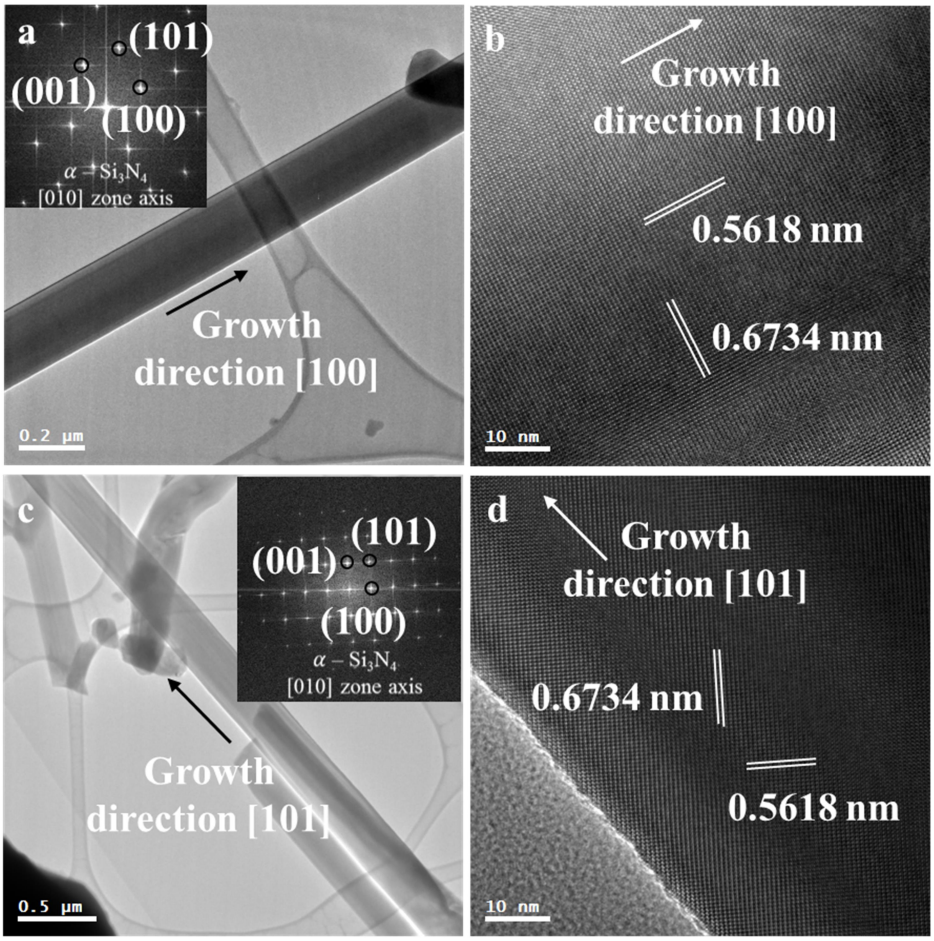

Fig. 4-3. TEM images of the Si_3N_4 nanowires heat-treated for 1 h at 1550 ^oC under 20% NH_3/N_2 atmosphere: (a) and (c) are typical TEM, and (b) and (d) are HR-TEM images of the sample. Insets are SAED patterns corresponding to single crystalline α-Si_3N_4, indicating that the nanowires were growing along the (a) [100] direction and (c) [101] direction.

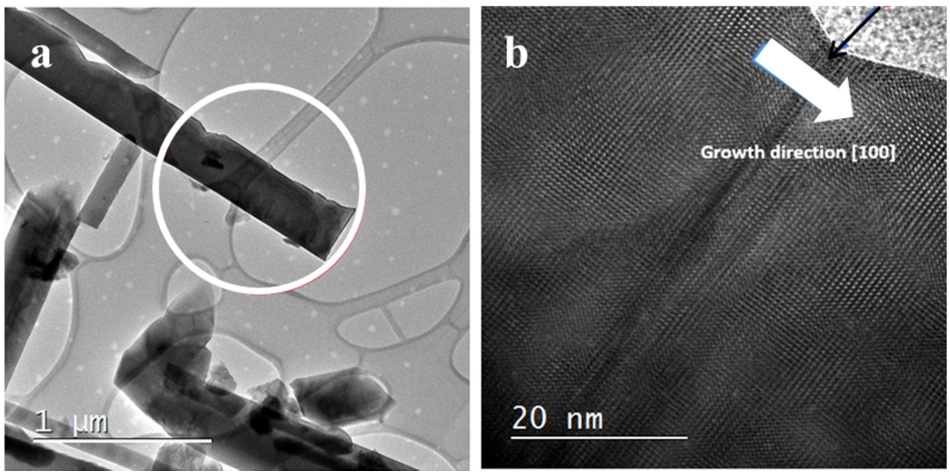

Fig. 4-4. TEM images of the Si_3N_4 nanowires heat-treated for 1 h at 1550 ^oC under 20% NH_3/N_2 atmosphere: (a) a typical TEM image of the sample and (b) an HR-TEM image of the stacking fault of the sample.

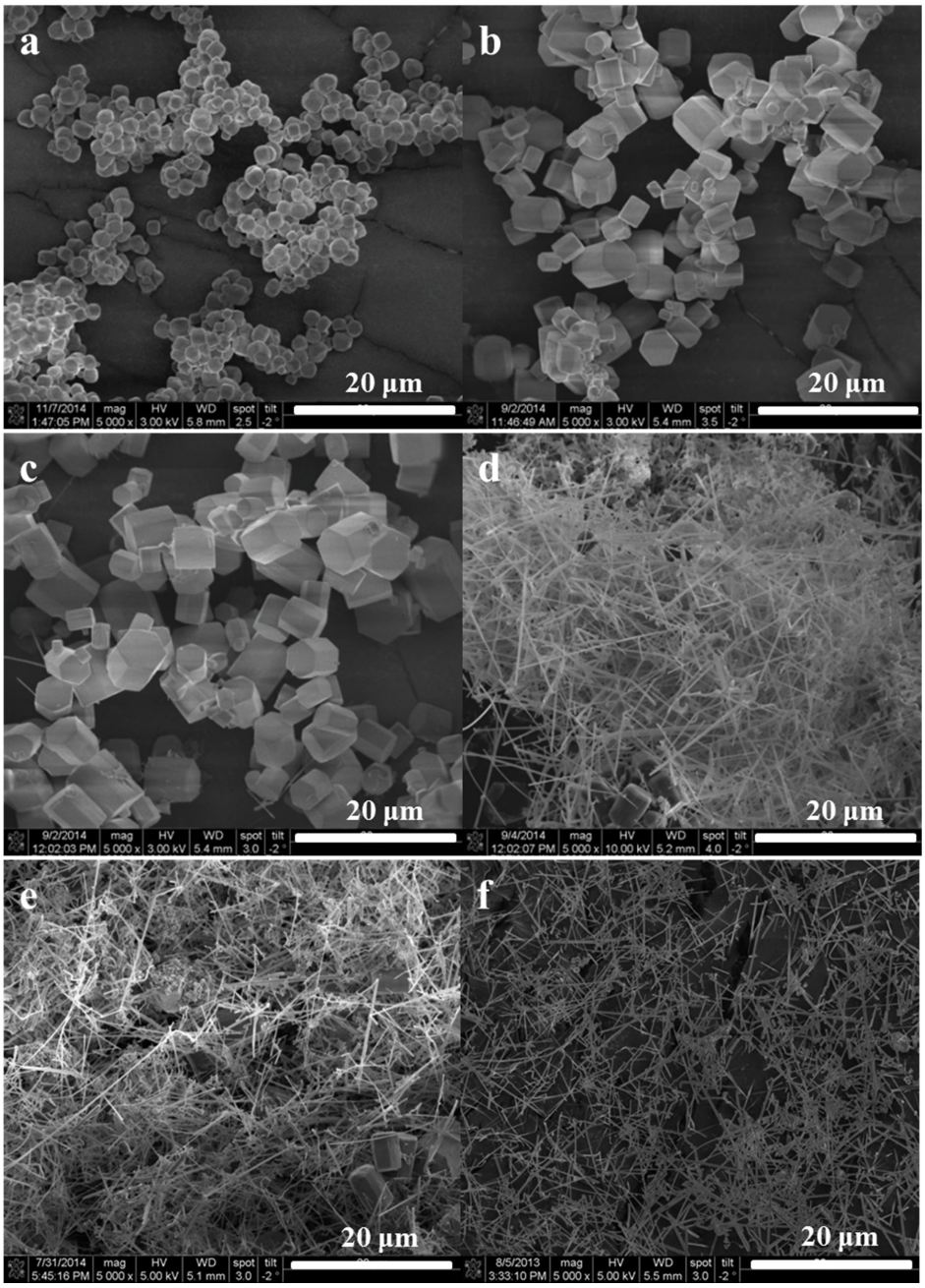

Fig. 4-5. SEM images of silicon nitride powders and nanowires: the samples were heat-treated at 1550 ^{o}C for 1 h under (a) N_2, (b) 1% NH_3/N_2, (c) 3% NH_3/N_2, (d) 5% NH_3/N_2, (e) 10% NH_3/N_2 and (f) 20% NH_3/N_2 atmosphere.

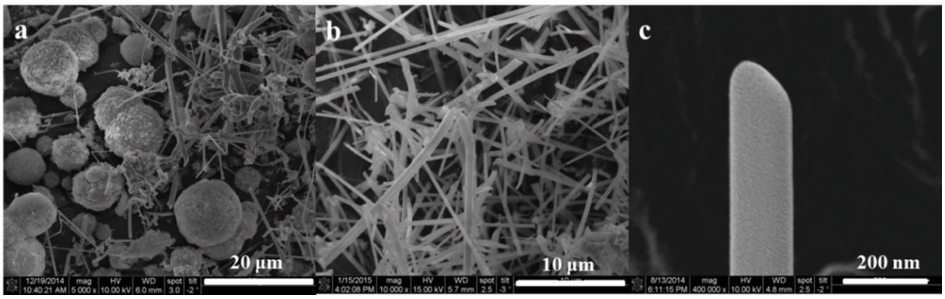

Fig. 4-6. SEM images of nanowires obtained from a-Si_3N_4 powder with Fe which was heat-treated under 20%NH_3/N_2 atmosphere at (a) 1400 ^oC for 3 h and (b) 1550 ^oC for 1 h. (c) high-magnification SEM image of the nanowire heat-treated at 1550 ^oC for 1 h.

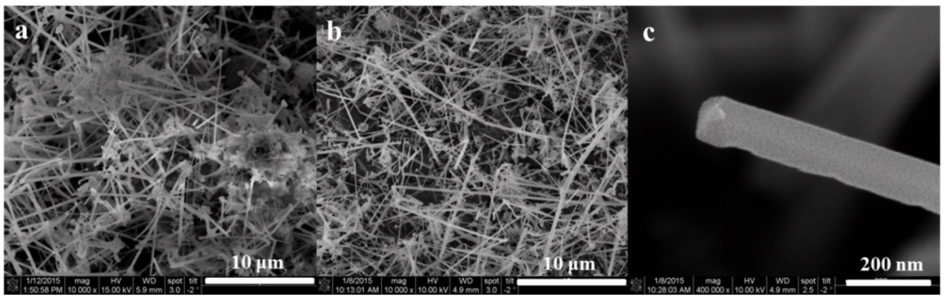

Fig. 4-7. SEM images of nanowires obtained from a-Si_3N_4 powder with Ni which was heat-treated under 20%NH_3/N_2 atmosphere at (a) 1400 ^oC for 3 h and (b) 1550 ^oC for 1 h. (c) high-magnification SEM image of the nanowire heat-treated at 1550 ^oC for 1 h.

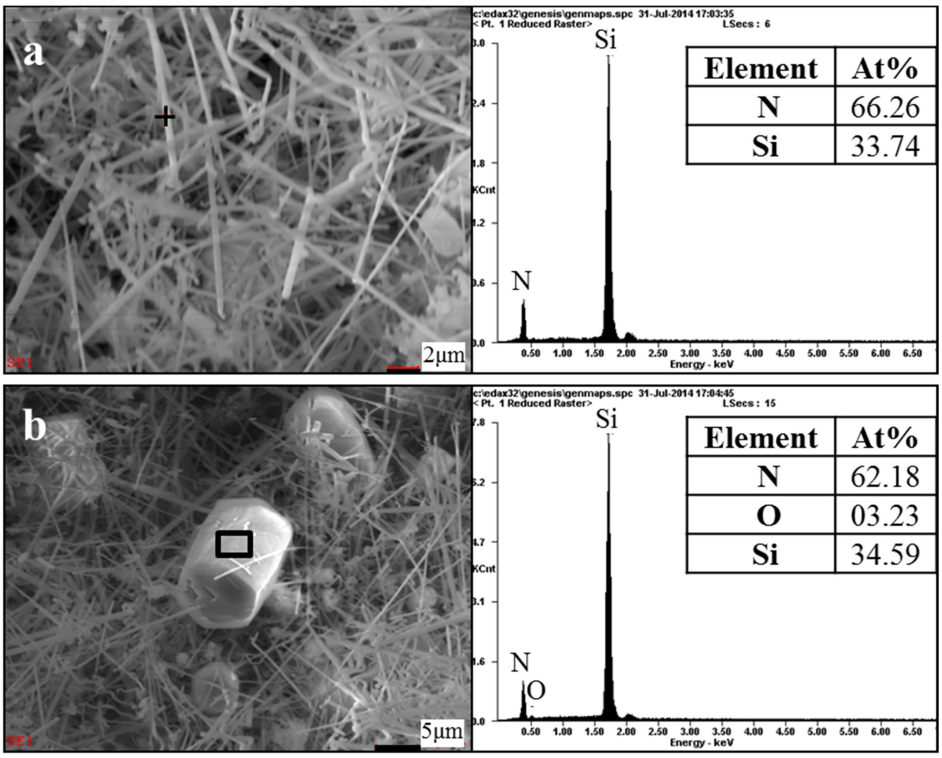

Fig. 4-8. SEM images and corresponding EDX spectrums of silicon nitride nanowires heat treated at 1550 ^{o}C for 1 h under 10% NH_3/N_2 atmosphere: (a) nanowires and (b) rod like particles and nanowires. Insets are the elemental analysis results of EDX.

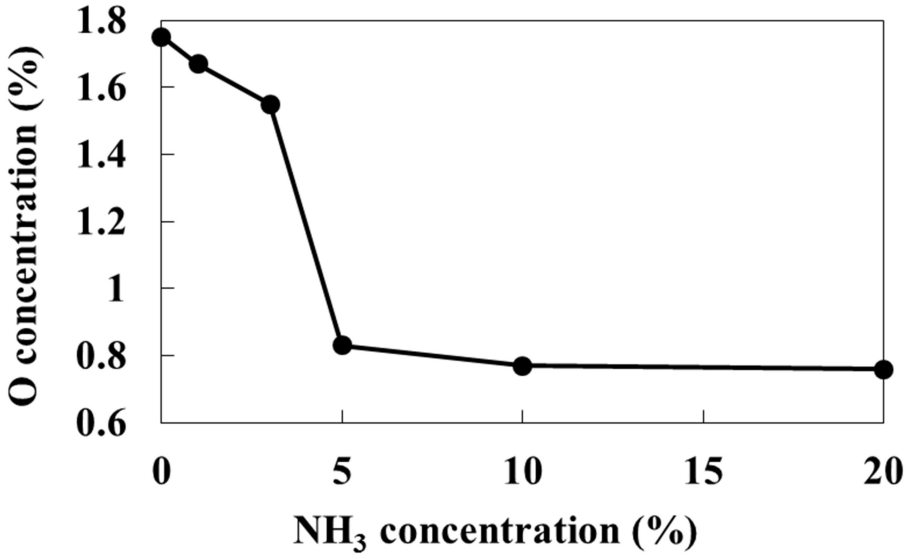

Fig. 4-9. Oxygen contents of Si_3N_4 nanowires heat treated at 1550 ^oC for 1 h under various NH_3 concentrations measured by N/O analyzer (LECO, ONH836).

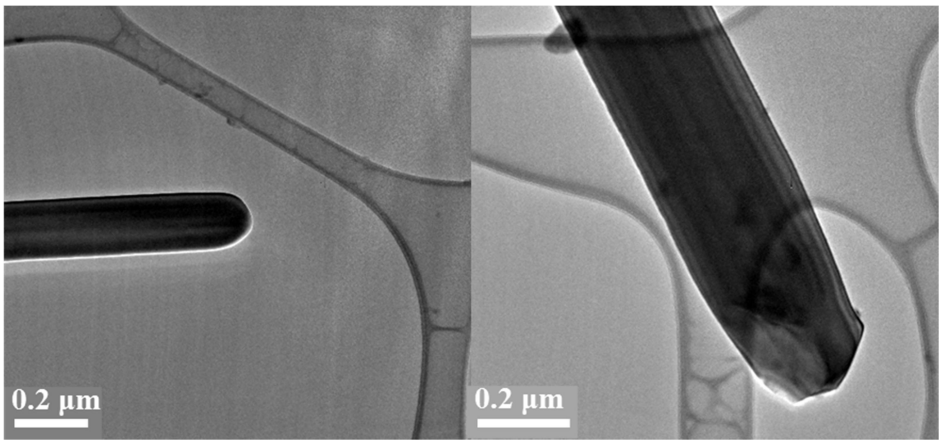

Fig. 4-10. TEM images of Si_3N_4 nanowires heat-treated at 1550 ^oC for 1 h under 20% NH_3/N_2 atmosphere.

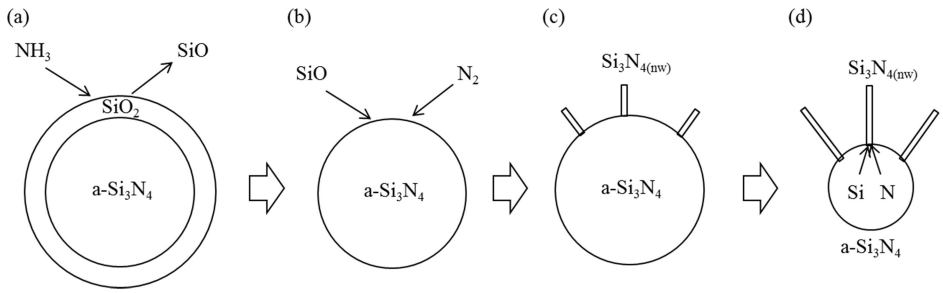

Fig. 4-11. A schematic of nanowire growth mechanism - VSS(Vapor-Solid-Solid) mechanism: (a) reduction of SiO_2 to SiO on the surface of a-Si_3N_4 powder by NH_3, (b) reaction of SiO and N_2, (c) formation of Si_3N_4 nanowire seeds, and (d) growth of Si_3N_4 nanowires from re-arrangement of Si and N atom.

Reference

[1] Y. Huang, X. Duan, L. J. Lauhon, K. H. Kim and C. M. Lieber, *Science*, 2001, **294**, 1313–1317.

[2] Z. W. Pan, Z. R. Dai and Z. L. Wang, *Science*, 2001, **291**, 1947–1949.

[3] M. S. Hu, W. M. Wang, T. T. Chen, L. S. Hong, C. W. Chen, C. C. Chen, Y. F. Chen, K. H. Chen and L. C. Chen, *Adv. Funct. Mater.*, 2006, **16**, 537–541.

[4] J. Zang, Z. H. Xu, R. A. Webb and X. Li, *Nano Lett.*, 2010, **11**, 241–244.

[5] J. Huang, Z. Huang, Y. Liu, M. Fang, K. Chen, Y. Huang, S. Huang, H. Ji, J. Yang, X. Wua and S. Zhang, *Nanoscale*, 2014, **6**, 424–432.

[6] K. R. Carduner, C. S. Blackwell, W. B. Hammond, F. Reidinger and G. R. Hatfield, *J. Am. Chem. Soc.*, 1990, **112**, 4676-4679.

[7] Y. J. Xu, C. B. Cao, Z. Chen, J. Li, F. C. Wang and H. N. Cai, *J. Phys. Chem. B*, 2006, **110**, 3088-3092.

[8] C. C. Tang, Y. Bando, T. Sato and K. J. Kurashima, *J. Mater. Chem.*, 2002, **12**, 1910-1913.

[9] F. Munakata, K. Matsuo, K. Furuya, Y. Akimune, J. Ye and I. Ishikawa, *Appl. Phys. Lett.*, 1999, **74**, 3498–3500.

[10] F. H. Lin, C. K. Hsu, T. P. Tang, J. S. Lee, J. Y. Lin and P. L. Kang, *Mater. Chem. Phys.*, 2005, **93**, 10–15.

[11] G. Shen, Y. Bando, B. Liu, C. Tang, Q. Huang and D. Golberg, *Chem. Eur. J.*, 2006, **12**, 2987–2993.

[12] W. Yang, Z. Xie, H. Miao, L. Zhang, H. Ji and L. An, *J. Am. Ceram. Soc.*, 2005, **88**, 466–469.

[13] F. Wang, G. Q. Jin and X. Y. Guo, *J. Phys. Chem. B*, 2006, **110**, 14546–14549.

[14] K. Huo, Y. Ma, Y. Hu, J. Fu, B. Lu, Y. Lu, Z. Hu and Y. Chen, *Nanotechnology*, 2005, **16**, 2282–2287.

[15] G. Feng, M. He, X. Y. Kong, H. Lin, J. Li and L. Z. Fan, *Appl. Phys. A*, 2009, **97**, 729–734.

[16] J. Huang, S. Zhang, Z. Huang, Y. Wen, M. Fang and Y. Liu, *CrystEngComm*, 2012, **14**, 7301–7305.

[17] F. Gao, W. Yang, Y. Fan and L. An, *Solid State Chem.*, 2008, **181**, 211–215.

[18] S. Liu, M. Fang, Z. Huang, J. Huang, H. Ji, H. Liu, Y. G. Liu and X. Wu, *Sci. Rep.*, 2015, **5**, 8998 DOI:10.1038/srep08998.

[19] J. Huang, Z. Huang, S. Yi, Y. Liu, M. Hang and S. Zhang, *Sci. Rep.*, 2013, **3**, 3504 DOI:10.1038/srep0350.

[20] L. W. Yin, Y. Bando, Y. C. Zhu and Y. B. Li, *Appl. Phys. Lett.*, 2003, **83**, 3584–3586.

[21] L. D. Zhang, G. W. Meng and F. Phillipp, *Mat. Sci. Eng. A*, 2000, **286**, 34-38.

[22] Y. Zhang, N. Wang, R. He, J. Liu, X. Zhang and J. Zhu, *J. Cryst. Growth*, 2001, **233**, 803-808.

[23] H. Y. Kim, J. Park and H. Yang, *Chem. Phys. Lett.*, 2003, **372**, 269-274.

[24] T. Xie, G. S. Wu, B. Y. Geng, Z. Jiang, X. Y. Yuan, Y. Lin, G. Z. Wang and L. D. Zhang, *Appl. Phys. A*, 2005, **80**, 1057-1059.

[25] H. Zhang, S. Zhang, S, Pan and J, Hou, *J. Am. Ceram. Soc.*, 2005, **88**, 566-569.

[26] M. Nakamura, Y. Kuranari and Y. Imamura, *Silicon Nitride 1*, Edited by S. Somiya et al., Elsevier, London 1987, 90.

[27] F. W. Dorn, W. Krause and F. Schroder, *Adv. Mater.*, 1992, **4**, 221–224.

[28] H. Lange, G. Wotting and G. Winter, *Angew. Chem. Int. Ed. Engl.*, 1991, **30**, 1579–1597.

[29] G. Zou, B. Hu, K. Xiong, H. Li, C. Dong, J. Liang and Y. Qian, *Appl. Phys. Lett.*, 2005, **86**, 181901-181903.

[30] F. Xu, X. Zhang, W. Xi, J. Hong and Y. Xie, *Chem. Lett.*, 2003, **32**, 600-601.

[31] R. S. Wagner and W. C. Ellis, *Appl. Phys. Lett.*, 1964, **4**, 89-90.

[32] D. Y. Chen, B. L. Zhang, H. R. Zhuang, W. L. Li and S. Y. Xu, *Mater. Lett.*, 2002, **57**, 399-402.

[33] F. H. Lin, C. K. Hsu, T. P. Tang, J. S. Lee, J. Y. Lin and P. L. Kang, *Mater. Chem. Phys.*, 2005, **93**, 10-15.

[34] Y. K. Chung, J. H. Koo, S. A. Kim, E. O. Chi, J. H. Hahn and C. Park, *Ceram. Int.*, 2014, **40**, 14563-14568.

[35] M. J. Wang and H. Wada, *J. Mater. Sci.*, 1990, **25**, 1690-1698.

[36] X. H. Sun, C. P. Li, W. K. Wong, N. B. Wong, C. S. Lee, S. T. Lee and B. K. Teo, *J. Am. Chem. Soc.*, 2002, **124**, 14464–14471.

[37] H. Cui and B. R. Stoner, *J. Mater. Res.*, 2001, **16**, 3111-3115.

[38] G. Gundiah, G. V. Madhav, A. Govindaraj, Md. M. Seikh and C. N. R. Rao, *J. Mater. Chem.*, 2002, **12**, 1606-1611.

[39] G. Y. Li, X. D. Li, H. Wang and Z. Q. Li, *Appl. Phys. A*, 2008, **93**, 471-475.

[40] K. Komeya and H. Inoue, *J. Mater. Sci.*, 1975, **10**, 1243-1246.

[41] R. A. Gardner, *J. Solid State Chem.*, 1974, **9**, 339-344.

[42] G. Han and H. Y. Sohn, *J. Am. Ceram. Soc.*, 2005, **88**, 882-888.

[43] Z. L. Wang, Z. W. Pan and Z. R. Dai, *Microsc. Microanal.*, 2002, **8**, 467-474.

Chapter 5. Industrial Application

5.1 Introduction

Multicrystalline (multi) silicon is the most widely used material in the solar cell industry, accounting for ~50% of the global solar cell market.[1] Cell manufacturers must decrease manufacturing costs, and improve solar cell performances to be competitive. Silicon nitride (Si_3N_4) coated crucibles for directional solidification are a promising alternative to silica (SiO_2) crucibles. The use of Si_3N_4 coated-crucibles has two main advantages: (i) the reusability of the crucible for several castings and (ii) potentially very low oxygen content in the solidified ingots. Si_3N_4 is a well-known material for high temperature applications owing to its tolerance for thermal shocks and chemical stability. [2] Hence, its application as a crucible material for multi-Si ingots casting can overcome the single-run limitation related to the use of SiO_2 crucibles. Silica crucibles undergo phase transformation from quartz (higher density) to cristobalite (lower density) during the melting of the Si charge. During the post solidification cooling, the crucibles recrystallize into quartz, and the resulting stresses lead to crucible fracture. Therefore the cost of multi-Si ingots can be appreciably decreased by replacing a single-use silica crucible with a reusable silicon nitride coated crucible. Moreover, diffusion of oxygen into the melt from the silica crucible walls and the silicon nitride coating layer has been reported as a relevant source of oxygen contamination in the solidified ingot.[3–5] Hence, using a silicon nitride based crucible for casting of multi-Si ingots allows eliminating one source of

contamination for the silicon melt, and thus it offers the potential to solidify multi-Si ingots with very low oxygen concentrations. A novel technique to produce crucibles of silicon nitride has been developed.[6] In this study, for the solidification furnace, numerical and experimental investigations of such crucibles reported by Bellmann *et al*. were followed.[7] They suggested increasing the furnace temperature by 20 K during melting to counterbalance the higher heat loss through the bottom owing to higher heat conductivity of the silicon nitride coated crucibles compared to silica crucibles. In this study, Si_3N_4 powder synthesized by low-temperature vapor-phase reaction was coated on the 5G (W880 mm × D880 mm x H420 mm) SiO_2 crucibles, and the synthesized Si_3N_4 coated-crucible was used to directionally solidify multi-Si ingots for solar cells. The thickness and uniformity of the coating layer were measured. The effect of coating layer on the ingot properties are presented and compared to those of the reference ingots cast in commercial crucibles, under standard solidification parameters.

5.2 Experimental Procedure

5.2.1 Si_3N_4 Powder Coating

Si_3N_4 powder (α-phase: 100%, O content: 0.78%, metal impurities: <140 ppm, average particle size: 1.65 μm) synthesized by low-temperature vapor-phase reaction was coated on the 5G (W880 mm × D880 mm × H420 mm) SiO_2 crucibles by automatic coating process shown in Fig. 5-1. 700 g of Si_3N_4 powder was mixed in 2300 g of water. The resulting mixture was sprayed on the crucible with the flow rate of 36 g/min. For the first coating of 20th layer, the coating layer

was dried for 30 min at room temperature. After coating the 20th layer, the coating layer was dried for 10 min per every coating of 10th layer until the mixture was consumed completely. The coated crucible was dried at room temperature for 7 days and then was heated at 1100 °C for 5 h at a heating rate of 73 °C/h. The thickness and uniformity of coating layer were measured by the depth gage.

5.2.2 Polysilicon Ingot Growing

400 kg of polysilicon was charged in the synthesized Si_3N_4 coated-crucible. The polysilicon was melted for 12 h and stabilized for 2 h, followed by growing and then cooling for 35 and 12 h, respectively. The process is presented in Fig. 5-2. After ingot growing, the crucible was removed from the ingot. The ingot was cut into 25 bricks. Then, every brick was inspected to check the presence of crack or inclusion by IR spectroscopy. Crack free brick was sliced into slugs to investigate minority carrier lifetime (WT-2000PVN), resistivity (WT-2000PVN), Oi, and Cs contents (FT-IR, QS-1200), and metal impurities (ICP-OES).

5.2.3 Si_3N_4 sintering

Sintering aids such as 5 wt% Y_2O_3, 2 wt% MgO, and 1 wt% La_2O_3 were added to the amorphous Si_3N_4 powder. The mixture was ball milled in ethanol for 24 h. 2.5 wt% PVA and 2.5 wt% PEG were added to the mixture as a binder. The ball-milled mixture was dried at 70 °C for overnight. The starting material was pelletized by uniaxial press and cold isotropic press. The green body was heated at various temperatures under nitrogen atmosphere at 0.1 Mpa. The density and

microstructure of the sintered body were measured. For comparison, Ube E10 powder was sintered under the same conditions as explained above.

5.3 Results and Discussion

5.3.1 Si_3N_4 Powder Coating

The thickness of the coating layer was measured at the 100 points of the coating layer of inside of the crucible. The average thickness and standard deviation were calculated. Uniformity was calculated by standard deviation. The crack free ratio was calculated by the summation of the cracks existed at each points. The measured points and the results are presented in Fig. 5-3. The average thickness of coating layer was 257 μm, whereas the thickness of commercial crucible was 150 μm. Uniformity was 27.15%, and cracks were not observed. When the coated crucible is used for multi-Si ingot, it will more protect the ingot from the contamination of oxygen and impurities from SiO_2 crucible than when commercial crucible is used because of thicker coating layer.

5.3.2 Polysilicon Ingot Growing

Multi-Si ingot was grown from the synthesized Si_3N_4 coated-crucible, and the results of quality assessment are presented in Table 5-1. The crucible was removed from the ingot, and the surface of the ingot was investigated by naked eyes whether coating layer was remained on it. The surface was clean, and any crack was not observed. The ingot was cut into 25 bricks, and the inside crack and inclusion in

each brick were investigated by IR spectroscopy. Any crack or inclusion was not observed in the 25 bricks. The brick was sliced into slugs, and the slugs were collected from the top, middle, and bottom of the brick to carry out MCLT, resistivity, Oi & Cs, and metal impurities. The average MCLT and resistivity of the slugs were 3.9 μs and 4.4 Ω·s, respectively, whereas the slugs grown from commercial crucible showed the average MCLT and resistivity of 4.2 μs and 4.7 Ω·s, respectively. The contents of O, C, and metal impurities were 4.4, 1.1, and 7.3 ppm, respectively, whereas the slugs grown from commercial crucible contained 4.4 ppm of O, 1.1 ppm of C, and 7.3 ppm of metal impurities. Those results indicate that the performance of Si_3N_4 coated crucible was almost similar to the commercial one.

5.3.3 Si_3N_4 sintering

The density and microstructure of the sintered body were measured, and the results are presented in Figs. 5-5 and 5-6, respectively. Pressureless sintering of the synthesized powder showed 99% sintering density at 1650 °C, whereas Ube E10 powder showed 96% sintering density. Sintering onset temperature was lower compared to UBE powder. The synthesized powder showed different microstructures, which need to be modified.

5.4 Conclusions

The Si_3N_4 powder synthesized by low-temperature vapor-phase reaction was coated on the 5G crucible for multi-Si ingot. Multi-Si ingot was grown from the synthesized Si_3N_4 powder coated-crucible. The quality of the coating layer was investigated. The thickness of the coating layer was 257 μm with a uniformity of 27.15%. The inside crack and inclusion were not observed in the 25 bricks. The average MCLT and resistivity of the slugs were 3.9 μs and 4.4 Ω·s, respectively. The contents of O, C, and metal impurities were 4.4, 1.1, and 7.3 ppm, respectively. Those results indicate that the performance of synthesized Si_3N_4 coated-crucible was almost similar to the commercial one. To apply for the structural ceramics, pressureless sintering of the synthesized powder was carried out. The density and microstructure of the sintered body were measured, and the results were compared to the sintered body from Ube E10 powder. Pressureless sintering of the synthesized powder showed 99% sintering density at 1650 °C, whereas Ube E10 powder showed 96% sintering density. The density of the synthesized power was higher than that of Ube E10 powder. The Si_3N_4 powder synthesized by low-temperature vapor-phase reaction will be a good candidate for the coating and the structural ceramics materials.

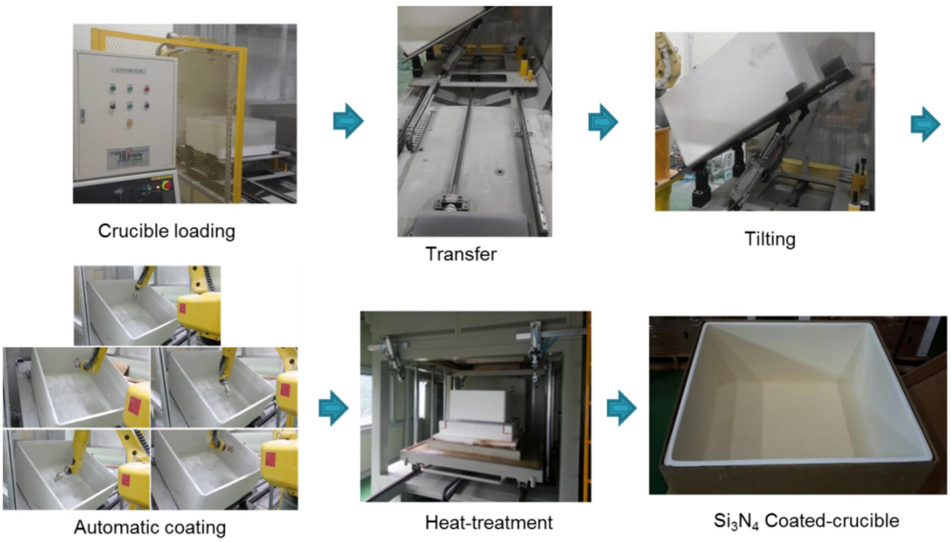

Fig. 5-1. Automatic coating process

Fig. 5-2. Polysilicon ingot growing process

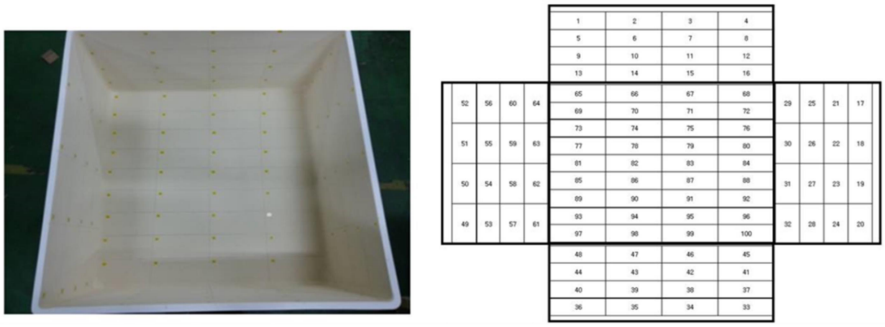

	Si_3N_4 coated crucible	Commercial crucible
Thickness (μm)	257	150
Crack free (%)	100	100
Uniformity (%)	27.15	-

Fig. 5-3. Coating results

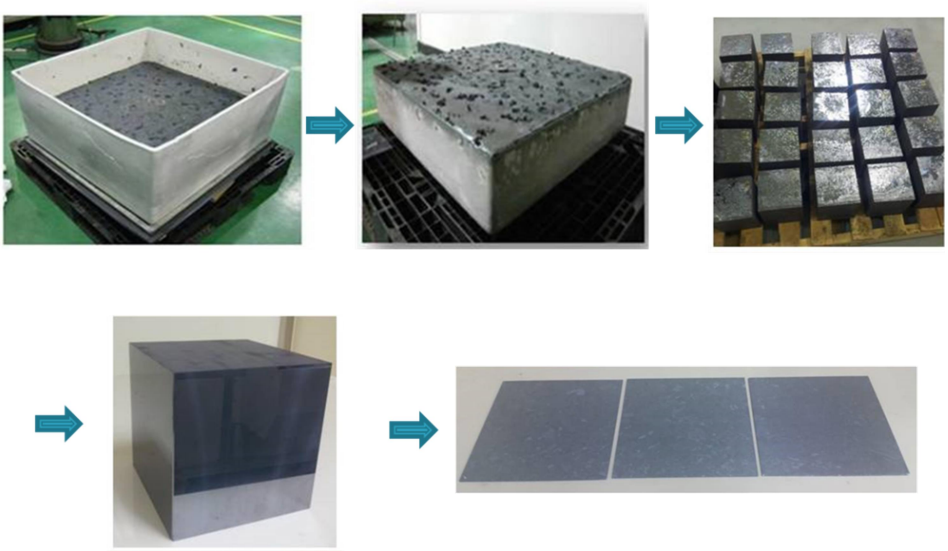

Fig. 5-4. Preparation process of slug

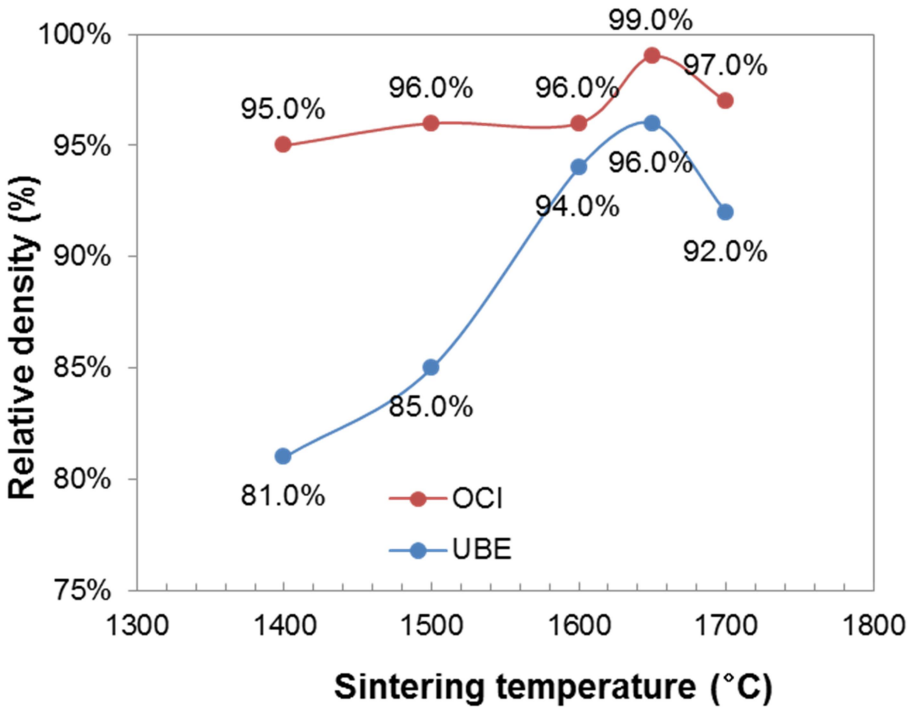

Fig. 5-5. Density of the sintered body from synthesized powder and Ube E10 powder

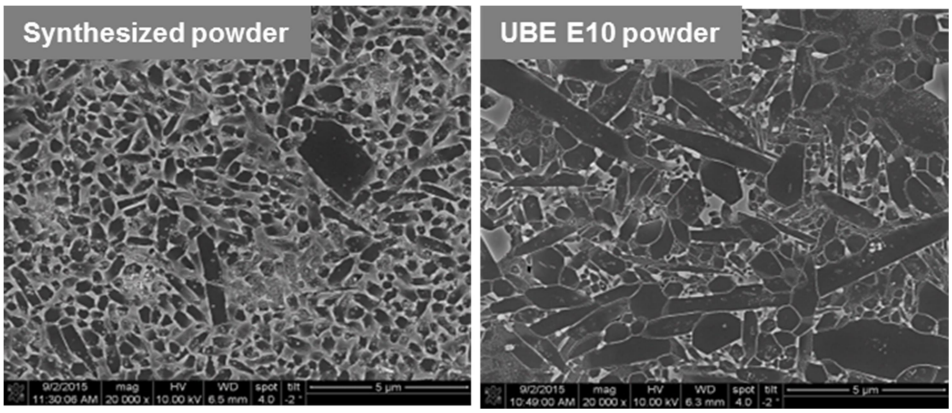

Fig. 5-6. Microstructure of the sintered body from synthesized powder and Ube E10 powder

Table 5-1 Result of quality assessment of ingot

Analysis	**Unit**	**Commercial crucible**	**Si_3N_4 coated crucible**	**Comparison**
Exfoliation	-	Good	Good	Good
MCLT	μs	4.2	3.9	Better
Resistivity	Ω·cm	4.7	4.4	Good
Oi/Cs	ppm	5.7/1.5	4.4/1.1	Better
Crack-free	%	100	100	Good
Metal Impurities	ppb	7.3	7.3	Good

Reference

[1] G. Hering, Year of the tiger, *Photon International* 3 (2011) 186–218.

[2] F.L. Riley, Silicon nitride and related materials, *J. Am. Ceram. Soc.* 83 (2000) 245–265.

[3] H. Matsuo, R.B. Ganesh, S. Nakano, L. Liu, Y. Kangawa, K. Arafune, Y. Ohshita, M. Yamaguchi, K. Kakimoto, Thermodynamical analysis of oxygen incorporation from a quartz crucible during solidification of multicrystalline silicon for solar cell, *J. Cryst. Growth* 310 (2008) 4666–4671.

[4] R. Kvande, L. Arnberg, C. Martin, Influence of crucible and coating quality on the properties of multicrystalline silicon for solar cells, *J. Cryst. Growth* 311 (2009) 765–768.

[5] E. Olsen, E. Øvrelid, Silicon nitride coating and crucible—effects of using upgraded materials in the casting of multicrystalline silicon ingots, *Progress in Photovoltaics: Research and Applications* 16 (2008) 93–100.

[6] E. Olsen, A. Solheim, H. Sørheim, Mould parts of silicon nitride and method for producing such mould parts, *International Patent* no. WO 2004/016835 A1, 2004.

[7] M.P. Bellmann, E.A. Meese, M. Syvertsen, A. Solheim, H. Sørheim, L. Arnberg, Silica versus silicon nitride crucible: influence of thermophysical properties on the solidification of multi-crystalline silicon by Bridgman technique, *J. Cryst. Growth* 318 (2011) 265–268.

Chapter 6. Summary

In this study, the synthesis and decomposition temperatures of $Si(NH)_2$ were studied to investigate the reaction phenomena and parameters of low-temperature vapor-phase reaction for the synthesis of $Si(NH)_2$. In addition, the effects of the flow rates of the reactants and the carrier gas on the particle size, the reaction temperature, and the yield were investigated. The reaction product was grown on the nozzle, because the reaction zone was formed near the nozzle. The convection caused by the heat of reaction played an important role of product growing phenomena. The down-top flow reaction was the best way to prevent product from the deposition. The concentration of the reactant affected the particle size of the product. No reaction was observed at temperatures >200 °C because of the decomposition of $Si(NH)_2$. The reaction temperature increased as the reactant flow rates increased because of the exothermic nature of the reaction, thus lowering the yield. The reaction yield decreased with increasing Ar flow rate; this process can be used to cool the reactor. The flow rates of $SiCl_4$, NH_3, and Ar were increased to 48, 1000, and 1000 mL min^{-1}, respectively, for the optimization, affording 87% yield in the reactor used in this study (D100 mm × H500 mm, 4L).

Amorphous silicon nitride powder was heated at various temperatures for different periods of time to examine the crystallization behavior. The effects of the heat-up rate on the particle size, and its distribution, of the α-phase silicon nitride powder were investigated. The phase transition from amorphous to α-phase occurred at temperatures >1400 °C. The crystallization process completed after heat treatment

at 1500 °C for 3 h or at 1550 °C for 1 h. The crystallization process starts at the surface of the amorphous particles, the outer regions of the particles become crystalline, whereas the inner part remains amorphous. The re-arrangement of the Si and N atoms on the surface of the amorphous particle leads to the formation of hexagonal crystal structures separated from the host amorphous particles. The nucleation occurred at temperatures <1400 °C.

The particle size and distribution was tuned by varying the heat-treatment profile (namely, the heat-treatment temperature, heating rate, and heating duration at the specified treatment temperature), which can be used to control the relative extent of nucleation and growth. The completion of most of the nucleation by lowering the heat-up rate was used to achieve a singlet particle size distribution. Conversely, a bi-modal particle size distribution was achieved by adopting a fast heat-up rate during the crystallization process. The amorphous Si_3N_4 (a-Si_3N_4) powder synthesized by low-temperature vapor-phase reaction method was used to synthesize highly crystallized Si_3N_4 nanowires by heating under ammonia atmosphere. The synthesis process of Si_3N_4 nanowires from a-Si_3N_4 powder and the growth mechanism were established. To supply SiO needed to grow nanowires, ammonia gas was introduced during the heat treatment of a-Si_3N_4 powder. The SiO formed by the reduction of SiO_2 on the surface of a-Si_3N_4 powder reacted with N_2, leading to the growth of Si_3N_4 nanowires. A minimum concentration of ammonia (~5%) was required for the growth of nanowires. The nucleation of nanowire occurs on the surface of a-Si_3N_4 powder covered by a thin layer of SiO_2. The Si and N atoms of the surface of the amorphous powder move to the nanowire seed formed from the reaction between SiO and N_2, and the nanowires grow from the re-

arrangement of Si and N atoms of a-Si_3N_4 powder. The growth of nanowires from the seed formed on the a-Si_3N_4 powder under NH_3 atmosphere followed the VSS mechanism, and the crystal growth of α-Si_3N_4 nanowires occurred along the [100] and [101] directions. The reduction of SiO_2 to SiO by ammonia was promoted in the presence of Ni catalyst, and the growth was observed at lower temperature when Ni was added to the a-Si_3N_4 power. The process parameters to synthesize Si_3N_4 nanowires from a-Si_3N_4 powder synthesized by low-temperature vapor-phase reaction method were optimized, and its growth mechanism was investigated. The Si_3N_4 powder synthesized by low-temperature vapor-phase reaction was coated on the 5G crucible for multi-Si ingot. Multi-Si ingot was grown from the synthesized Si_3N_4 powder coated-crucible. The quality of the coating layer was assessed. The thickness of the coating layer was 257 μm with a uniformity of 27.15%. The inside crack and inclusion were not observed in the 25 bricks. The average MCLT and resistivity of the slugs were 3.9 μs and 4.4 Ω·s, respectively. The contents of O, C, and metal impurities were 4.4, 1.1, and 7.3 ppm, respectively. These results indicate that the performance of synthesized Si_3N_4 coated-crucible was almost similar to the commercial one. To apply for the structural ceramics, pressureless sintering of the synthesized powder was carried out. The density and microstructure of the sintered body were measured, and the results were compared to the sintered body from Ube E10 powder. Pressureless sintering of the synthesized powder showed 99% sintering density at 1650 °C, whereas Ube E10 powder showed 96% sintering density. The density of the synthesized power was higher than that of Ube E10 powder. We believe that Si_3N_4 powder synthesized by

low-temperature vapor-phase reaction would be a good candidate for the coating and structural ceramics materials.

	Reaction phenomena	Process optimization		Applications	
		Imide synthesis	Crystallization	Sintering	Coating
Contents	▪ Rxn Phenomena ▪ Reactor design ▪ Nozzle design	▪ Rxn parameters -. Temperature -. Flow rate ▪ Optimization -. Particle size -. yield	▪ Powder -. Temperature -. Duration -. Heat-up rate -. Cryst. Mechanism ▪ Nanowire -. NH_3 concentration -. Effect of catalyst -. Growth mechanism	▪ Pressure less sintering ▪ Density	▪ 5th generation crucible coating ▪ Performance evaluation -. Crack, Thickness ▪ p-Si ingot growing ▪ Performance evaluation -. Crack, MCLT, Oi/Cs, impurities, Resistivity
Results	▪ Development of LT vapor-phase reaction method ▪ Down-top flow reactor ▪ Separate nozzle	▪ Particle size control ▪ Optimization -. yield >85% -. Temp.: <150°C	▪ Si_3N_4 powder -. α-phase: 100% -. Size: <1.5μm -. O: <0.8% ▪ Si_3N_4 nanowire -. D: hundreds of nm -. L: tens of μm -. Growth: [100], [101] VSS mechanism	▪ Temp.: 1650°C ▪ Density: 99%	▪ Coating layer -. Thickness: 306 μm -. Uniformity: ±7.4% -. Crack: free ▪ p-Si ingot -. MCLT: 3.9μs -. Oi/Cs: 4.4/1.1 ppm -. Impurities: 7.3 ppm -. Resistivity: 4.4 Ω·cm
Publications	▪ Patent: 4	▪ Patent: 5 ▪ Paper: 1	▪ Patent: 2 ▪ Paper: 2		

Fig. 6-1 Summary of Si_3N_4 powder production and application

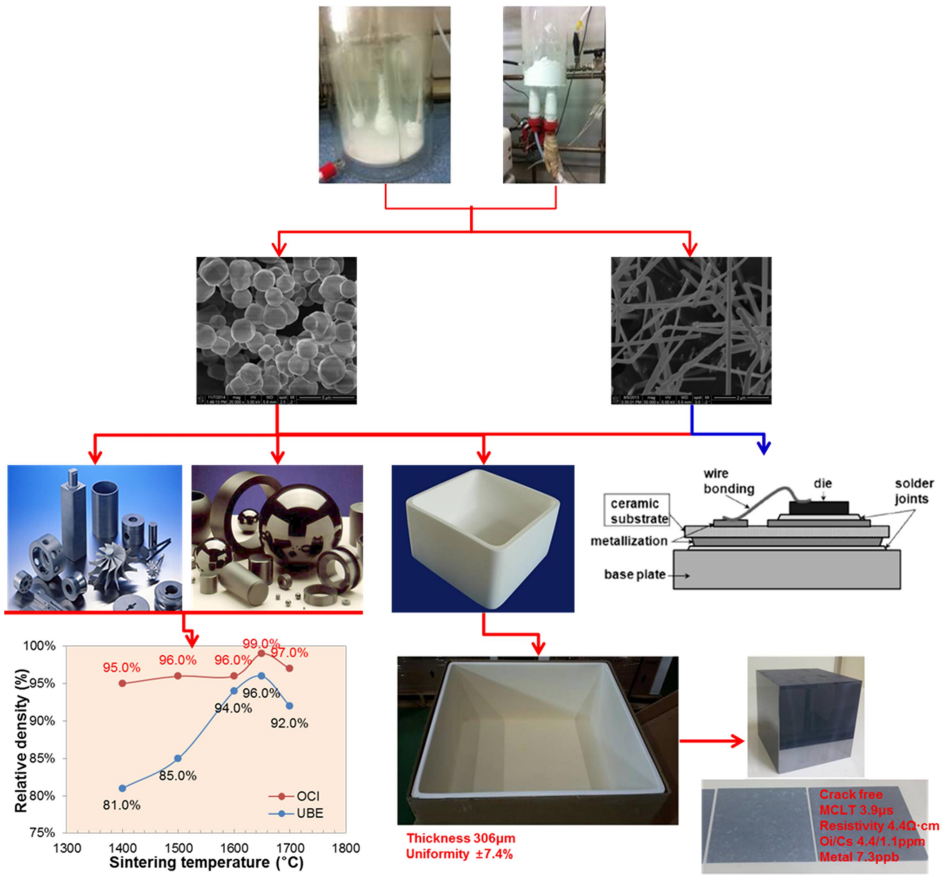

Fig. 6-2 Scheme of Si_3N_4 powder production and application

초록

극한의 조건에서 상업적으로 사용되는 대부분의 질화규소 분말은 이미드 열분해법에 의해 생산되고 있다. 이미드는 -50°C ~ 0°C 에서 솔벤트를 사용하는 액상 반응에 의해 합성된다. 이 공정은 에너지를 많이 소비하는 단점이 있다. 에너지 소비가 적은 방법 중 질화규소 분말을 합성하기에 적합한 방법은 원료인 $SiCl_4$와 NH_3를 기상에서 반응하여 질화규소를 제조하는 방법이다. 본 연구에서는 이미드를 합성하기 위하여 도입된 새로운 방법인 저온기상합성법에 대한 연구를 진행하였다. 저온기상합성 공정 변수를 파악하고 최적화 하는 연구를 수행하였다. 상온에서 반응을 진행하였고, 원료는 반응기 하부에서 상부 방향으로 분사되도록 하였고, 고체 생성물은 반응기 하부에 쌓일 수 있도록 반응기를 설계하였다. 반응 생성물인 이미드는 TG 분석결과 150°C 이상에서 완전히 분해되는 것으로 나타났다. 발열반응으로 인하여 반응 온도는 반응물의 유량을 증가할수록 증가하였고, 케리어 가스의 유량을 증가할수록 감소하는 것으로 나타났다. 반응 수율은 케리어 가스의 유량을 증가할수록 감소하였고, 87%의 반응 수율을 얻을 수 있도록 반응 조건을 최적화 하였다.

저온기상합성법에 의해 합성된 무정형 질화규소를 다양한 온도에서 다양한 시간동안 열처리 하여 결정화 거동에 대한 연구를 진행하였다. 열처리 온도와 시간이 결정화도에 미치는 영향과, 승온속도가

입자크기와 입자크기분포에 미치는 영향에 대해서 고찰하였다. 무정형에서 알파상으로의 상전이는 1400°C 이상에서 나타났다. 1500°C에서 3시간동안 열처리를 하거나, 1550°C에서 1시간 동안 열처리를 할 경우 완전하게 결정화가 진행되었다. 무정형 질화규소 입자의 표면에서부터 결정화가 진행되었고, 실리콘과 질소 원소들의 재배열에 의해 헥사고날 구조를 보이는 알파상 질화규소로 결정이 성장하였다. 입자 크기분포는 승온속도에 영향을 받았다. 승온속도가 낮은 조건에서는 핵생성 속도가 빠른 온도구간에서 충분한 열처리에 의해 핵이 균일하게 발생하였고, 생성된 핵이 모두 균일하게 결정 성장하여 입자 크기 분포가 균일하였으며, 승온속도가 빠른 조건에서는 핵생성 속도가 빠른 온도구간에서 충분하게 열처리가 되지 않아 균일하게 핵생성이 되지 못하였고, 결정화 속도가 빠른 온도구간에서 핵생성과 결정 성장이 동시에 발생하게 되어 상대적으로 입자 크기가 분균일하게 결정이 성장하였다.

분위기 가스가 결정 성장에 미치는 영향을 파악하고자 암모니아 가스 분위기에서 열처리를 하였고, 그 결과 무정형 질화규소가 알파상 질화규소 나노와이어로 상전이 되었음을 관찰하였다. 두께가 200 ~ 300 nm, 길이가 수십 마이크로미터, [100], [101] 방향으로 성장한 질화규소 나노와이어가 합성되었다. XRD, TEM, SEM/EDS, N/O 분석을 통해 나노와이어 성장 메커니즘을 규명하였다. 무정형 질화규소 표면에 존해하는 SiO_2 층이 암모니아 가스와 반응하여 SiO를 생성하였고,

생성된 SiO가 N_2와 반응하여 Si_3N_4 나노와이어로 성장하였다. SiO와 N_2 반응에 의해 생성된 질화규소 나노와이어는 무정형 질화규소 표면에서부터 합성되었고, 무정형 질화규소의 실리콘과 질소 원소의 재배열에 의해 나노와이어가 성장하였다. 이를 기체-고체-고체 성장 메커니즘으로 명명하였다. 니켈 촉매를 첨가할 경우 SiO_2와 NH_3가 반응하여 SiO가 생성되는 환원 반응의 촉매 역할을 하여 반응온도가 낮아지는 효과를 관찰하였다

저온기상합성법에 의해 합성된 질화규소의 상업적 이용을 위해 분말의 소결 특성을 파악하였고, 태양전지 제조를 위한 다결정 실리콘 잉곳 제조용 도가니 내벽에 코팅하여 코팅 특성을 파악하였다. 코팅 결과 257 μm 두께의 27.15% 균일도를 보이는 코팅층이 형성되었고, 이를 실리콘 잉곳을 성장시켜 제조한 웨이퍼의 성능을 평가함으로써 코팅제로써의 영향을 파악하였다. 웨이퍼의 특성 평가 결과 MCLT 3.9 μs, 비저항 4.4 Ω·s, 산소함량 4.4 ppm, 탄소함량 1.1 ppm, 금속 불순물 7.3 ppm으로 나타났다. 이는 상업적으로 사용되는 상용 도가니에서 성장한 잉곳의 웨이퍼 성능과 유사한 것으로 나타났다.

질화규소 분말의 소결 특성을 파악하고자 상압소결을 하였고, 이를 우베 E10분말과 비교 평가를 하였다. 그 결과 1650°C에서 밀도 99%를 보였으며 이는 우베 E10 분말의 밀도가 96% 보다 높은 것으로 나타났다. 코팅제로써의 성능 평가 결과와 소결후 밀도 측정 결과로부터 본 연구를 통해 합성된 질화규소를 상업적으로 적용이 가능 할 것으로 사료된다.

Keywords: 실리콘 다이이미드, $Si(NH)_2$, 질화규소, Si_3N_4, 기상반응, 이미드 열분해, 결정화, 나노와이어, 질화규소 분말 코팅

학번: **2013-30187**